MICROWAVE IRRADIATION EFFECT IN THE MODIFICATION OF VANADIUM PHOSPHORUS OXIDE CATALYSTS SYNTHESISED VIA SESQUIHYDRATE ROUTE

KANG JO YEE

A thesis submitted to the Department of Chemical Engineering,
Faculty of Engineering and Science,
Universiti Tunku Abdul Rahman,
in partial fulfilment of the requirements for the degree of Master of Science

May 2014

MICROWAVE IRRADIATION EFFECT IN THE MODIFICATION OF VANADIUM PHOSPHORUS OXIDE CATALYSTS SYNTHESISED VIA SESQUIHYDRATE ROUTE

ABSTRACT

Three series of vanadyl pyrophosphate (VPOs) catalysts were prepared via sesquihydrate route. All the precursors were synthesised through vanadyl phosphate dihydrate ($VOPO_4 \cdot 2H_2O$) in 1-butanol instead of using isobutanol/benzyl alcohol as reducing agent, which were commonly used in conventional method. In the first series, microwave drying process is employed on Stage 1 and/or Stage 2 during the synthesis and was compared with the VPOs catalyst produced by conventional oven drying process. The effect of the drying method of the catalyst precursors will be the key study of this research. The second series, Gallium is used as dopant and 0.1 mol%, 0.3 mol% and 0.5 mol% of gallium were added into the series of VPOs catalysts prepared via sesquihydrate route and microwave drying. For the third series, microwave irradiation process employed in Stage 1 and/or Stage 2 during the synthesis was compared with the VPOs catalyst produced by conventional reflux method. All the modified precursors were calcined under a flow of 0.75% *n*-butane/air at 733K to generate the active vanadyl pyrophosphate ($(VO)_2P_2O_7$) catalysts. In this research, the physico-chemical properties, reactivity and catalytic performances of all the VPOs catalysts were investigated using XRD, SEM-EDX, BET, ICP-OES, redox titration and TPR in H_2. Catalysts dried with microwave irradiation shows structure with crystal-like clusters that

stacked up into rosette shape and they showed to have better catalytic performances with the increment in both activity and selectivity as compared to catalyst produced via only conventional oven drying method. VPOs-MM is used as control for further research in Series 2 and Series 3 due to its balance improvement in activity, selectivity and specific surface area. Catalysts added with gallium exhibited good crystalline with characteristics peaks of vanadyl pyrophosphate phase and their surface morphologies are of more compact structures with further agglomeration of the crystal-like clusters layering in rosette shape. The combination of microwave energy level and Ga-dopant bonding in the VPOs catalysts has improved the mobility of oxygen atoms (O^-) associated with V^{4+} phase, which caused the VPOs-Ga0.5% to contribute the highest conversion rate of *n*-butane to MA with minimal specific surface area. When microwave irradiation was involved at Stage 1 during the synthesis of VPOs catalyst precursors, it was found that the BET specific area had increased with the formation of more prominent V^{5+} phase as shown in the XRD profile. VPOs-M_sM_s showed to be the best catalyst among all three series due to its ability to produce more maleic anhydride with minimum by-products.

ABSTRAK

Tiga siri mangkin-mangkin vanadium fosfat telah dimodifikasi melalui prekursor vanadyl hydrogen fosfat sesquihydrida ($VOPO_4 \bullet 2H_2O$). Semua mangkin-mangkin disintesis dalam 1-butanol. Dalam siri pertama, proses pengeringan mikrogelombang digunakan dalam sintesis di peringkat 1 dan/atau peringkat 2. Mangkin-mangkin yang diproses melalui pengeringan mikrogelombang dibandingkan dengan VPOs mangkin yang disintesis melalui pengeringan konvensional. Dalam siri kedua, Galium digunakan sebagai dopan dan 0.1 mol%, 0.3 mol% dan 0.5mol% gallium ditambahkan dalam siri mangkin-mangkin VPOs yang disediakan melalui laluan sesquihydrida dan pengeringan mikrogelombang. Bagi siri ketiga, sinaran mikrogelombang digunakan dalam peringkat 1 dan/atau peringkat 2 semase proses sintesis. Semua prekursor yang telah dimodifikasi dikalsinasi dalam aliran 0.75 % *n*-butana/udara pada suhu 733 K untuk menghasilkan mangkin vanadyl pirofosfat ($(VO)_2P_2O_7$) yang aktif. Teknik-teknik yang telah digunakan untuk mencirikan mangkin-mangkin tersebut adalah: XRD, SEM, BET, ICP-OES, titrasi redoks, TPR dalam H_2. Morfologi mangkin-mangkin yang dikeringkan oleh sinaran mikrogelombang mengpamerkan bentuk kelompok kristal yang disusun ke dalam bentuk roset. Mangkin-mangkin yang dikeringkan oleh sinaran mikrogelombang menunjukkan prestasi pemangkin yang lebih baik, dimana kedua-dua activiti dan pemilihan meningkat apabila dibandingkan dengan mangkin yang disintesis melalui pengeringan konvensional. VPOs-MM digunakan sebagai kawalan untuk penyelidikan lanjut dalam Siri 2 dan Siri 3 disebabkan oleh peningkatan kira-aktiviti, pemilihan dan kawasan permukaan

tertentu. Pemangkin-pemangkin yang didopkan dengan galium menunjukkan struktur yang lebih padat dengan penumpuan kristal berkelompok dalam bentuk roset. Gabungan tahap tenaga gelombang mikro dengan Ga-pendopan dalam pemangkin VPOs telah meningkatkan mobiliti atom oksigen (O-) yang berkaitan dengan V^{4+} fasa yang menyebabkan VPOs-Ga0.5% memiliki kadar penukaran tertinggi *n*-butana ke MA dengan minimum kawasan permukaan tertentu. Apabila sinaran mikrogelombang terlibat dalam sintesis peringkat 1, mangkin-mangkin VPOs didapati mengandungi permukaan spesifik yang tinggi dengan formasi fasa V^{5+} seperti yang dipamerkan dalam profil XRD. VPOs-M_sM_s merupakan pemangkin yang terbaik di kalangan ketiga-tiga siri kerana kemampuannya untuk menghasilkan lebih banyak maleic anhydride dengan minimum sisa produknya.

ACKNOWLEDGEMENTS

I would like to thank everyone who had contributed to the successful completion of this project. I would like to express my gratitude to my research supervisor, Asst. Prof. Dr. Leong Loong Kong for his invaluable advice, guidance and his enormous patience throughout the development of the research. Thank you for believing in me and constantly encouraging me to do my best. I am grateful to him for advising me to be humble and hardworking in life.

I would also like to express my gratitude to my loving parent who had given me encouragement and for guiding me through my ups and downs. Special thanks to my beloved mother for being emotionally strong for me and family. Thank you for teaching me: to face the problems, to solve them, and to let it go.

In addition, I would also like to express my gratitude to my friends, Max Ling Kuan Hoe and Catherine Loh Pei Xuan. Thank you for their supports during my time as postgraduate. Through our ups and downs, not only have they helped in making the problems smaller, they also helped me to grow as a better person. I would also like to thank my wonderful friends and colleagues for making my study and work life exciting and fill with joys.

Lastly, I am grateful to UTAR for giving me this opportunity to carry out my research and providing me with the facilities.

FACULTY OF ENGINEERING AND SCIENCE

UNIVERSITI TUNKU ABDUL RAHMAN

APPROVAL SHEET

I certify that this project report entitled **"MICROWAVE IRRADIATION EFFECT IN THE MODIFICATION OF VANADIUM PHOSPHORUS OXIDE CATALYSTS SYNTHESISED VIA SESQUIHYDRATE ROUTE"** was prepared by **KANG JO YEE** and submitted as partial fulfilment of the degree of Master of Science at Universiti Tunku Abdul Rahman.

Approved by,

_____ Date: _____

(Asst. Prof. Dr. Leong Loong Kong)

Supervisor

Department of Chemical Engineering

Faculty of Engineering and Science

Universiti Tunku Abdul Rahman

FACULTY OF ENGINEERING AND SCIENCE

UNIVERSITI TUNKU ABDUL RAHMAN

Date: _____

SUBMISSION OF THESIS

It is hereby certified that KANG JO YEE_ (ID No: 0909095) has completed this thesis entitled "**MICROWAVE IRRADIATION EFFECT IN THE MODIFICATION OF VANADIUM PHOSPHORUS OXIDE CATALYSTS SYNTHESISED VIA SESQUIHYDRATE ROUTE**" under the supervision of Dr. Leong Loong Kong from the Department of Chemical Engineering, Faculty of Engineering and Science,

I understand that University will upload softcopy of my in pdf format into UTAR Institutional Repository, which may be made accessible to UTAR community and public.

Yours truly,

_____

(*KANG JO YEE)*

TABLE OF CONTENTS

LIST OF TABLES

LIST OF FIGURES

LIST OF APPENDICES

CHAPTER 1

INTRODUCTION

1.1 Catalysis and Catalysts

The term “catalysis” is first introduced by Jöns Jakob Berzelius at 1835. He derived it from the Greek words ‘kata’, which stands for down, and ‘lysein’, which means to split or break. For catalysis to occur there must be a chemical interaction between the catalyst and the reactant-product system. The main purpose of solid catalyst is to develop a commercial product that can be used as an active, selective, and stable material for a determined catalytic process (González-Cortés and Imbert, 2013).

According to Boudart (1991), catalyst is a substrate which transforms reactants into products, through an uninterrupted and repeated cycle of elementary steps in which the catalyst participates while being regenerated to its original form at the end of each cycle during its lifetime. According to Clugston (1998), the catalyst generally enters into chemical combination with the reactants but is ultimately recoverable at the end unchanged in chemical composition or mass. A catalyst influences not only the reaction rate, but also the distribution of products.

A catalyst provides an alternative pathway for the reaction to occur, thus reducing the activation energy and increasing the reaction rate without involving itself in reactant and product as shown in Figure 1.1 (Chorkendorff and

Niemantsverdriet, 2007). Since the presence of catalyst does not alter the equilibrium constant, the quotient of the rates for the forward and reverse reactions also remain unchanged. The catalyst does however increase the forward rate; it must also increase the reverse rate by the same factor (Bond, 1987).

Figure 1.1 showed the process of reactants, which is considered as an exothermic process. The main difference in the diagram is the activation energy for both the reactions. Activation energy is the minimum amount of energy required for the reaction to occur. With the aid of catalyst, the activation energy (blue curve) needed is much lower as compared to the activation energy (green curve) without the catalyst. However, the final products are still the same. The reduction of activation energy (Ea) increases the number of reactant molecules with enough to reach the activation energy and form the product.

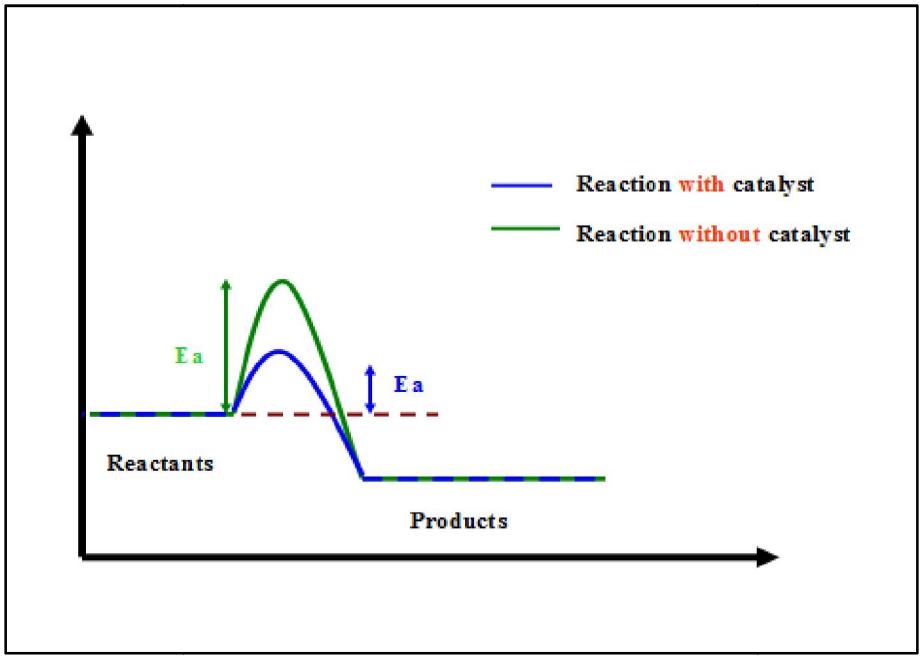

Figure 1.1: The activation energy (Ea) and enthalpy of formation (ΔH) with and without catalyst

1.2 Types of Catalysis

Generally, catalytic systems are classified as either homogeneous or heterogeneous while enzyme catalysis is the catalysis of chemical reactions by specialized proteins called enzymes. The mechanism of enzyme catalysis is similar in principle to other types of chemical catalysis. However, enzymes are neither homogeneous nor heterogeneous catalysts (Cavani and Trifiro, 1994a).

1.2.1 Homogeneous Catalysis

Homogeneous catalysis is molecularly dispersed with the reactants in the same phase. This may take place either in the gas or liquid phase. Homogeneous catalysis allow for greater mixing and interaction with the reaction mixture. Another advantage of homogeneous catalysis is that the catalysts used are reproducible because they have a definite stoichiometry and structure. Although homogeneous catalysis provides easy access to the catalytic site but it can make the separation of catalyst and products difficult. Therefore, homogeneous reactions generally result in yield loss of the desired product. Furthermore, most of homogeneous catalysis are usually highly acidic (sulphuric acid) or base (sodium hydroxide), hence are highly corrosive to the reactor unit. Moreover, homogeneous catalysis may also represent a significant safety hazard in the case of fast and highly exothermic reaction, for example, reactions involving oxygen and hydrocarbons (Hutchenson et al., 2010).

Homogeneous catalysis is used in variety of industrial applications, as it allows for an increase in reaction rate without an increase in temperature. Example of homogeneous catalysis is the nitrogen oxide which catalyses the oxidation of sulphur dioxide. Another example is the catalytic carbonylation of methanol to acetic acid by $[Rh(CO)_2I_2]^-$ complexes in solution (Chorkendoff and Niemantsverdrient, 2003).

1.2.2 Heterogeneous Catalysis

Heterogeneous catalysis is a reaction where the catalyst used existed in a separate phase to the reactants with a distinct interface between them (Hartley, 1985). Typical examples of heterogeneous catalysis involve a solid catalyst with the reactants as either liquids or gases. This catalysis is the process whereby reactants adsorb onto the surface of a solid catalyst, are activated by chemical interaction with the catalyst surface, and transformed to adsorbed products rapidly and selectively, which desorbed from the catalyst surface (Figure 1.2). Usually catalyst used in heterogeneous catalysis is in solid state and can easily be separated and recycled from reactants and products. Thus the catalysts can be regenerated for several years before being replaced.

Examples of heterogeneous catalysis include the nickel in the manufacture of margarine, alumina and silica in the cracking of alkanes and platinum rhodium palladium in catalytic converters. In this research, the oxidation of *n*-butane to maleic anhydride with vanadyl pyrophosphate acting as a catalyst is a heterogeneous catalysis (Cavani and Trifiro, 2004).

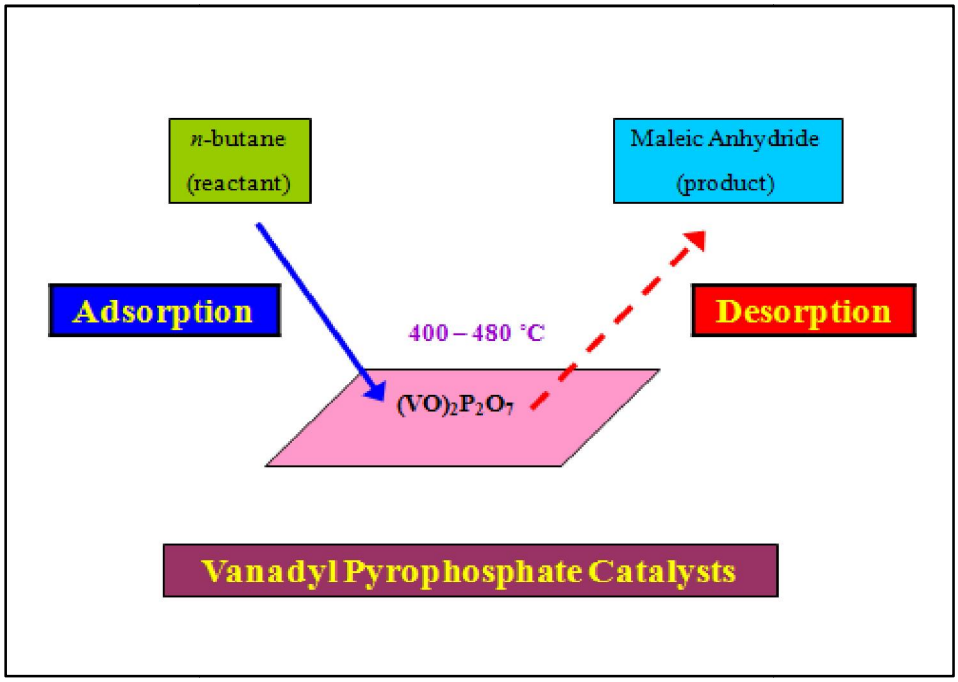

Figure 1.2: *n*-butane Oxidation to Maleic Anhydride

Table 1.1: Phases of Catalysts and Reactants used in Heterogeneous Catalysis

(Bond, 1987)

Catalyst	**Reactant**	**Example**
Liquid	Gas	Polymerization of alkenes catalysed by phosphoric acid.
Solid	Liquid	Decomposition of hydrogen peroxides catalysed by gold.
Solid	Gas	Ammonia synthesis catalysed by iron.
Solid	Liquid + Gas	Hydrogenation of nitrobenzene to aniline catalysed by palladium.

Generally, in heterogeneous reactions, we can divide the catalytic process in five main steps (Thomas and Thomas, 1997):

1. diffussion of reactants from the fluid into the catalyst support porous structure, reaching the internal surface
2. adsorption of reactants on the catalyst active sites
3. chemical reaction between the reactants
4. desorption of the reaction products from the active sites
5. diffussion of products through the catalyst support, reaching the external fluid

Different possible mechanisms for reactions on surfaces are known, depending how the adsorption takes place, based on Langmuir-Hinshelwood and Eley-Radical (Bond 1987). Frequently, the trasportation of reactants and products from one phase to another plays a dominant role in limiting the reaction rate (Ramaswamy, 2002).

1.3 Essential Properties of Good Catalysts

Generally, a commercially useful catalyst must possess three major desirable features: long life span, high activity, and reasonably good selectivity (Hartley, 1985). A good catalyst should capable to be regenerated a lot of times and should be able to sustain the desired ion over prolonged periods. The longer a catalyst can be regenerated, the lower the cost needed to carry out the reaction process.

Activity of a catalyst is defined as the rate which the chemical reaction reaches the equilibrium or a thermodynamic quantity that measure the effective concentration or intensity of a particular substance in a given chemical system (Sharp, 2003). Another definition of activity is the amount of reactants transformed into product per unit of time and unit of reactor volume. Higher activity gives rise of higher conversion of end products. Catalysts must have a reasonable activity per unit volume of reactor space and the cost of the catalyst per unit of product being produced should be low. This in turn implies a high turnover number (Hartley, 1985). Turnover Number (TON) is a measure of efficiency of a catalyst; the number of molecular conversions per molecule of catalyst (Sharp, 2003).

Selectivity of a catalyst is defined as the rate of reactant conversion into the desired products. If a catalyst does not exhibit high selectivity, the cost of separating the products will be prohibitive. Therefore, a good catalyst must fulfill the characteristic of high selectivity. Selectivity usually depends on reaction parameters such as temperature, pressure, reactants composition and also on the catalyst nature (Fadoni and Lucarelli, 1999). A catalyst must be able to effect the desired reaction at an acceptable rate under conditions of temperature and pressure that are practicable because the use of extreme conditions such as high temperature and pressure usually attain good yields but it proves to be very costly. Hence, it is essential to synthesis a catalyst that will operate under the mildest possible conditions. With minimized side reactions (Bond 1987; Cavani and Trifiro, 1994a).

1.4 Sustainable and Green Chemistry

The term “green chemistry”, also known as sustainable chemistry is a philosophy of chemicals and formulation of processes that minimize the use of hazardous substances to reduce the environment pollution. According to Sheldon (2000), “green chemistry” efficiently utilises raw materials, eliminates waste and avoids the use of toxic and/or hazardous reagents and solvents in the manufacture and application of chemical products.

Nowadays, industrial processes have moved towards more efficient use of resources and improvement in selectivity due to the facts that both aspects correspond to an improvement in the process economics. Example of this improved process is the synthesis of maleic anhydride where the starting material of this catalytic process had been substituted with butane instead of using benzene.

Butane is now adopted worldwide due to the following reasons (Taufiq-Yap et al., 2009):

i. Use of non-toxic reactants.
ii. Improved atom economy.
iii. Waste formation id minimized.
iv. Cheaper than benzene and also requires less costly safety equipment.
v. The molar yield starting from butane instead of benzene is lower, but the weight yield (the relevant industrial parameter) is higher.

vi. When a selective catalyst is available, reduction of process complexity means a reduction in both fixed costs and variable cost (utilities, labour, etc.).

vii. Gas-phase reactions reduce the costs of separation.

viii. The formation of by-products and waste, besides a loss in selectivity, also implies higher costs of separation.

1.5 Selective Oxidation of Light Hydrocarbons

The possibility of developing new lower environmental impact and lower cost processes has recently generated interest in the transformation of light alkanes to valuable oxygenated compounds and alkenes by selective oxidation due to the abundance and low cost of the light alkanes such as ethane, propane and butane (Centi, Cavini and Trifirò, 2001). The application of oxide-based catalysts includes selective oxidation, total oxidation, hydrogenation, dehydrogenation, and environmental applications.

Examples of catalytic oxidation of hydrocarbon and its desired products are as follows (Sheldon et al., 2007):

i. ortho-Xylene to phthalic anhydride on vanadium pentoxide / titanium catalyst.

ii. Propane to acrolein on bismuth molybdenum composite oxide catalyst.

iii. Ethene to ethene oxide silver based catalyst.

iv. Propene to acrylonitrile on iron antimony oxide catalyst.

v. Isobutene to methyl methacrylate on molydenum-bismuth with catalyst.

vi. *n*-butane to maleic anhydride with vanadium phosphorus oxide (VPO) as catalyst.

The oxidation of *n*-butane to maleic anhydride is the only industrial process of selective oxidation of paraffin and *n*-butane selective oxidation on vanadium phosphorus oxide catalyst is a much studied reaction in heterogeneous catalysis. Vanadyl pyrophosphate catalysts have been studied extensively for selective oxidation of *n*-butane to maleic anhydride (Asghar et al., 2010). Vanadyl pyrophosphate, $(VO)_2P_2O_7$ is known to be the active and selective catalyst phase of the *n*-butane oxidation to maleic anhydride. The use of highly active catalysts makes it possible to increase selectivity and conversion of *n*- butane to maleic anhydride.

1.6 Aim and Objectives

It is often observed that the selectivity and activity of catalyst are low by using dihydrate precursor ($VOPO_4 \cdot 2H_2O$) route. The high formation of by-products during the oxidation of *n*-butane to maleic anhydride using catalysts synthesised via dihydrate precursor is one of the problems encountered during the synthesis of VPO catalysts too. Thus, the aim of my research is to synthesise VPO catalysts with higher production of maleic anyhydride and least amount by-products.

The objectives of this study are set as follows:

i. To synthesise VPO catalysts via sesquihydrate precursor route using different drying methods, doped system and synthesis methods to improve activity and selectivity of the VPOs catalysts.
ii. To study the physico-chemical characteristics of the synthesised VPO catalysts.
iii. To study the catalytic performances of the synthesised VPO catalysts in the *n*-butane conversion to MA.

CHAPTER 2

LITERATURE REVIEW

2.1 Maleic Anhydride (MA)

Maleic anhydride ($C_4H_2O_3$) is chemically known as 2,5-furandione, also called as dihydro-2-5-dioxofuran, toxillic anhydride or cis-butenedioic anhydride (Felthouse et al., 2001). MA crystallizes as orthorhombic crystalline needles and is available from producers either as a molten liquid or as briquettes. Figure 2.1 shows the atomic structure of MA.

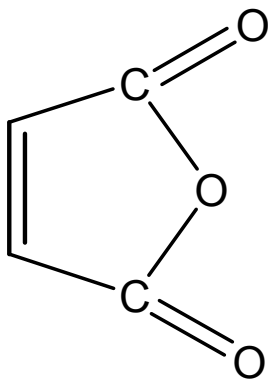

Figure 2.1: Atomic structure of maleic anhydride

Maleic anhydride (MA) was first produced 150 years ago by the dehydration of maleic acid and later on MA was produced by the vapour phase oxidation of

benzene or other aromatic compounds (Trivedi and Culbertson, 1982). However, since 1974, *n*-butane was successfully replaced as the feed for MA production where the reaction is carried out at 673 K in gas phase and vanadium phosphorus oxide (VPO) is used as catalyst.

Butane-based technology is the predominant area of research due to the reason that it produce maleic anhydride from butane, eight hydrogen atoms must be abstracted, three oxygen atoms inserted and a ring closure performed. Another reason is all of the commercial processes use the same catalyst and this catalyst selectively produces maleic anhydride from butane (Felthouse et al., 2001).

2.1.1 Oxidation of *n*-Butane to Maleic Anhydride

The oxidation of *n*-butane to maleic anhydride is the only industrial process of selective oxidation of paraffin and the vanadium phosphorus oxide catalyst is used. Oxidation of *n*-butane is also the only large-scale commercial partial oxidation process that uses low cost alkane as a direct feedstock. The main reaction of the oxidising *n*-butane to maleic anhydride is as below:

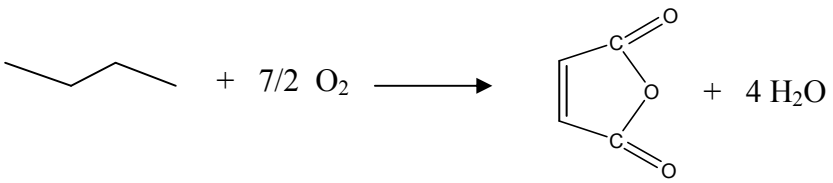

(2.1)

The reaction mechanisms of the oxidation of *n*-butane to maleic anhydride involves the stepwise abstraction of weight hydrogen atoms leading to the formation of four water molecules and the insertion of three oxygen atoms (Frey et al., 2010). As shown in Figure 2.2, *n*-butane undergoes oxidative dehydrogenation to form butane and causing the lost of two hydrogen molecules in the first step of chain reaction mechanism. Butane is then undergoes allylic oxidation to form butadiene with two more hydrogens lost during the reaction. Next, butadiene undergoes insertion of 1.4-oxygen to form 2,5-dihydrofuran which then further undergoes allylic H-abstraction to form furan. Lactone is formed when 2,5-dihydrofuran undergoes allylic oxidation. The oxidation of *n*-butane to maleic anhydride is completed when lactone and/or furan undergoes electrophilic oxygen to from maleic anhydride as the final product (Cavani and Trifiò, 1994a).

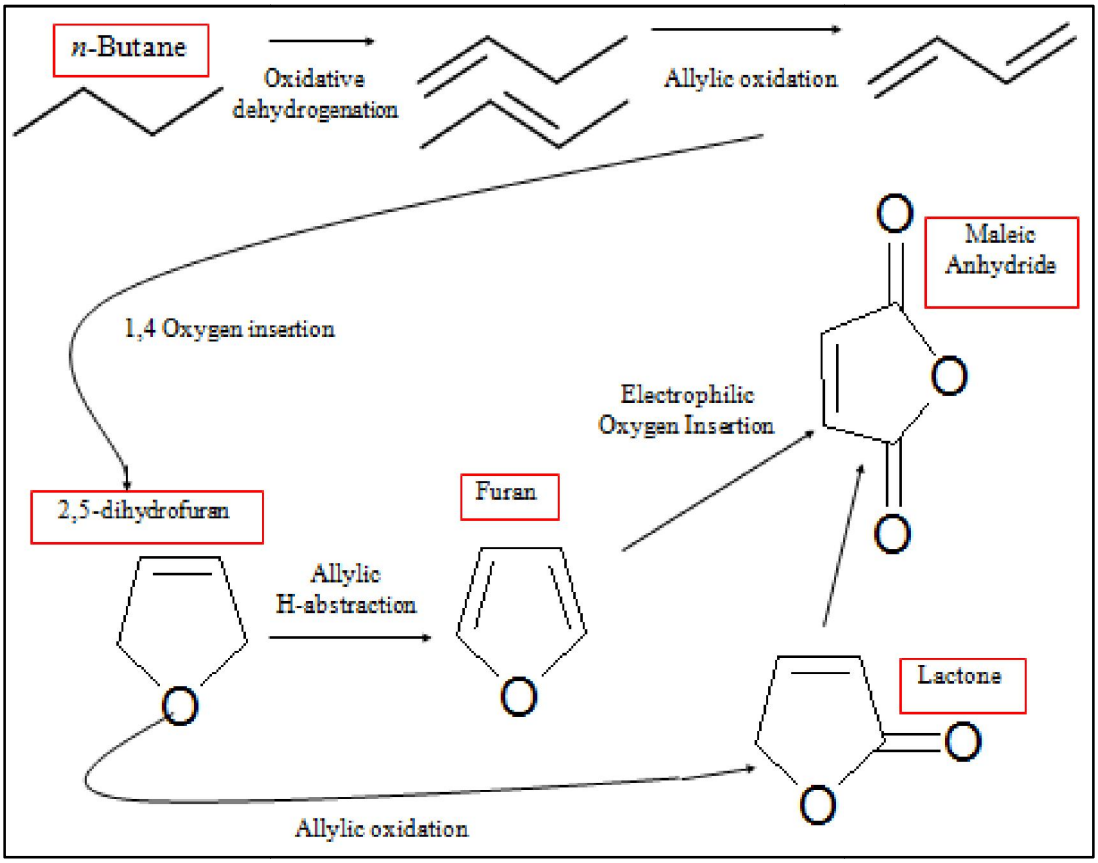

(Cavani and Trifirò, 1994b)

Figure 2.2: Mechanism of the oxidation of *n*-butane to maleic anhydride

2.1.2 World Consumption of Maleic Anhydride

Over half of total maleic anyhydride is used to produce unsaturated polyester resins. The reaction of maleic anhydride with phathalic anhydride with propylene glycol yields a commodity unsaturated polyester resin which is usually dissolved in styrene for use in reinforced compounds, artificial marble, *etc*. Other applications for MA are in the production of lube oil additives, alkyd resins, fumaric acid, assorted copolymers used for thickeners and dispersants (Figure 2.3). Global production of MA in 1995 was estimated at 1.8 billion pounds, with estimated value of $700 million. In 2010, approximately 52% of all maleic anhydride consumed was for the production of unsaturated polyester resins. Demand for unsaturated polyester resins is affected by the health of the construction industry and overall state of the economy. Figure 2.4 shows the world consumption of MA in year 2011. Recent report from Transparency Market Research which observes that global maleic anhydride demand was worth USD 4.11 billion in 2012 and is expected to reach USD 5.96 billion by 2018, growing at a CAGR of 6.4% from 2012 to 2018. Global volumes are expected to reach 2,752.4 kilo tons by 2018 (Maleic anhydride market for unsaturated polyester resins 2013). The developing regions will experience the highest growth in maleic anhydride for unsaturated polyester resin production since considerable amount of unsaturated polyester resin goes into infrastructure, construction, automotive, and marine industries. The global market for maleic anhydride is highly fragmented with top seven companies accounting for

approximately 30% of the total market. Huntsman Corporation, Lanxess AG, Polynt SpA, Flint Hills Resources, Ashland Chemical Co, DSM N.V., Nippon Shokubai Co Ltd and others are some of the major manufacturers of maleic anhydride.

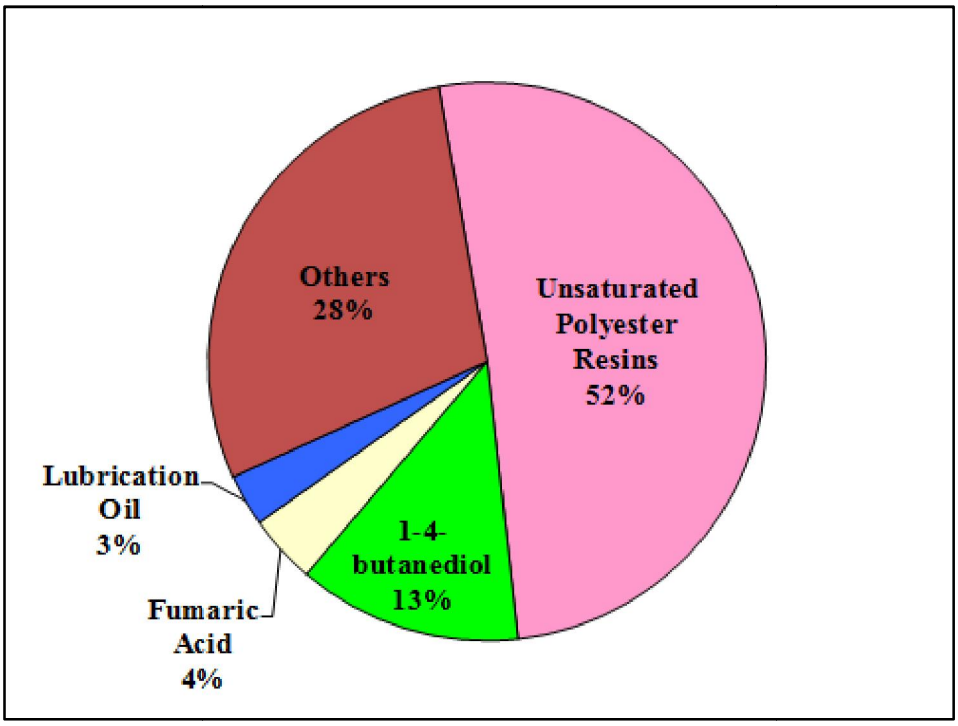

(Funada and Griner, 2011)

Figure 2.3: Uses of maleic anhydride as reported in 2011

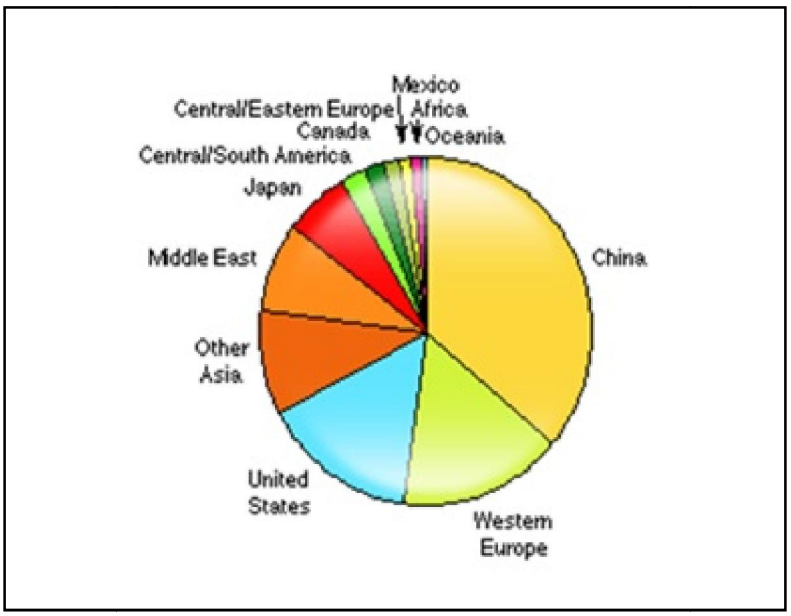

(Funada and Griner, 2011)

Figure 2.4: World consumption of MA in 2011

2.1.3 Reactor Technologies for the Production of MA

Industrially, there are three different ways to produce MA from *n*-butane which are fixed-bed, fluidised bed, and transported bed technologies. However, transported bed technology plant applied by DuPont has been shut down (Cavani and Trifirò, 2004). All these three technologies are differing in terms of:

i. Type of reactor (fixed, fluid or transported bed);
ii. Recovery method of crude MA (anhydrous or aqueous);
iii. Gas phase composition (from 1.8 % of *n*-butane in air in the case of fixed bed, to 5 % in fluidised bed);
iv. Employed catalyst (synthesis, activation step, presence of promoters and regeneration).

Table 2.1 below shows the comparison between the possible processes of MA production technologies:

Table 2.1: Industrial technologies for maleic anhydride production from *n*-butane

Process	Type of reactor	Recovery method
ALMA (Lonzagroup, Lummus)	Fixed-bed	Anhydrous
Lonzagroup	Fixed-bed	Anhydrous or Aqueous
Mitsubishi Chemicals	Fixed-bed	Anhydrous
Monsanto	Fixed-bed	Anhydrous

Denka Scientific Design	Fixed-bed	Anhydrous
DuPont	Transported-bed	Anhydrous
BP (Sohio) - UCB	Fixed-bed	Anhydrous

(Centi and Trifirò, 2001)

Figure 2.5 showed the fixed-bed technology used at industry level with fixed-bed condition of 673 – 723 K, space velocity: 1100 – 2600 h^{-1}, 1-2 bar, and 1-2.5 % *n*-butane in air. Multi-tubular reactors are used for the partial oxidation of *n*-butane due to its highly exothermic reactions. A cooling media is employed in this reactor in order to cool the reactor as a hotspots might destroy the catalyst and detrimental the reactor performance. Molten salt or oil is used to remain the temperature of reaction zone within the desired range. The long residence times with conditions above the explosive limit can be avoided by feeding *n*-butane and air separately (Mota et al., 2000).

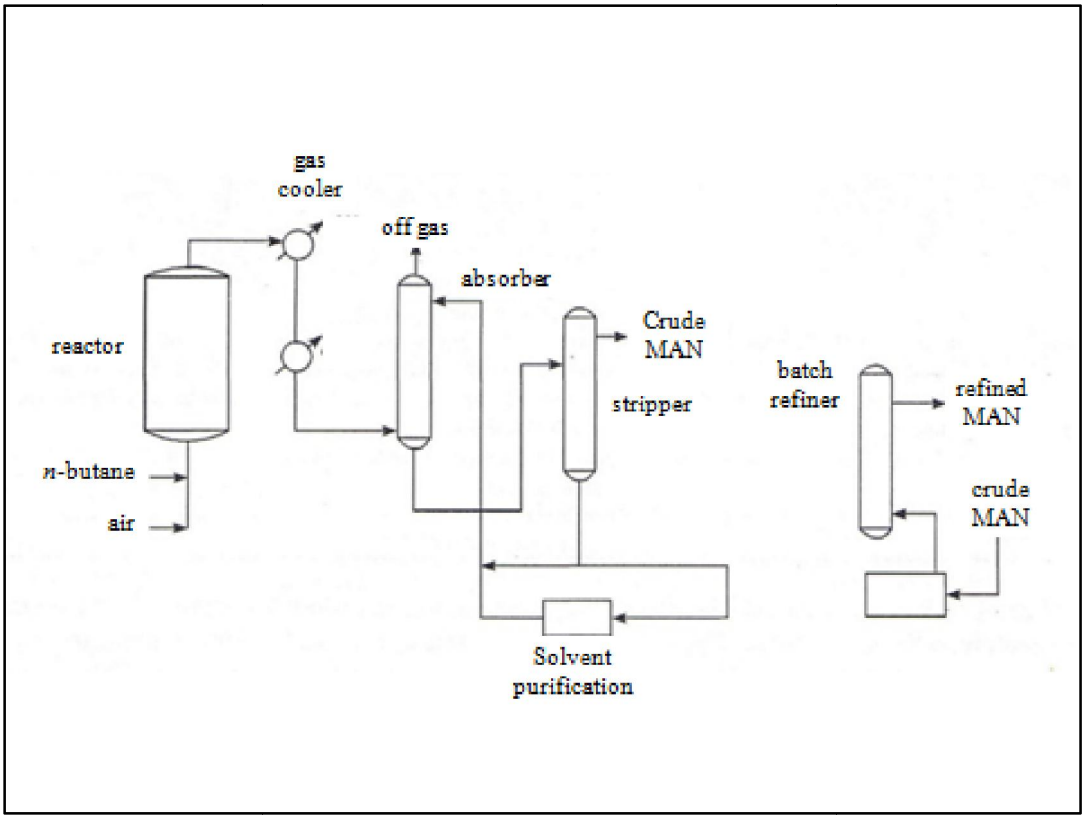

(Felthouse et al., 2000)

Figure 2.5: Fixed-bed reactor

Hutchenson et al. (2010) proposed a study on DuPont circulating fluidised bed (CFB) technology to produce maleic anyhydride from *n*-butane with a proprietary vanadyl pyrophosphate catalyst. CFB reactor operating conditions fall within the flammability envelope of the reactant and products to maximise reactor productivity, which is possible since the solids phase tends to suppress non-selective homogeneous reactions (combustion); while at the same time promoting the desired selective catalytic reactions.

Figure 2.6 shows the commercial CFB facility consisting of a transport bed operating in the turbulent fluidisation regime (fast bed), a riser, a stripper, and a regenerator. Catalyst entered the base of the fast bed through a tapered standpipe and was transported upwards to the riser. The gas-powder mixture will then exited the riser and entered the stripper tangentially, which provided a sufficiently high level of separation to avoid overloading of the cyclone.

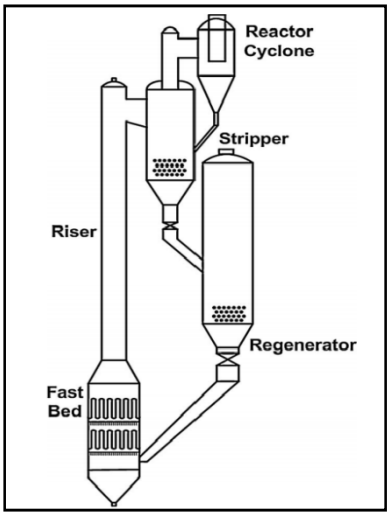

(Hutchenson et al., 2010)

Figure 2.6 : Circulating fluidised-bed reactor

2.2 Vanadyl Pyrophosphate Catalyst $(VO)_2P_2O_7$

Vanadium-phosphorus oxides represent a class of redox catalysts of high commercial significance due to their ability to induce selective oxidation of alkanes; especially for the synthesis of maleic anhydride (Upadhyaya and Samant, 2013). It is widely assumed that vanadyl pyrophosphate, $(VO)_2P_2O_7$ is the main component of VPO catalysts which overcome the defect sites (amorphous and crystalline) phases (Frey et al., 2010). Thus, vanadyl pyrophosphate $(VO)_2P_2O_7$ is known as the active site of the catalyst for the oxidation of *n*-butane to maleic anhydride.

Vanadyl pyrophosphate $(VO)_2P_2O_7$ is transformed from $VOHPO_4 \cdot 0.5H_2O$ in an *n*-butane/air gas mixture at about 673 K for an extended time period. This resultant catalyst consists of a complex mixture of vanadium phosphorus oxide phases such as α-, β-, γ-$VOPO_4$, $VOHPO_4 \cdot 4H_2O$, $VOHPO_4 \cdot 0.5H_2O$, $VO(PO_3)_2$ and β-, γ- $(VO)_2P_2O_7$ (Centi et al., 1988; Borders, 1987). The use of highly active

catalysts makes it possible to increase selectivity and conversion of *n*-butane to maleic anhydride. These combination of $VOPO_4$ (V^{5+} phases) and $(VO)_2P_2O_7$ (V^{4+} phase) indicate good activity and selectivity of VPO catalyst.

The catalyst $(VO)_2P_2O_7$ is special in executing the mechanism in the oxidation of *n*-butane to maleic anhydride. Vanadyl pyrophosphate consists of the ability to carry out the first step, which is the activation of *n*-butane, with high selectivity. Other catalysts such as phosphate catalyst or molybdenum oxide catalyst only show to be active and selective to the oxidation of butenes and butadiene to MA but not selective to *n*-butane. Another essential feature of $(VO)_2P_2O_7$ catalyst is that the rate of dehydrogenation is higher than the rate of oxygen insertion into butenes. This is important in achieving high selectivity (Cavani and Trifiro, 1994a).

According to Hutchings (1991), vanadyl pyrophosphate, $(VO)_2P_2O_7$ has a layered structure in which two octahedral pairs share edges (Figure 2.7). The octahedral pairs are connected by PO_4 tetrahedra which gives a layer structure in a (0 2 0) plane while double vanadyl chains are present in perpendicular to the (0 2 0) plane.

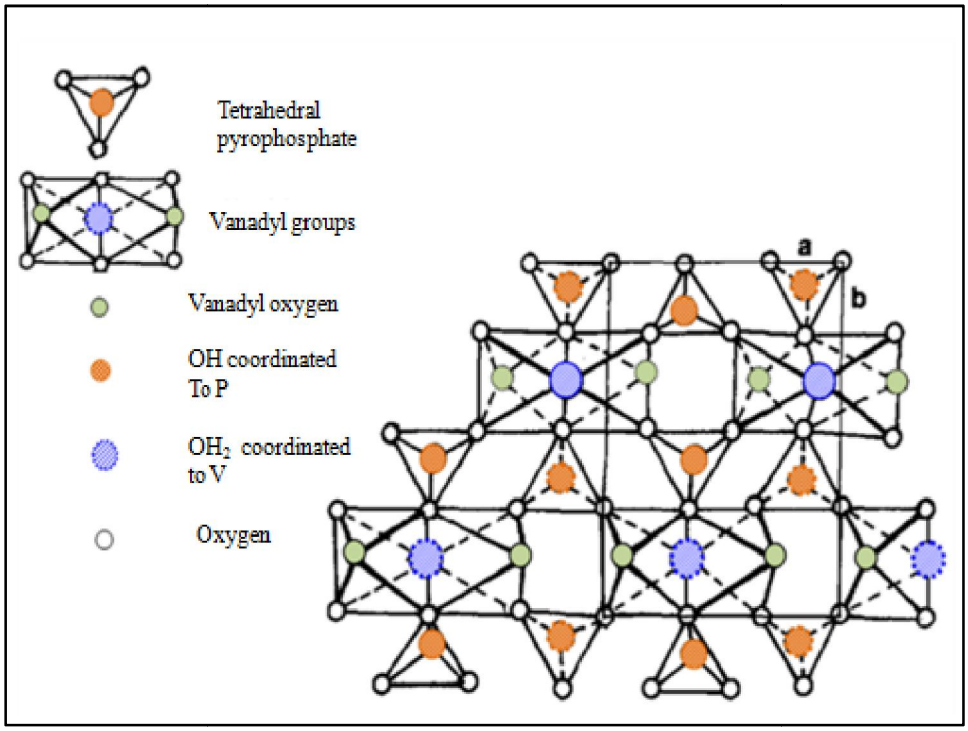

(Borders, 1987)

Figure 2.7: Idealised structure of (0 0 1) plane of $VOHPO_4 \cdot 0.5H_2O$

Previous study had showed that the defects in the (1 0 0) plane of $(VO)_2P_2O_7$ (Figure 2.8) plays an important role in the selective oxidation of *n*-butane (Bordes, 1987). The best performance of $(VO)_2P_2O_7$ is directly related to the presence and extent of exposed (0 2 0) facets, which is related to the (0 0 1) facet of $VOHPO_4 \cdot 0.5H_2O$ (O'Mahony et al., 2005). As illustrated in Figure 2.9, Misono (2002) has proposed that the (1 0 0) basal plane of $(VO)_2P_2O_7$ is active for selective oxidation where V-O-V pair sites are located and that the side planes are non-selective.

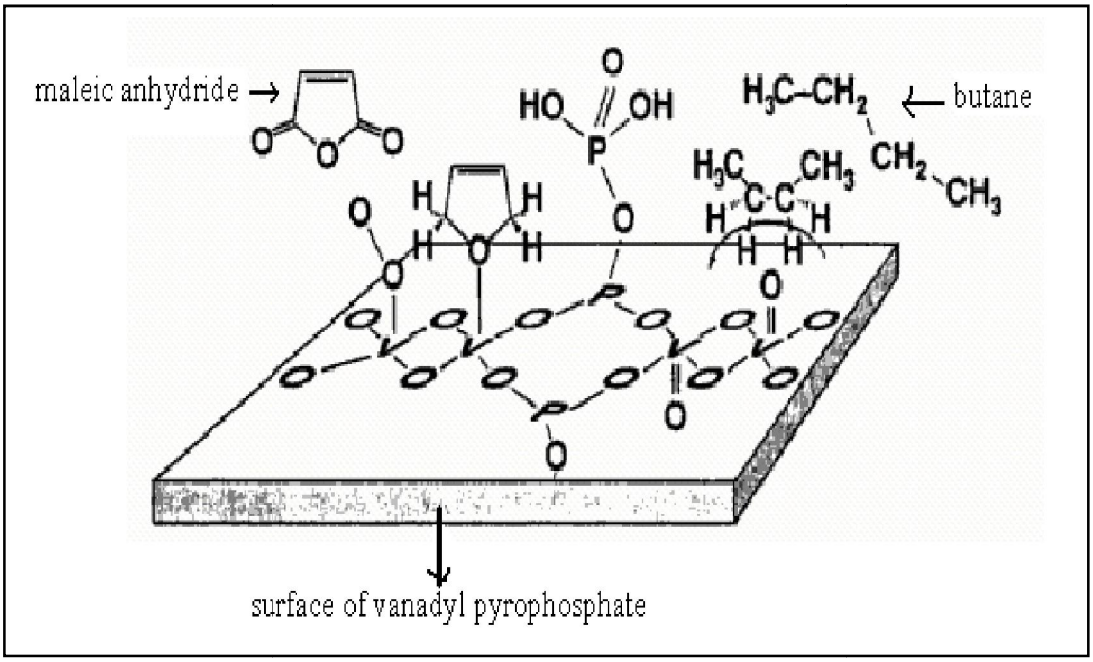

Figure 2.8: The oxidation of butane to maleic anhydride on the surface of vanadyl pyrophosphate perpendicular to (1 0 0)

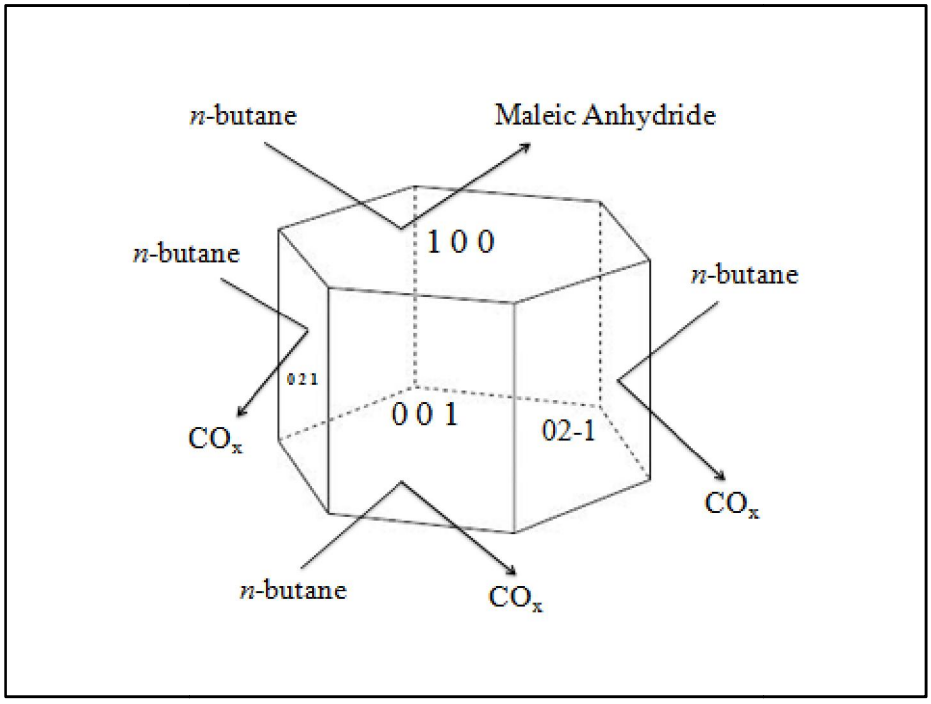

(Misono, 2002)

Figure 2.9: Selective and unselective oxidation site on crystal faces of $(VO)_2P_2O_7$

2.2.1 Parameters that Affect the Performance of Vanadium Phosphorus Oxide Catalyst

The parameters which will affect the characteristic and performance of the $(VO)_2P_2O_7$ catalyst include:

i. Type of reducing agent or precursor;
ii. Phosphorus-to-vanadium (P/V) ratio;
iii. Addition of promoters;
iv. Application of support system;
v. Effect of calcinations conditions: temperature (T), duration (D), and environment (E).
vi. Effect of microwave irradiation

2.2.2 Parameter: Preparation of Precursor

VPO catalysts can be prepared via different routes. In general, V_2O_5 is used as a source of vanadium, and H_3PO_4 is used as a source of phosphorus. Different reducing agents which result in different kind of precursors can be used and the precursors will transform to vanadyl pyrophosphate catalyst after calcination process at high temperature. Védrine et al. (2013) proposed that by controlling the morphology of the precursor, we can control the morphology of the final catalyst, which is why the preparation of precursor is important to produced high performances catalyst. The methods for preparation of the catalyst precursor can be classified into few methods *i.e.* aqueous, organic, dihydrate, and hemihydrates. An alternative route via vanadyl

hydrogen phosphate sesquihydrate precursor was developed by reducing the $VOPO_4.2H_2O$ in 1-butanol (Ishimura et al., 2000; Taufiq-Yap et al., 2004).

Equations below showed the summary of preparation routes for VPO, VPA, and VPD catalysts (Védrine et al., 2013):

VPA Route

$$V_2O_5 + HCl \xrightarrow[H_3PO_4]{\Delta_1\ 2\ h} VOHPO_4{\cdot}0.5H_2O \qquad (2.2)$$

VPO Route

$$V_2O_5 + H_3PO_4 + alcohol \xrightarrow{\Delta_1\ 16\ h} VOHPO_4{\cdot}0.5H_2O \qquad (2.3)$$

VPD Route

$$V_2O_5 + H_3PO_4 \xrightarrow[\Delta_1\ 16\ h]{H_2O} VOPO_4{\cdot}2H_2O \xrightarrow[\Delta_1\ 16\ h]{alcohol} VOHPO_4{\cdot}0.5H_2O \qquad (2.4)$$

i. Aqueous method, VPA

The aqueous method, VPA was used in early research and was the originally the preparation method for VPO catalyst. VPA method uses water as the solvent and used V_2O_5 as a source of vanadium while H_3PO_4 is used as source of phosphorus. A reducing agent is required to synthesis the V^{4+} precursor phase. In aqueous medium, V_2O_5 is reduced by a mineral agent such as hydrochloric acid, followed by addition of the phosphorus component, usually as 85 % *ortho*-H_3PO_4. The precursor prepared is more crystalline and was isolated by evaporation of the solvent. The presence of traces of chlroride in the aqueous medium cause difficulty in industrial

production, as it is corrosive to reactors. Significant amounts of an impurity $VO(H_2PO_4)_2$ was also obtained (Hutchings, 2004). When vanadium phosphorous oxide (VPO) catalyst is prepared via aqueous medium, the final catalyst tends to have low surface area where the catalyst activity is directly proportional to surface area. Therefore, these catalysts exhibit poor performance for butane oxidation.

ii. **Organic method, VPO**

In organic method, both acid and water needed in the aqueous method were substitutes with organic solvents in order to overcome the major disadvantage of the VPA method mentioned above. In organic medium, the reduction of V_2O_5 particles are first suspended in the medium by strong agitation, then vanadium with H_3PO_4 emulsified in alcohol is added to the medium reaction and the precipitates are isolated by filtration after cooling (Hodnett, 2000). By using the organic medium in the preparation of catalyst, there are possibilities of obtaining high value of surface area, reducibility, and mobility of oxygen species (Taufiq-Yap et al., 2001).

iii. **Dihydrate method, VPD**

Dihydrate precursor, $VOPO_4 \cdot 2H_2O$, method was first proposed by Johnson et al. (1984) and further described by Ellison et al. (1994). In 1997, Hutchings and Higgins have shown that a very active catalyst can be prepared via two-stage synthesis method via VPD route. In the first stage, the reaction of V_2O_5 with *ortho*-H_3PO_4 and water will leads to the formation of the V^{5+} dihydrate phase $VOPO_4 \cdot 2H_2O$ (Hutchings, 2004). The dihydrate mixture is recovered

and dried then refluxed with alcohol to form hemihydrate. The alcohol in second stage reflux reduced the $VOPO_4 \cdot 2H_2O$ to $VOHPO_4 \cdot 0.5H_2O$ and produce catalyst precursor with better surface morphology. Dihydrate method can give the $(VO)_2P_2O_7$ phase with the highest surface platelet morphology exposing preferentially the (1 0 0) active plane for maleic anhydride formation (Hutchings et al., 1997). Therefore, catalyst produced will lead to improvement in activity of *n*-butane conversion due to the large amount of active oxygen species removed from the catalyst especially those linked to the V^{4+} phase (Taufiq-Yap et al., 2009).

iv. **Hemihydrate method, VHP**

Hemihydrates precursor ($VOHPO_4 \cdot 0.5H_2O$) prepared via aqueous medium or organic medium used the same reactants, but different reducing agents. In 2001, Felthouse et al. proposed that the most effective catalyst, vanadium phosphorus oxide, is produced during the pyrolysis of vanadyl (IV) hydrogen phosphate hemihydrates (VHP). In organic hemihydrates method, the precursor forms by the reaction of V_2O_5 with H_3PO_4 in benzyl alcohol or isobutanol (Cavani and Trifirò, 1994a). As mentioned above, catalysts prepared in an organic medium will show a higher specific reactivity. This happens to the catalyst prepared via hemihydrates precursor as well where the catalysts show a higher activity due to the higher surface area and higher density of active sites. Due to this reason, almost all the industrial preparations are done by the organic route to improve the catalyst in activity and selectivity.

v. **Sesquihydrate method, VPOs**

The sesquihydrate precursor is obtained by reducing $VOPO_4 \cdot 2H_2O$ in 1-butanol, which is more environmental friendly reducing agent (Matsuura et al., 1995). Among all the preparation methods, $VOHPO_4 \cdot 0.5H_2O$ is particularly important since the precursor of the $(VO)_2P2O_7$ phase observed in the final activated catalyst (O'Mahony et al., 2004). The layer structure of sesquihydrate with wide spacing capable of intercalating additives appears of benefits for preparing improved catalysts (Leong et al., 2011). After calcinations, the catalyst prepared via sesquihydrate route showed a high specific activity in selective oxidation of *n*-butane to maleic anhydride (Taufiq-Yap et al., 2004).

2.2.3 Parameter: P/V Atomic Ratio

Ruiz et al. (1993) proposed that P/V ratio to be an important factor in determining the activity and selectivity of the catalyst. The optimal composition of P/V ratio will present a slight excess of phosphorus with respect to the stoichiometric value of the precursor (Horowitz et al., 1988). A slight excess of catalyst phosphorus (P/V atomic ratio =1.1) was found to stabilise a $(VO)_2P_2O_7$ phase which was active and selective in *n*-butane oxidation; a larger excess of phosphorus was found to enhance the selectivity of $(VO)_2P_2O_7$ phase at the expense of catalyst activity (Nakamura et al., 1974; Hodnett et al., 1983, Robert and Glenn, 1986).

In 1983, Hodnett et al. proposed that low P/V ratio (< 1) will causes the catalyst to be very poor in selectivity but high in activity. Gopal and Calvo (1972) reported that low P/V ratios will favour the formation of β-VPO_5 with average oxidation state of vanadium close to +5. The average vanadium (AV) value of catalyst could be assumed as a consequence of the stabilizing effect of excess phosphorus which controls the mobility of oxygen anions via the lattice. In other words, the slight defect of phosphorus (P/V = 0.95) will produced catalyst which favoured selectivity but less activity.

2.2.4 Parameter: Addition of Promoters

One of the key areas of study in VPO catalysts is the promotion effect of metal compounds, named dopants or promoters. A promoter defined as a material added in a small amount to the catalyst during; in itself it is of low activity or inactivity, but in the reaction it enhances the activity, stability or selectivity of the active component (Bartholomew and Farrauto, 2006).

Several studies have been published concerning the synthesis of VPO precursors as well as the role that promoters can play in improving catalytic performance. A wide range of cations have been added to vanadium phosphate catalysts beneficial effects have been reported. For example, Hutchings and Higgins (1996) findings showed that Zr, Zn, and Cr could be used as structure promoters and Fe, Cs, and Ag showed a decrease in the specific activity. The addition of promoters were considered to act in two ways; namely structural effects due to an enhancement

in the surface area of the activated catalysts and electronic which has been demonstrated in very few systems to date (Sartoni et al., 2004).

In general, there is an ideal concentration of the promoter at which its favourable effect reaches a maximum, this latter being observed within a narrow range of promoter concentration only. For instance, the addition of low levels of Mo (Hutching et al., 1996) is found to enhance both selectivity and activity whereas the addition of low levels of Co affects mainly the activity (Abdelouahab et al., 1995; Mota et al., 2000). Due to the reason that the considerably increased activity, smaller amounts of the expensive active component are necessary, hence the catalyst becomes more economic. In the presence of promoters, the activation energy of the catalysed reaction decreases in which the adsorption is stronger and the amount of material adsorbed is greater (Bartholomew and Farrauto, 2006).

The addition of first row transition metals to VPO catalyst is claimed to produce an improvement in the activity of the catalyst. The replacement of V^{4+} phase by the promoter cation is said to introduce defects into the structure as well as influencing the oxidation of the surface. Both of these effects may be important to the promotion of VPO catalyst performances. Hence, it is an interplay of structural and electronic factors that is important (Hutchings, 2001). Therefore, the way which the promoters are introduced is important.

In previous publications, Kourtakis et al. (2010) proposed a method in which promoter cations are incorporated into the precursors by cation substitution into the VPO lattice during its synthesis. During the activation through calcination, the

promoter cations migrate into the bulk of the catalyst in varying degrees to form new microstructures which showed improvements in catalystic performance. Promoter compounds can be added either together with the vanadium and phosphorus compounds prior to preparation of the catalyst precursor; or by impregnation of the catalyst precursor prior to formation of the final catalyst by heat treatment (Hutchings, 1991).

There has been very little interest shown in doping by group 13 cations even though gallium, Ga has been shown to be effective as a catalyst component in the activation of methane. However, Sartoni et al. (2004) have shown that Ga can act as a promoter for vanadium phosphate catalysts and made a detailed study of the structure of Ga-doped and found that Ga acts as both a structural and an electronic promoter.

In Sartoni et al. (2004) studies, low Ga-doped of catalyst has been synthesised by via VPO route with different Ga salts and Gallium(III) Acetylacetonate, $Ga(acac)_3$ derived catalytic material gave a significant increase in surface area and enhanced activity as compared to that from Ga_2O_3 and $GaPO_4$. A series of catalysts had been tested in the study include 0.1 %-1.5 % of Ga-doped catalysts prepared using Ga(acac)3 and 0.1 % mol of Ga produced using Ga(acac)3 shown to have the best activity , with 73 % *n*-Butane conversion (Sartoni et al. 2004). It is believed that further modification of Ga-doped VPO catalyst could improves overall performances of catalyst.

2.2.5 Parameter: Application of Support System

Another parameter that could improve the performance of VPO catalyst is through employment of support system in the catalyst. Catalyst support is viewed as the skeletal and binding materials of the active component whereas this active component is either applied onto the support surface by impregnation, or the support, too, is formed during preparation of the catalyst. Support system has a critical impact on the catalyst activity, selectivity, and recycle rate of catalyst. Unlike promoters, most supports do not directly enhance the catalytic activity. In fact, catalyst supports are porous, high surface area metal oxides or carbon having significant pore volume and capacity for preparing and preserving stable, well-dispersed catalytic phases during reaction.

Alumina support, γ-Al_2O_3, has moderately high surface, thermal stability over a wide range of temperature relevant to catalytic process (up to 90 °C), and its ability to be moulded into mechanically stable pellets are among the reason why alumina is widely used as catalyst support. Al-MCM-41 supported VPO catalysts were produced by Nie et al. (2001; 2003) which the supported VPO catalysts exhibited a remarkable enhancement in MA selectivity with slight decrease in *n*-butane conversion. The decrement of activity of this supported VPO catalysts might due to the unique interaction involved.

Previously, study shows the use of heat-conducting supports (β-SiC) gave rise of significant improvements in *n*-butane oxidation (Ledoux et al., 2000). The active

phase of β-SiC-supported catalyst has shown to improve in MA yield when used in a fixed-bed reactor due to the better control of the catalyst surface temperature. Furthermore, the chemical inertness of the support did not show to modify the reactivity properties of precursor and active phase.

2.2.6 Parameter: Effect of calcinations condition

Calcination is a process which involves high-temperature in air at which its purpose is to decompose and volatilize the catalyst precursors into final catalyst. It has been known that the temperature, duration, and atmosphere of calcinations treatment can affect the transformation of precursor to active phase (Taufiq-Yap et al., 2001). Calcination temperature generally is not set on high value due to the reason that sintering effect will occur at high temperature.

Ma et al. (2012) reported that prepared catalyst, when calcined at high temperature (especially above 1123 K), agglomeration occurred which result in drastically decrease of surface area and pore volume. He also proposed that the particles size of catalyst would remain stable at low temperature but would increase at high temperature, causing the catalyst to become bulkier in crystallite size. In short, high temperature of calcination will leads to sintering effect and cause the deactivation of surface area and pore structure decrease (Ma et al., 2012). However, if the catalyst is calcined at temperature lower than 573 K, the precursor will fail to transform to the active phase $(VO)_2P_2O_7$. Therefore, the VPO catalyst is in optimum working condition after calcinations in at 673 – 753 K range.

The duration of calcinations is another condition that will affect the formation of catalyst. Longer duration of calcinations process will leads to the increasing total surface area of catalyst due to the reason that the morphology of catalyst (rosette shaped for VPO catalyst) clusters will become more cracked and rougher during the long period of calcinations treatment. The increase in the surface area leads to the increase in the number of platelets that form the rosette structure in VPO catalyst (Taufiq-Yap et al., 2001). Hence, long period time of calcinations duration indirectly improve the activity of conversion of *n*-butane to MA.

Previous studies have shown that the calcinations atmospheres can affect the catalyst's morphology, activity, and selectivity in *n*-butane oxidation. In order to maintain the active phase (V^{4+}) VPO catalyst, the reducing property of *n*-butane is needed and the non-reactive environment using inert gases (N_2/CO_2) to prevent oxidisation. However, this non-reactive environment required high temperature during calcinations causing sintering phenomenon. Therefore, the calcinations atmosphere of VPO catalyst has been set at 0.75 % *n*-butane in air, where the explosive limit (~1.75 %) is not reached (Cheng and Wang 1997). Wu et al. (2004) previous studies reported that calcinations atmosphere has been found to have significant effects on the photocatalytic activity of titanium oxide (TiO_2) catalyst and the calcinations in either inert gas hydrogen or vacuum results in a high defect density and low surface coverage resulting a low activity in the catalyst prepared.

2.2.1 Parameter: Effect of microwave irradiation

Nowadays, the use of microwave energy to directly heat chemical reactions has become an increasingly popular technique in the scientific community (Ravichandran and Karthikeyan, 2011). The influence of microwave heating on solid catalyst systems has been studied intensively in recent years and there have been numerous reports indicating the increase in the rate of chemical reactions and product selectivity when microwave radiation is used during catalyst preparation step (Conde et al., 2001 and Rownaghi, 2009).

Microwave irradiation is believed to offer substantial benefits in the synthesis of heterogeneous catalysts by increasing the catalyst activity. The microwave coupling dielectric heating effect lies in the capacity of an electric field to polarize charges in the material. The other substantial advantages offered by microwave irradiation are (i) significant reduction in catalyst synthesis costs due to shorter processing time and (ii) improved catalytic properties of synthesized catalysts (Rownaghi et al., 2009b). It is believed that the microwave irradiation shows effect on the structural morphology of VPO catalyst when used in synthesis and drying of catalyst precursors.

Previous studies reported the XRD patterns of VPO catalysts prepared via $VOPO_4 \cdot 2H_2O$ with microwave irradiation method used in synthesis appears to be different from that of the conventionally prepared catalyst (Taufiq-Yap et al., 2007; Rownaghi et al., 2009a). The yield of maleic anyhydride was reported to significantly increase from 21.3% for conventional catalyst to 37.9% for the synthesis with microwave irradiation (Rownaghi et al., 2010). The microwave irradiation synthesis method represents a simple, efficient, and low-cost technique

for the synthesis of VPO catalyst with improved catalytic performance in selective oxidation of *n*-butane.

Microwave irradiation, too, shows to affect the morphology and catalytic performances of catalysts when employed in drying process (Rownaghi et al., 2009b). The microwave energy has been widely used in materials synthesis and chemical reactions due to its advantages of rapid volumetric heating and dramatic increase in reaction rates. Microwave-promoted technique has shown to provide a better performance than conventional heating dried by microwave heating materials such as solvents and reagents can absorb microwave energy and convert it to heat which leads to an increased heating rate and efficient drying.

CHAPTER 3

MATERIALS AND METHODOLOGY

3.1 Materials and Gases used in Synthesis

Below are the chemicals and gas used throughout the synthesis:

Table 3.1: Gases and materials for preparation of vanadyl pyrophosphate catalysts

Materials/ Gas	Brand	Purity
Vanadium (V) pentoxide, V_2O_5	Merck	99 %
ortho-Phosphoric acid, *o*-H_3PO_4	Merck	85 %
1-Butanol, $CH_3(CH_2)_3OH$	Merck	99.5 %
Gallium(III) Acetylacetonate, $Ga(C_5H_7O_2)_3$	Aldrich	99.99 %
0.75 % *n*-butane in air	Malaysia Oxygen Berhad (MOX)	0.75 %

3.2 Methodology

The production of vanadyl pyrophosphate catalyst has been developed via vanadyl hydrogen phosphate sesquihydrate precursor, $VOHPO_4 \cdot 1.5H_2O$ (Matsuura, 1995). In this research, sesquihyrate route was employed due to the usage of more environmental friendly reducing agent (1-butanol), microwave irradiation and dopant - Gallium(III) Acetylacetonate, $Ga(C_5H_7O_2)_3$ were used in modifying of the VPOs catalysts with the expectation to increase the conversion rate of *n*-butane to maleic anhydride and to reduce the formation of by-products. The synthesis methods of VPOs catalyst in this research are based on the concept of previous studies by L.K.

Leong et al., (2012), Rownaghi et al., (2009c), Taufiq-Yap et al., (2004), and Taufiq-Yap et al., (2007). By using their researches as references, a series of try-and-error experiments on the microwave irradiation duration were carried out to obtain the optimal synthesis methods. The optimal duration obtained was further used in preparation of VPOs catalysts in all three series. At least 3 repetition of experimental set were prepared for every sample for more accurate analysis.

3.2.1 Series 1: Preparation of Bulk Catalysts

The synthesis of sesquihydrate precursor has been divided into a two-step procedure, which involving vanadyl phosphate dihydrate, $VOPO_4 \cdot 2H_2O$ as an intermediate before obtaining the precursor.

In Stage 1, Vanadium (V) oxide, V_2O_5 (15.0 g from Merck), was suspended with continuous stirring into a mixture of *ortho*-phosphoric acid, *o*-H_3PO_4 (90 ml, 85% from Merck) and distilled water (360 mL). This mixture was stirred and refluxed at 393 K for 24 h. The mixture was cooled to room temperature and the resulting yellow solid ($VOPO_4 \cdot 2H_2O$) was recovered by centrifugation. The resulting yellow solid was then divided into two parts. One part was dried by microwave irradiation method for 15 mins. The drying conditions were set at 2450 MHz and an output power of 300 W. The second part was oven-dried at 358 K for 72 h. The resulting yellow solids were shown to be $VOPO_4 \cdot 2H_2O$.

In Stage 2, both $VOPO_4 \cdot 2H_2O$ (10.0 g, 50.5 mmol) dried by microwave irradiation and conventional oven-dried were refluxed for 21 h with 1-butanol (233 ml from Merck). The resulting whitish blue solids was recovered by centrifugation and washed sparingly with a small amount of acetone. The resulting whitish blue solids were then divided into two parts. One part was dried by microwave irradiation method for 15 mins. The drying conditions were set at 2450MHz and an output power of 300W. The second part was oven-dried at 358 K for 72 h. The precursors obtained were then calcined in a reaction flow of 0.75% *n*-butane in air mixtures at 733 K for 18 h to generate the active catalysts, $(VO)_2P_2O_7$.

The activated catalysts were denoted as VPOs-MM, VPOs-MO, VPOs-OM, and VPOs-OO. The following are the applied drying processes during the synthesis of the catalysts:

VPOs-MM : catalyst dried by microwave irradiation on both stages.

VPOs-MO : catalyst dried via microwave irradiation in Stage 1 and conventional oven-dried in Stage 2.

VPOs-OM : catalyst prepared via conventional oven drying in Stage 1 and microwave drying in Stage 2.

VPOs-OO : catalyst dried using conventional oven on both stages

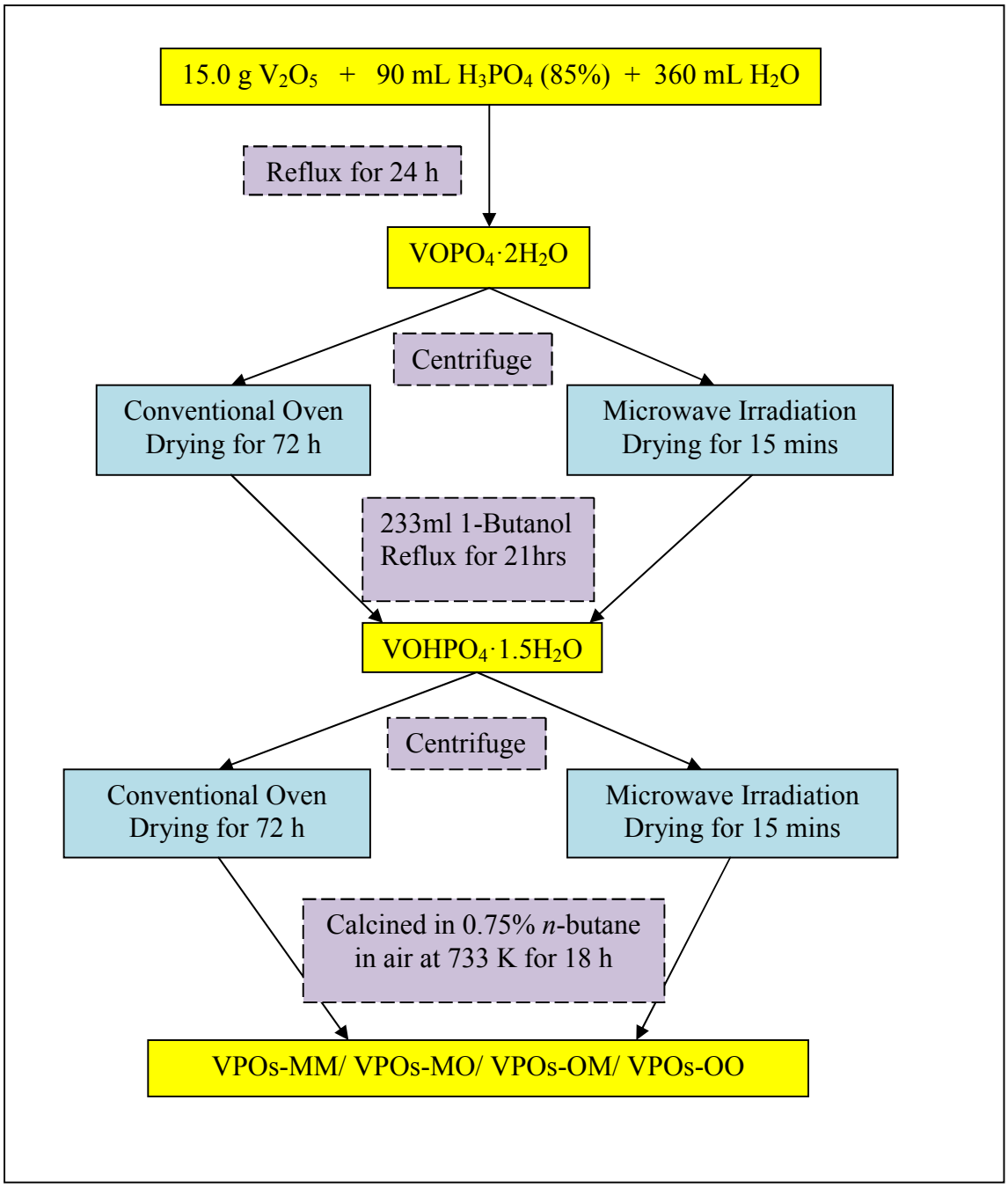

Figure 3.1: Series 1: Flow chart of preparation for bulk VPOs catalysts

3.2.2 Series 2: Preparation of Undoped and Ga Doped VPOs Catalysts

The preparation of VPOs catalysts in Series 2 were prepared as shown in Chapter 3.2.1 with the microwave irradiation as drying method on both Stage 1 and Stage 2. For 0.1% Ga-doped VPOs catalysts, 0.1% gallium were added into 10g of $VOPO_4 \cdot 2H_2O$ precursor. Compound of Gallium (III) Acetylacetonate, $Ga(acac)_3$ was used as Ga dopant source. Together with 233 ml 1-butanol, Ga doped VPOs precursor was refluxed for 21 hours. Stage 2 reflux was repeated with the addition of different dosage of gallium as dopant (0.3% and 0.5%).

Both undoped and Ga-doped VPO_s precursors were then calcined in a reaction flow of 0.75% *n*-butane in air mixture for 18 hours 723 K. The activated catalysts were denoted as VPOs-MM (as undoped), VPOs-Ga0.1%, VPOs-Ga0.3%, and VPOs-Ga0.5%.

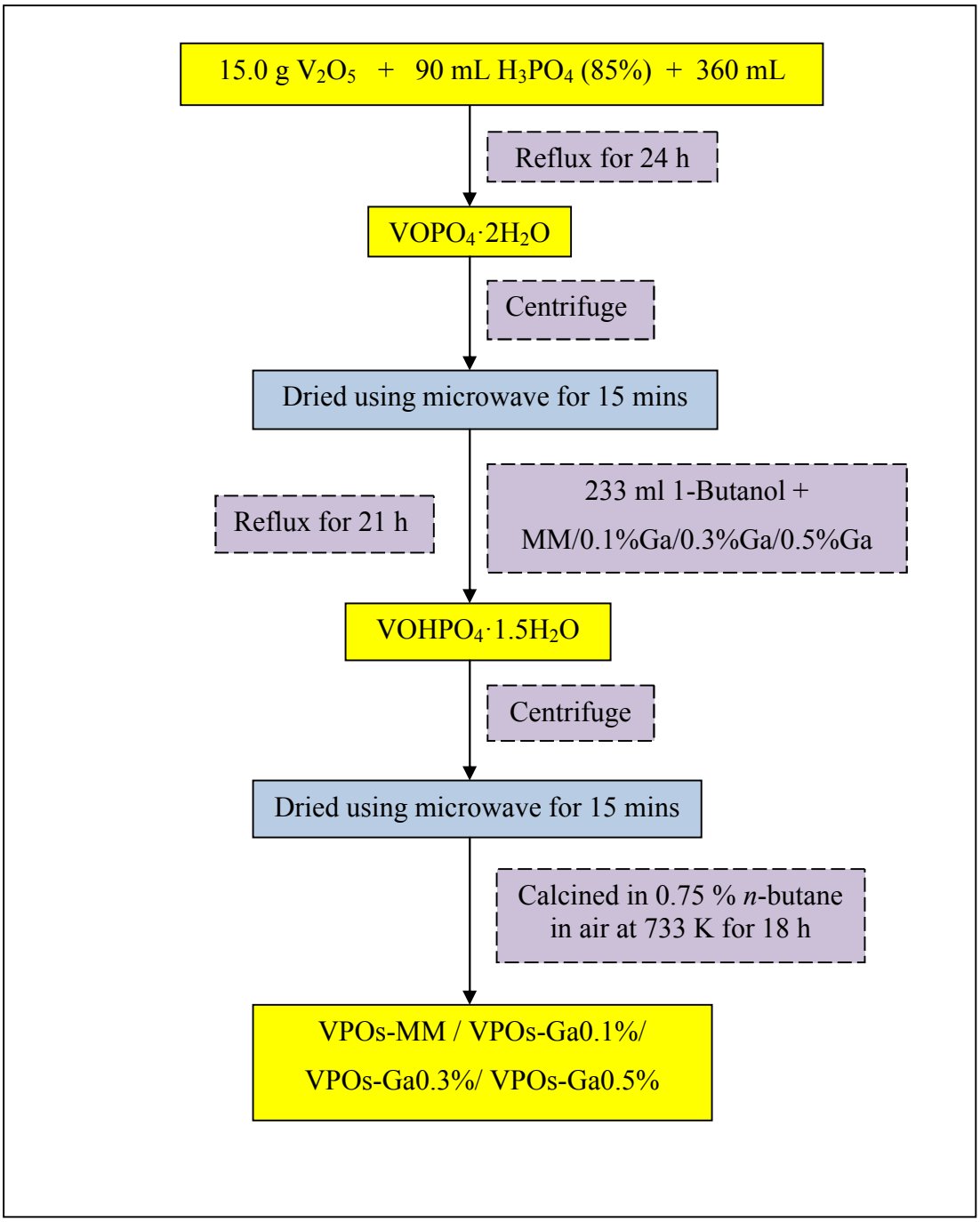

Figure 3.2: Series 2: Flow chart of preparation for doped VPOs catalysts

3.2.3 Series 3 Preparation of Bulk Catalysts

In Stage 1, dihydrate precursor was prepared using two different methods – reflux and microwave digester method. In reflux method, V_2O_5 (15.0 g from Merck), was suspended with continuous stirring into a mixture of *o*-H_3PO_4 (90 ml, 85% from Merck) and distilled water (360 mL). This mixture was stirred and refluxed at 393 K for 24 h.

While in microwave digester methods, 6 sets of the mixture of 2.5 g V_2O_5, 15 ml of *o*-H_3PO_4 and 60 ml of deionised water were prepared by using 6 same species of Teflon-lined microwave vessels. All the 6 vessels were then undergone microwave treatment for 2 hours at 393 K. Both mixtures from both synthesis methods were cooled to room temperature and the resulting yellow solid ($VOPO_4 \cdot 2H_2O$) was recovered by centrifugation. The resulting yellow solid, $VOPO_4 \cdot 2H_2O$ was then dried by microwave irradiation method for 15 mins. The drying conditions were set at 2450 MHz and an output power of 300 W.

In Stage 2, both $VOPO_4 \cdot 2H_2O$ synthesised by reflux and microwave digester were separated into two portions. First portion of 10 g $VOPO_4 \cdot 2H_2O$ was refluxed for 21 h with 1-butanol (233 ml from Merck). Second portion was separated into 6 Teflon-lined microwave vessels with 2.5 g of $VOPO_4 \cdot 2H_2O$ and 60 ml of 1-butanol each vessel. All the 6 vessels were then undergone microwave treatment for 2 hours at 120 °C using microwave digester. The resulting whitish blue solids was recovered by centrifugation and washed sparingly with a small amount of acetone. The

resulting whitish blue solids from both synthesis methods were then dried by microwave irradiation method for 15 mins. The drying conditions were set at 2450 MHz and an output power of 300 W. The precursors obtained were then calcined in a reaction flow of 0.75% *n*-butane in air mixtures at 733 K for 18 h to generate the active catalysts, $(VO)_2P_2O_7$.

The activated catalysts were denoted as VPOs-M_sM_s, VPOs-R_sR_s, VPOs-R_sM_s and VPOs-M_sR_s where VPOs represents the catalyst prepared via sesquihydrate route; M_s represents microwave irradiation synthesis process; and R_s represents the reflux synthesis process. The position of M_s/R_s represents the Stage 1 and Stage 2 synthesis respectively.

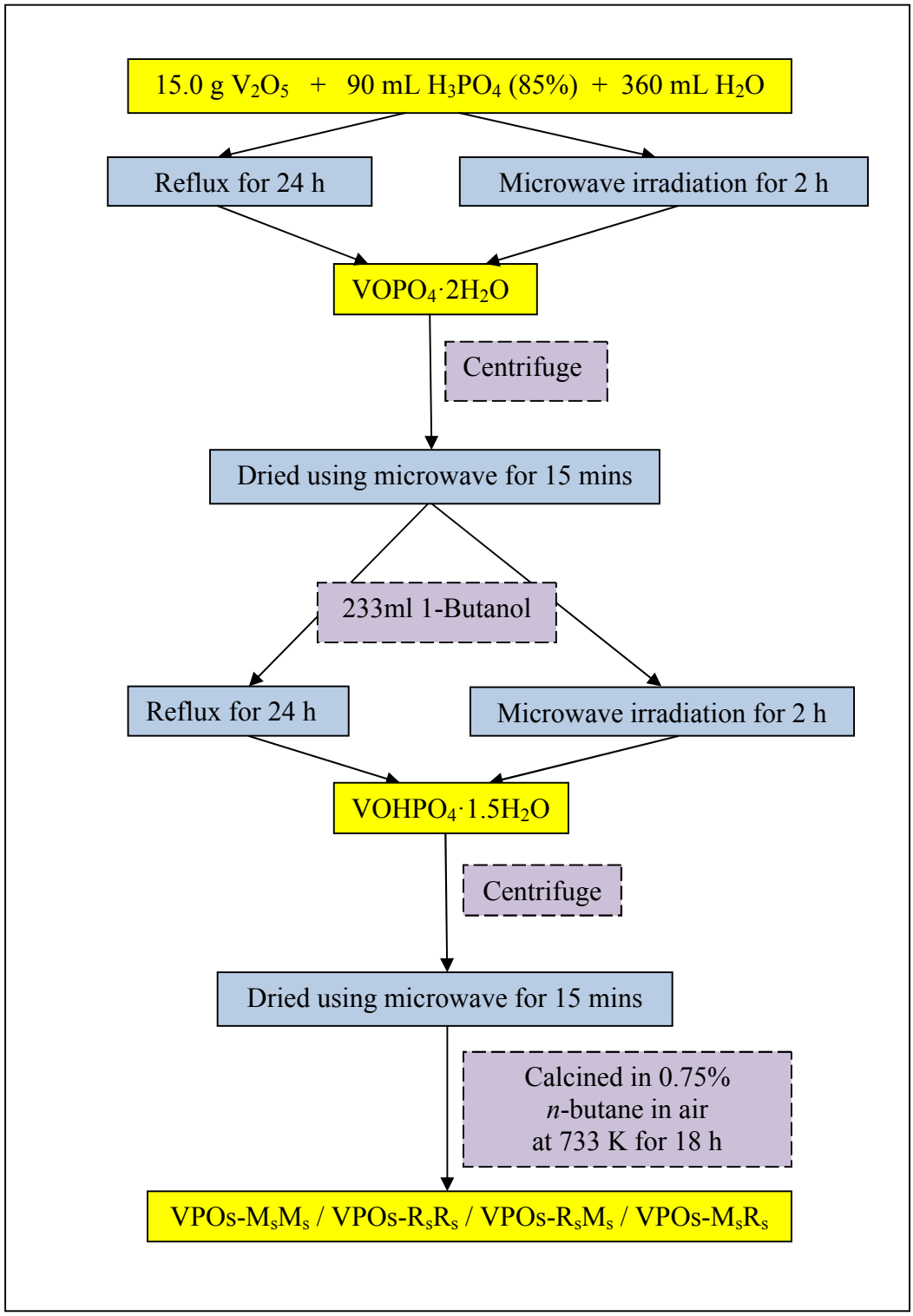

Figure 3.3: Series 3: Flow chart of preparation for bulk VPOs catalyst

(a) Stage 1 reflux

(b) $VOPO_4.2H_2O$ formed

(c) Centrifugation

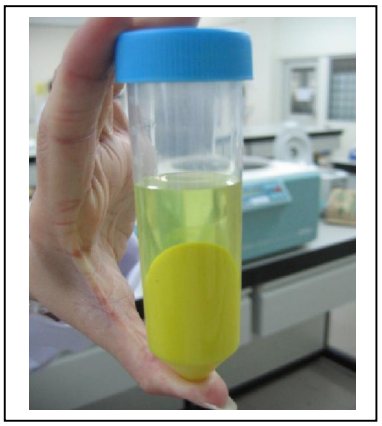

(d) $VOPO_4.2H_2O$ after centrifuged

(e) $VOPO_4.2H_2O$ before drying

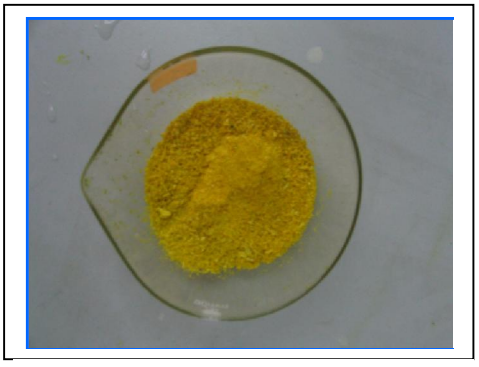

(f) $VOPO_4.2H_2O$ after drying

Figure 3.4: Preparation of $VOPO_4.2H_2O$ intermediate in Stage 1

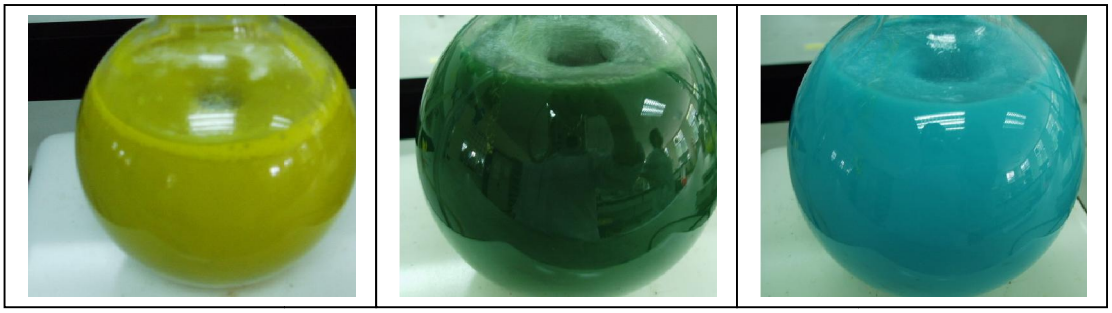

(a) Stage 2 – solution colour changes during reflux

(b) $VOHPO_4.1.5H_2O$ before and after centrifuga

(c) $VOHPO_4.1.5H_2O$ after drying

(d) $VOHPO_4.1.5H_2O$ before calcination

(e) $VOHPO_4.1.5H_2O$ after calcination

Figure 3.5: Stage 2 reflux and the activation of VPOs catalysts

3.3 Characterisation Technique and Instrumentations

Throughout the research, there are certain instruments and technique involved to examine the physical and chemical properties of the catalysts produced. The machines and techniques used are notably, X-Ray Diffractometer (XRD), Scanning electron Microscopy (SEM), Energy-dispersive X-ray (EDX) spectroscopy, Brunauer-Emmett-Teller (BET) surface Area Measurements, Inductively Coupled Plasma-Optical Emission Spectrometry (ICP-OES), Temperature Programmed Desorption Reduction Oxidation (TPDRO), and Redox Titration technique by Niwa and Murakami (1982).

3.3.1 Materials and Gases used in Characterisation of VPO catalysts

Table 3.2: Gases and Materials used in Analysis

Instrumentation/ Technique		Brand	Purity
BET surface area measurements			
Material	Material liquid Nitrogen, N_2	MOX	
Gases	Purified Nitrogen, N_2	MOX	99.999%
	Purified Helium, He	MOX	99.999%
ICP-OES			
Materials	Nitric acid, HNO_3	Merck	69-70%
	Vanadium (V) pentoxide, V_2O_5	UNI Chem	
	Gallium(III)Acetylacetonate, Ga(acac)	Aldrich	99.99%
	ortho-Phosphoric acid, *o*-H_3PO_4	MERCK	85%
Redox titration			
Materials	potassium permanganate, $KMnO_4$	Fisher Scientific	
	sulphuric acid, H_2SO_4	Merck	95–97%
	Ammonia dihydrogen orthophosphate, $NH_4H_2PO_4$	Ajax chemicals	
	diphenylamine, $(Ph)_2NH$	Acros Organics	
	ammonium metavanadate, NH_4VO_3	BDH Chemicals	
	ammonium iron(II) sulphate, $(NH_4)_2Fe(SO_4)_2 \cdot 6H_2O$	Systerm	
Temperature Programmed Reduction (TPR in H_2 / N_2)			
Gases	hydrogen in air, H_2/air		5.55%
	purified nitrogen, N_2		99.999%

3.3.2 X-ray diffraction (XRD) Analyses

XRD analysis is one of the most powerful and efficient techniques for qualitative and quantitative analysis of crystalline compounds. It is use to determine the phase composition of catalysts at ambient temperature and under normal atmospheric conditions. It relies on the dual wave or particle nature of X-Rays to obtain information about the structure of crystalline materials. The sample is prepared for analysis by compressing a small amount of sample into the sample holder.

The phenomenon of diffraction occurs when the penetrating radiation, X-rays enters a crystalline substance and is scattered. The scattered X-Rays will undergo constructive and destructive interference in a process termed as diffraction. In order for a beam to be 100% diffracted, the distance it travels between rows of atoms at the angle of incidence must be equal to an integral multiple of the wavelength of the incident beam. D-spacings which are greater or lesser than the wavelength of the directed X-ray beam at the angle of incidence will produce a diffracted beam of less than 100% intensity. Sample will rotate during the analysis to reduce any heating to the sample. Resulting diffractogram will confirm the identity of a solid material as a pharmaceutical powder. The diffraction of X-Rays by crystals is described by Bragg's Law. X-Rays are reflected from a crystal only if the angle of incidence satisfies the condition $n\lambda = 2d \sin \theta$.

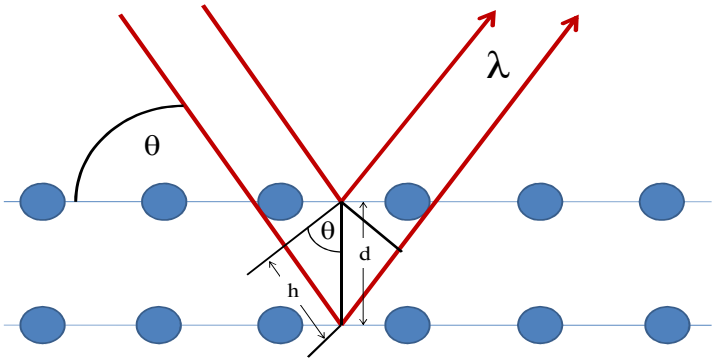

Figure 3.6: Bragg's Law Diagram

X-ray diffraction has been in use in two main areas: the fingerprint characterization of crystalline materials and the determination of their structure. Each crystalline solid has its unique characteristic X-ray powder pattern which may be used as a "fingerprint" for its identification. Once the material has been identified, X-ray crystallography may be used to determine its structure, *i.e.* how the atoms pack together in the crystalline state and what the interactatomic distance and angle are *etc*. Therefore, size and the shape of the unit cell for any compound most easily determined by using the diffraction of X-rays. In catalysis, X-ray diffraction analysis is carried out to determine the phase compositions of catalysts at ambient temperature and under normal atmospheric conditions. Therefore, the relative abundance of V^{4+} and V^{5+} can be determined. The crystallite sizes can also be determined by using Debye-Scherrer equation:

$$t = \frac{0.89\lambda}{\beta_{hkl}\cos\theta_{hkl}} \qquad (3.1)$$

where t is the crystallite size for (h k l) phase, λ is the X-ray wavelength of radiation for CuKα, $\beta_{h\,k\,l}$ is the full-width at half maximum (FWHM) at (h k l) phase and $\theta_{h\,k\,l}$ is the diffraction angle for (h k l) phase (Klug and Alexander, 1974).

The XRD patterns were obtained by using a Shimadzu model XRD-6000 diffractometer (Figure 3.7) employing Cu Kα radiation (λ = 1.54 Å) to generate diffraction patterns from powder crystalline samples at 40 kV generated by a glass diffraction x-ray tube (Toshiba, A-40-Cu) normal focus 2.0 kW type at ambient temperature. The samples were compressed on an aluminium sample holder and the basal spacing was determined via powder technique. Samples were scanned with wavelength range of 0.5–2 Å at range of 2θ = 2.0000 – 60.0000° with a scanning rate of 1.2000° per minute.

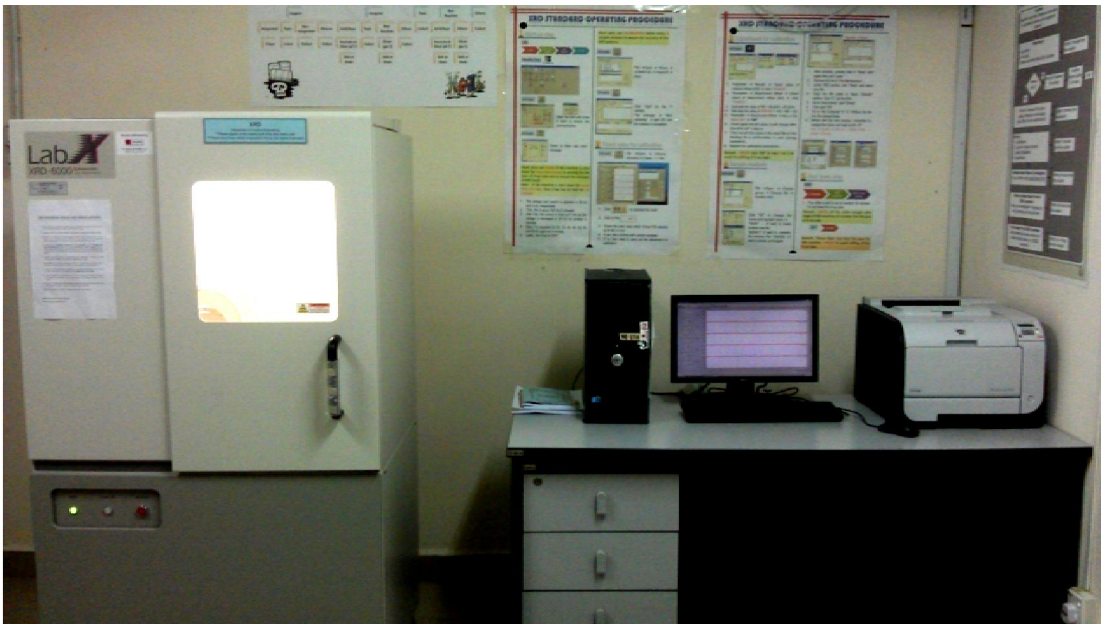

Figure 3.7: Shimadzhu diffractometer Model XRD-6000

3.3.3 Brunaur-Emmett-Teller (BET) Surface Area Measurement

The BET surface area analysis involves the nitrogen adsorption-desorption at low temperature (77k), has been used for the determination of the total specific surface area of porous catalysts. This was done by using a Thermo Finnigan Sorptomatic 1990 nitrogen adsorption-desorption analyzer (Figure 3.8).

Prior to analysis, approximately 0.5 g of catalyst was degassed at 423 K for overnight and the specific surface area of the powder is determined by physical adsorption of a gas on the surface of the solid. The determination is normally carried out at the temperature of liquid nitrogen. The amount of gas adsorbed can be measured by a volumetric or continuous flow procedure. The specific surface area of the catalyst is determined by calculation the amount of adsorbate gas corresponding to monomolecular layer on surface area using the BET equation (Brunauer et al., 1938).

$$\frac{p}{V(p_o - p)} = \frac{1}{V_m C} + \frac{(C-1)p}{CV_m p_o} \tag{3.2}$$

where V is the volume, reduced to standard conditions, i.e. the standard temperature and pressure (STP) of gas adsorbed per unit mass of adsorbent at a given pressure, p and constant temperature; p_0 is the saturation pressure at the measurement temperature; V_m is the volume of gas required to form a complete monolayer adsorbed layer at STP per unit mass of adsorbent, when the surface is covered by a monolayer of adsorbate; and C is a constant related to free energy of adsorption which is represented by the equation below:

$$C = \mathrm{A_{r\,exp}}\left(\frac{(\Delta \mathrm{H_1} - \Delta \mathrm{H_2})}{RT}\right) \tag{3.3}$$

where A_r is the pre-exponential factor; $\Delta \mathrm{H_1}$ is the heat of adsorption of the first layer; $\Delta \mathrm{H_2}$ is the heat of liquefaction; R is the gas constant; and T is the absolute temperature in Kelvins. All the VPOs catalysts in this research shown a mesoporous adsorption curves in BET analysis indicated that the catalysts produce is in mesoporous texture of Type IV. The graphs were attached in Appendix I.

Figure 3.8: Thermo Finnigan Sorptomatic 1990

3.3.4 Chemical Analyses

The bulk chemical composition was determined by using a sequential scanning inductively coupled plasma-optical emission spectrometer (ICP-OES) Perkin Elmer Optical Emission Spectrometer Optima 2000 DV. 0.025 g of sample catalyst was digested with slight heating and continuous stirring in 10 mL of 8 M nitric acid. The resulting mixtures were diluted with deionised water to achieve a nominal concentration in the range of 100-120 ppm. The standard solutions of phosphorus and vanadium were prepared in concentrations of 10, 20, and 30 ppm, respectively. The standard solutions of gallium were prepared in concentrations of 2.5, 5.0, 10, 20 and 30 ppm. Deionised water was used as a blank control solution. All the solutions prepared were added with 10 mL of 8 M HNO_3 in order to be consistent with the sample solutions.

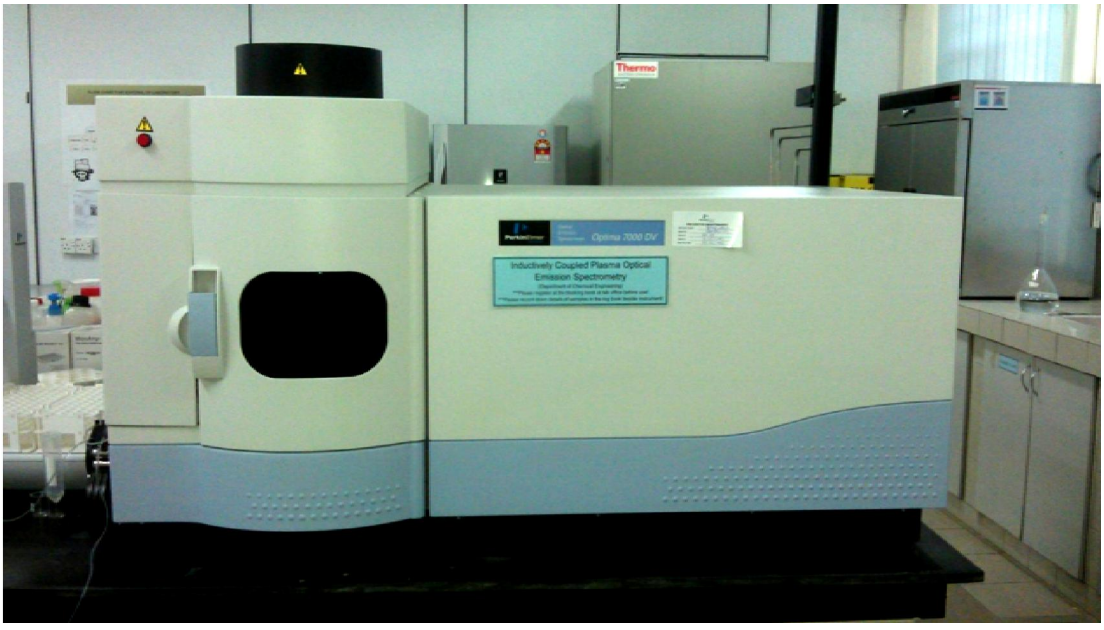

Figure 3.9: Perkin Elmer Optima 2000 DV optical emission spectrometer

3.3.5 Redox Titration Analyses

This method was developed by Miki Niwa and Yuichi Murakami in 1982. They had investigated the reaction mechanism of the ammoxidation of toluene on V_2O_5 / Al_2O_3 catalyst. The bifunctional activity of this catalyst which consists of the oxidation activity of V_2O_5 and the dehydration property of Al_2O_3 is stressed. However, some problems about the active sites of vanadium oxide and alumina and how they actually contribute to the ammoxidation of toluene remain a question (Niwa and Mukakami, 1982).

In this research, redox titration was carried out to determine the average vanadium valence (AV) of the VPO catalysts and/or to obtain the average oxidation state of vanadium. First, a known amount of the sample is dissolved in 100 ml sulphuric acid (2 M). It is then cooled to room temperature before being titrated with potassium permanganate solution (0.01 M). This titrant is used to oxidise V^{3+} and V^{4+} in the solution to V^{5+}. The end point is reached when the change of colour from the original greenish blue to pink was observed. The volume of potassium permanganate used was recorded as V_1. Then the oxidised solution was treated with ammonium iron (II) sulphate solution (0.01 M). This is to reduce V^{5+} to V^{4+} in the solution. Diphenylamine is used as an indicator. The end point is reached when the purple colour of the solution disappeared and became colourless. The volume of ammonium iron (II) sulphate used was recorded as V_2 (Niwa and Mukakami, 1982).

Another fresh 25 ml of the original solution was then titrated with 0.01 N ammonium iron (II) sulphate solution. Diphenylamine is also used as indicator. This stage of titration is to determine the V^{5+} in the original solution. The end point is reached when the solution changes from purple to greenish blue. The volume of ammonium iron (II) sulphate solution used was recorded as V_3.

The average oxidation state of vanadium (AV) can be determined by solving the equation below (Niwa and Mukakami, 1982):

$$AV = \frac{5V^{5+} + 4V^{4+} + 3V^{3+}}{(V^{5+} + V^{4+} + V^{3+})} \tag{3.4}$$

where V^{3+}, V^{4+} and V^{5+} are concentration of vanadium at different oxidation state. In order to obtain the values for V^{3+}, V^{4+} and V^{5+} values, respectively. The following equations are used:

$$\begin{gathered} V^{3+} = 20(0.01)V_1 - 20(0.01)V_2 + 20(0.01)V_3 \\ V^{4+} = 40(0.01)V_2 - 40(0.01)V_3 + 20(0.01)V_1 \\ V^{5+} = 20(0.01)V_3 \end{gathered} \tag{3.5}$$

where V_1 = the volume of potassium permanganate used and V_2 = the volume of ammonium iron (II) sulphate used.

Figure 3.10: Diagram shows the experiment of Redox Titration

3.3.6 Scanning Electron Microscopy (SEM) and Energy-dispersive X-ray (EDX) Spectroscopy

SEM is an electron microscope that produces images of a sample by scanning the sample with a focused beam of electron. The electron is generally scanned in a raster scan pattern and the beam's position is combined with the detected signal to produce an image. Various signals were produced when the electron interact with atoms in the sample. The signals produced contain information about the sample's surface topography and composition.

SEM analyses were done by using a Hitachi S3400N scanning electron microscope. A small amount of fresh catalyst was placed on the surface of a carbon tape, which had been fixed on an aluminium holder (diameter 15 mm). Then the catalysts were coated with palladium and gold with Sputter Coater machine. The

morphologies of the catalysts were captured by the electron detector in the SEM and the images were saved in a linked computer.

Energy-dispersive X-ray (EDX) analyses were carried out by using EDAX software. The Ametek EDX instrument was linked together with the SEM. The surface P/V atomic ratios of the catalysts were determined quantitatively by manipulating parameters, which will affect the x-ray spectrum, such as the process time, live time, dead time, probe current and the accelerating voltage.

Figure 3.11: Hitachi S-34000N Scanning Electron Microscope coupled with Ametek EDX

3.3.7 Temperature-programmed Reduction (TPR) in H_2 Analyses

Temperature Programmed Reduction (TPR in H_2) is used to determine the amount of bulk oxygen in the catalyst. TPR is also uses to study structural changes upon cyclic reduction/re-oxidation experiments, to study the reactivity and redox behaviour of catalysts, to obtain information such as the nature and oxidising species available from the catalyst, and to obtain information about the number and quantity of the reducible species in the sample.

This technique requires an oxidised catalyst precursor to be submitted to a programmed temperature rise, while a reducing gas mixture is flow over it (usually hydrogen diluted in some inert gas such as nitrogen or argon). As the catalyst is being reduced, hydrogen is consumed. The change in the thermal conductivity of the gas mixture before and after the reaction is measured by a thermal conductivity detector. During the TPR analyses, several products such as water, carbon monoxide or carbon dioxide are formed. All these undesired gas molecules need to be eliminated as to not to interfere in the signal output. To eliminate these impurities, pre-treatment is carried out before the analysis.

TPR in H_2 analyses were done by using a Thermo Electron TPDRO 1100 (Figure 3.12) instrument utilizing a thermal conductivity detector (TCD). In TPR analyses, the catalysts were cleaned at the beginning by heating them from room temperature to 473 K in a purified nitrogen flow (25 cm^3min^{-1}) and holding them to that flow at 473 K for 30 minutes before cooling them to ambient temperature. Next,

the flow is switched to 5% H_2/N_2 (25 cm^3min^{-1}).These reducing gas functions as to optimize the thermal conductivity difference between the reactant and the carrier gas. Following the conductivity of the eluted gas, the temperature was raised (5 $Kmin^{-1}$) to 1173 K.

TPR profile is a plot of the hydrogen consumption of a catalyst as a function of time, which will be converted to a function of temperature. The area of peaks observed in TPR provides information on the composition of reducible compounds mixture. The temperature of the peak maximum (T_{max}) is a characteristic of the reduction processes and may be used for “finger print" identification.

Figure 3.12: Thermo Electron TPDRO 1100

3.3.8 Catalytic Tests

Catalytic reactor is a fixed-bed microreactor used to determine the catalytic performance (selectivity and activity) of catalysts. The oxidation of *n*-butane was carried out in a fixed-bed microreactor at 673 K with GHSV = 2400 h^{-1} using a standard mass of catalyst (250 mg). A mixture of 1.0% *n*-butane and air was fed to the reactor via calibrated mass flow controller. The products were then fed via heated lines to an on-line gas chromatograph i.e. Thermo Scientific TRACE GC Ultra TM (Figure 3.13), which equipped for analysis. The TCD 66 detector allows the detection of the fixed gases O_2, N_2, CO, CO_2 etc and it is equipped with a Hysep-R packed column (1 m, 1/8") and Molecular Sieve 5A column (3 m, 1/8"). The flame ionization detector (FID) allows the detection of all hydrocarbon gases (C1-C4) and maleic anhydride, this channel equipped with a Rtx-1701 wide bore capillary column (30 m × 0.53 mm).

Figure 3.13: Fixed-bed microreactor with on-line Thermo Scientific TRACE GC Ultra™

CHAPTER 4

RESULTS AND DISCUSSION

4.1 Series 1: Effect of Microwave and Conventional Oven Drying Methods in the Synthesis of Vanadium Phosphorus Oxide Catalysts via Sesquihydrate Route

A series of vanadyl pyrophosphate (VPOs) catalysts were prepared via sesquihydrate route. Microwave drying process employed in Stage 1 and/or Stage 2 during the synthesis was compared with the VPOs catalyst produced by convection oven drying process. The activated catalysts were denoted as VPOs-MM, VPOs-MO, VPOs-OM, and VPOs-OO, where s represents the preparation method, i.e. via sesquihydrate route; M represents microwave irradiation drying method; and O represents oven drying method. The position of M/O represents the microwave drying method employed on Stage 1 and Stage 2, respectively.

4.1.1 Series 1: X-ray Diffraction (XRD) Analyses

XRD patterns VPOs-MM, VPOs-MO, VPOs-OM and VPOs-OO catalysts (Figure 4.1) showed similar diffraction patterns comprised of well-crystallised $(VO)_2P_2O_7$ phase. Three main characteristic peaks appeared at 2θ = 22.9 °, 28.4 °, and 29.9 °, which are corresponded to (0 2 0), (2 0 4), and (2 2 1) planes, respectively (JCPDS File No. 34-1381).

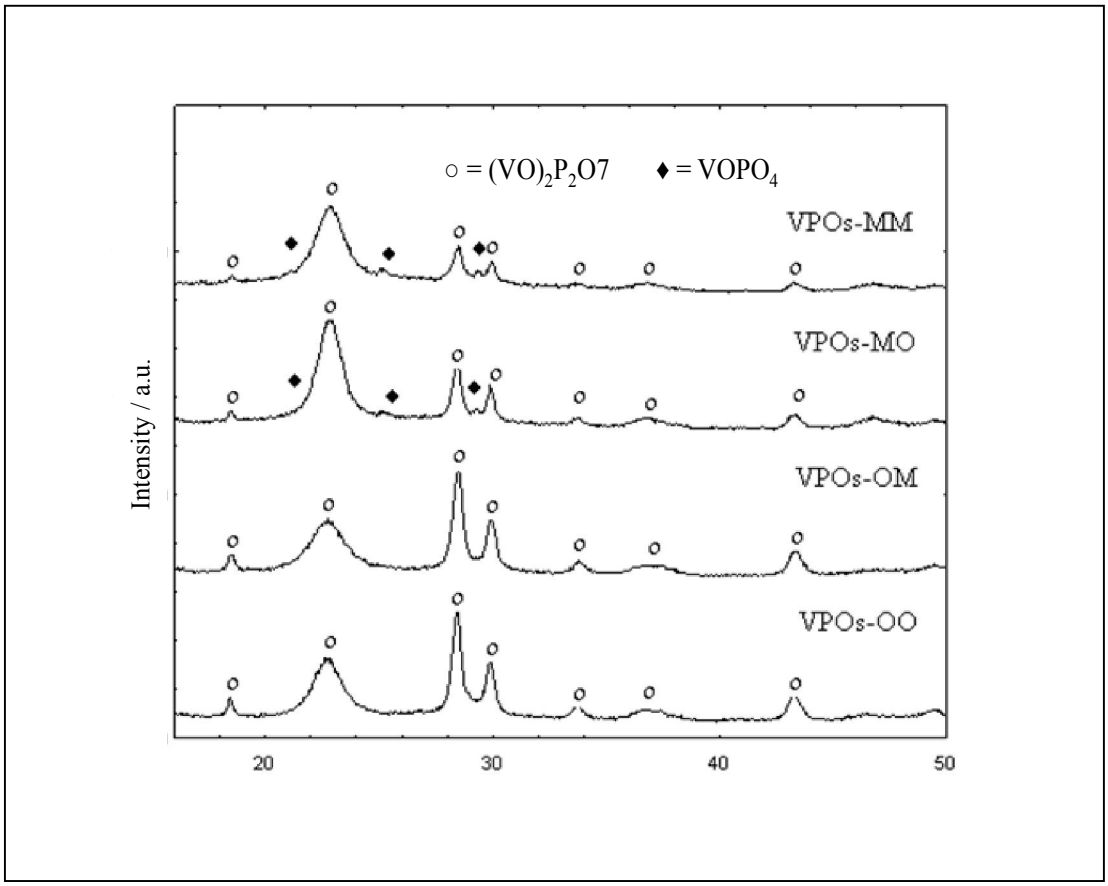

Figure 4.1: Series 1: Powder XRD pattern of bulk VPOs catalysts

As observed in Figure 4.1, there were additional weak peaks emerged at around 2θ = 21.3˚, 25.3˚, and 29.3˚ for VPOs-MM and VPOs-MO, which peaks are corresponded to various V^{5+} phases, such as β-$VOPO_4$ (JCPDS File No. 27-0948; 2θ= 21.3˚), and α_{I9I}-$VOPO_4$ (JCPDS File No. 34-1247) (2θ= 25.3˚ and 29.3˚). Catalysts dried by microwave irradiation at Stage 1 (VPOS-MM and VPOs-MO) would promote the formation of V^{5+} phases in the catalysts. This is in agreement with the findings by Rownaghi and co-workers indicated that microwave dried catalysts would favour the appearance V^{5+} phases, which was produced via hemihydrates route (Rownaghi et al., 2009c). No V^{5+} phase could be detected in the XRD profiles

of VPOs-OM and VPOs-OO, which could be due to the reason that the amount of this particular phase was below the detection limit of the XRD instrument. However, there are V5+ phase appeared in both VPOs-OM and VPOs-OO which is shown at Section 4.1.4 on TPR profile. As observed in the XRD profile, the catalysts dried by microwave irradiation on Stage 1 (VPOs-MM and VPOs-MO) was found to exhibit higher intensity on (0 2 0) plane. As for the catalysts which oven drying method was employed in Stage 1 (VPOs-OM and VPOs-OO), the reflection plane of (2 0 4) was found to be more intense as compared to the microwave drying counterparts.

The formula for the calculations of the crystallite size is given by Debye-Scherrer equation:

$$\mathrm{T}\ (\text{Å}) = \frac{0.89\lambda}{\beta_{hkl}\cos\theta_{hkl}} \tag{4.1}$$

where T is the crystallite size for (*h k l*) phase, λ is the X-Ray wavelength of radiation for Cu Kα, FWHM is the full width at half maximum at the peak and θ is the diffraction angle for the phase. According to Debye-Scherrer's equation, the crystallite size is inversely proportionally with linewidth of reflection plane (Klug and Alexander, 1974).

As shown in Table 4.1, the FWHM is used to calculate the crystallite size were calculated for both (0 2 0) and (2 0 4) planes for all the catalysts. The relation of FWHM and crystallite size had been proposed by Taufiq-Yap et al. (2001) in his previous study, whereby the decreased in the FWHMs of the (0 2 0) reflection with a long time on stream indicated that the thickness of particles in the (1 0 0) direction

increased. Although it has been proposed by some researchers that the oxidation of $(VO)_2P_2O_7$ catalyst starts at the side faces of the (1 0 0) plane, but this does not indicate that the contribution of VPOs catalyst performance only appeared at (1 0 0) plane. There are other V^{5+} phases, which will enhance the activity of the VPOs catalyst as well. Therefore, in XRD profile, it shows that microwave irradiation drying method will enhance the crystallinity of VPOs catalysts, but somehow it does not affect the crystallite size of the VPOs catalysts prepared in (0 2 0) and (2 0 4) planes.

Table 4.1: Series 1: XRD data of bulk VPOs catalysts

Catalysts	Linewidth[a] (0 2 0) (°)	Linewidth[b] (2 0 4) (°)	Crystallite size[c] (0 2 0) (Å)	Crystallite size[c] (2 0 4) (Å)
VPOs-MM	1.4853	0.7180	54	113
VPOs-MO	1.2648	0.6631	63	122
VPOs-OM	1.7484	0.6694	46	121
VPOs-OO	1.4773	0.7067	54	111

[a] Full-witdth half maximum (FWHM) of (020) reflection plane
[b] Full-witdth half maximum (FWHM) of (020) reflection plane
[c] Crystallite size by means of Scherrer's formula

4.1.2 Series 1: Brunauer-Emmett-Teller (BET) Surface Area Measurement and Chemical Analyses

As tabulated in Table 4.2, the specific surface area of VPOs catalysts are as follows; 18 m^2g-^{1} for VPOs-MM, 12 m^2g^{-1} for VPOs-MO, 21 m^2g^{-1} for VPOs-OM, and 15 m^2g^{-1} for VPOs-OO. Previously, Rownaghi et al., (2009c) had reported that catalyst prepared via VPD method and microwave drying process on both stages exhibited larger specific surface area than catalysts undergone conventional drying. This is in agreement with catalysts prepared via VPS method as well, where catalyst dried by microwave on both stages (VPOs-MM) has larger specific surface area as compared to conventional drying catalyst (VPOs-OO).

From the XRD profile (Figure 4.1), it could be notified that when catalyst undergoes microwave drying at Stage 1, extra V^{5+} phase occurred. At $2\theta = 21.3^{\circ}$, the V^{5+} phase was denoted by β-$VOPO_4$ which is known to form a bulkier structure inside the VPOs catalysts. While microwave at Stage 2 enhance the formation of V^{4+} phase which often appeared to be a thinner structure compare to β-$VOPO_4$ phase. Therefore, the specific surface area for VPOs-MM is smaller compare to VPOs-OM due to the formation of β-$VOPO_4$ at Stage 1 microwave drying process. However, it could be notified that VPOs catalysts prepared via microwave drying process on both stages exhibited larger specific surface area as compared to conventional drying catalyst. This is in agreement with the findings of Rownaghi et al., (2009) whereby the catalysts were prepared via hemihydrates route. Further analysis by secondary

electron images from SEM micrographs (Figure 4.2) proved that microwave irradiation had altered the surface structural of the catalysts.

ICP-OES is used to analyse the elements exist in VPOs catalyst and to test the P/V atomic ratio of the VPOs catalysts. As shown in Table 2, the P/V atomic ratio for VPOs-MM, VPOs-MO, VPOs-OM, and VPOs-OO are 1.30, 1.22, 1.18, and 1.28 respectively. As for EDAX analyses, results observed for P/V ratio fall within the range of 1.05 to 1.33. According to Centi (1993), the optimum P/V atomic ratio range in producing active and selective $(VO)_2P_2O_7$ phase fall within the range 1.0-1.2 (Centi, 1993) The high P/V atomic ratio of VPOs-MM indicated that microwave drying method induced the phosphorus surface enrichment.

The average oxidation numbers of vanadium and the composition of V^{5+} and V^{4+} oxidation states are tabulated in Table 4.2. The average oxidation number of VPOs-MM, VPOs-MO, VPOs-OM, and VPOs-OO is 4.4646, 4.5200, 4.4299, and 4.4419, respectively. Microwave irradiation method when used in Stage 1 increased the average oxidation number of the vanadium, which is in agreement with XRD profile showing the extra V^{5+} phases appeared. However, due to the reason when microwave irradiation drying method was used in Stage 1, the specific surface area was reduced. The decrement of specifc surface area was due to the increment of V^{5+} with bulkier structure. Therefore, VPOs-MM has a lower specific surface area compared to VPOs-OM. VPOs-OM showed the highest percentage of V^{4+} species appeared during the redox titration analysis, which is in agreement with the TPR profile and will be discussed later in Section 4.1.4.

Table 4.2: Series1: Percentages of V^{4+} and V^{5+} oxidation states present, Specific BET surfaces areas, and chemical compositions of VPOs catalysts

Catalysts	Surface Area (m^2/g)	P/V Ratio (ICP-OES)	P/V Ratio (EDX)	Average oxidation numbers of vanadium		
				V^{4+} (%)	V^{5+} (%)	V_{AV}
VPOs-MM	18	1.30	1.33	53.54	46.46	**4.4646**
VPOs-MO	12	1.22	1.13	48.00	52.00	**4.5200**
VPOs-OM	21	1.18	1.05	57.01	42.99	**4.4299**
VPOs-OO	15	1.28	1.19	55.81	44.19	**4.4419**

4.1.3 Series 1: Scanning Electron Microscopy (SEM) Analyses

The surface morphology of VPOs-MM, VPOs-MO, VPOs-OM, and VPOs-OO catalysts are shown in Figure 4.2(a)-(d). From the previous studies, it's well-known that VPO catalyst will formed secondary structures, consisting different sizes of plate-like crystal, which were agglomerated into the characteristics of rosette-shape clusters (Leong et al., 2010). These plate-like crystallites are compromised of agglomerates of $(VO)_2P_2O_7$ platelets that preferentially exposing the (1 0 0) crystal plane (Kiely et al., 1995).

As observed in Figure 4.2(a)-(b), catalysts dried by microwave irradiation shows structure with crystal-like clusters that stacked up into rosette shape, while catalyst prepared via conventional oven drying shows the typical rosette-type structure as observed in Figure 4.2(d). Catalysts prepared using microwave irradiation drying method in Stage 1 synthesised had shown to lost the folded-edges structure, which was deemed as the unique characteristics of catalysts prepared via sesquihydrate precursor route as shown in VPOs-OO. While microwave irradiation drying method in Stage 2 synthesised process does not affect the typical rosette-shape structure of VPOs catalyst with folded-edges but it decreased the size of platelets as shown in VPOs-OM. The decreased size of platelets is the reason of the higher specific surface area achieved in VPOs-OM.

According to Rownagni et al. (2009c) the microwave assisted prepared catalysts displayed a thin rosette-type structure with uniform crystal size and the smaller platelets observed in these catalysts resulted in higher surface area and hence improved catalyst performance. Both VPOs-MM and VPOs-OM showed to form a lot of smaller clusters compare to VPOs-MO and VPOs-OO. The SEM results obtained are in agreement with BET surface area analysis, which indicated that VPOs-MM and VPOs-OM has larger surface area as compared to catalyst prepared via conventional oven drying, VPOs-OO.

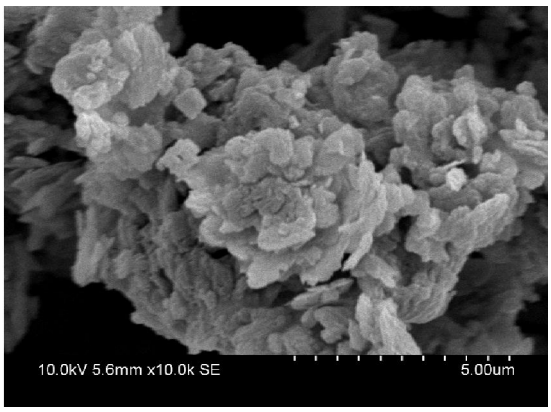

(a)

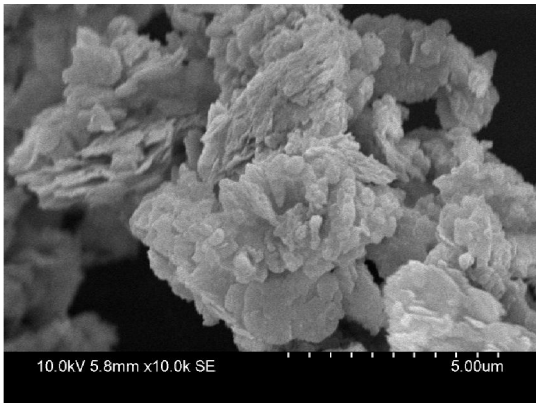

(b)

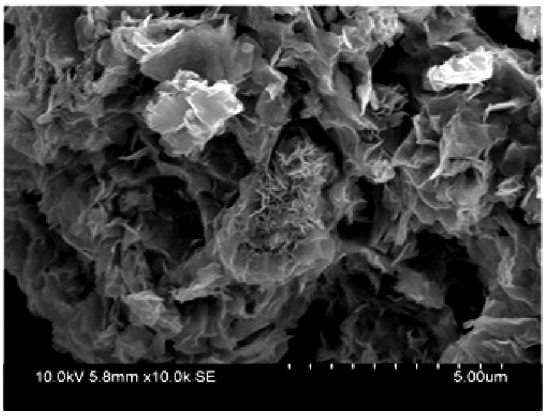

(c)

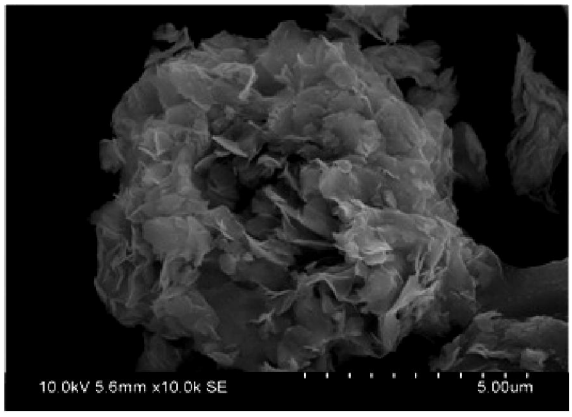

(d)

Figure 4.2: SEM micrographs of (a) VPOs-MM (b) VPOs-MO (c) VPOS-OM and (d) VPOs-OO catalysts

4.1.4 Series 1: Temperature Programmed Reduction (TPR of H_2/N_2)

As shown in Figure 4.3, all the bulk VPOs catalysts showed two characteristic reduction peaks. The first peak is the reduction of V^{5+} phase, whereas the second peak assigned to the removal of bulk oxygen from the active V^{4+} phase. The V^{4+} phase is considered the catalytically active phase while the V^{5+} phase is the selectivity phase for the conversion of *n*-butane to maleic anhydride (Hutchings, 1991). VPOs-MM catalyst showed 2 maxima peaks (Figure 4.3) at 793 K and 1007 K while VPOs-MO catalyst and VPOs-OM have 2 maxima peaks at 785 K and 1035 K, 789 K and 981 K respectively. As for VPOs-OO catalyst, the maxima peak appeared at 793 K and 981 K. This means that these catalysts had been reduced since the oxygen atoms being removed by the hydrogen gas.

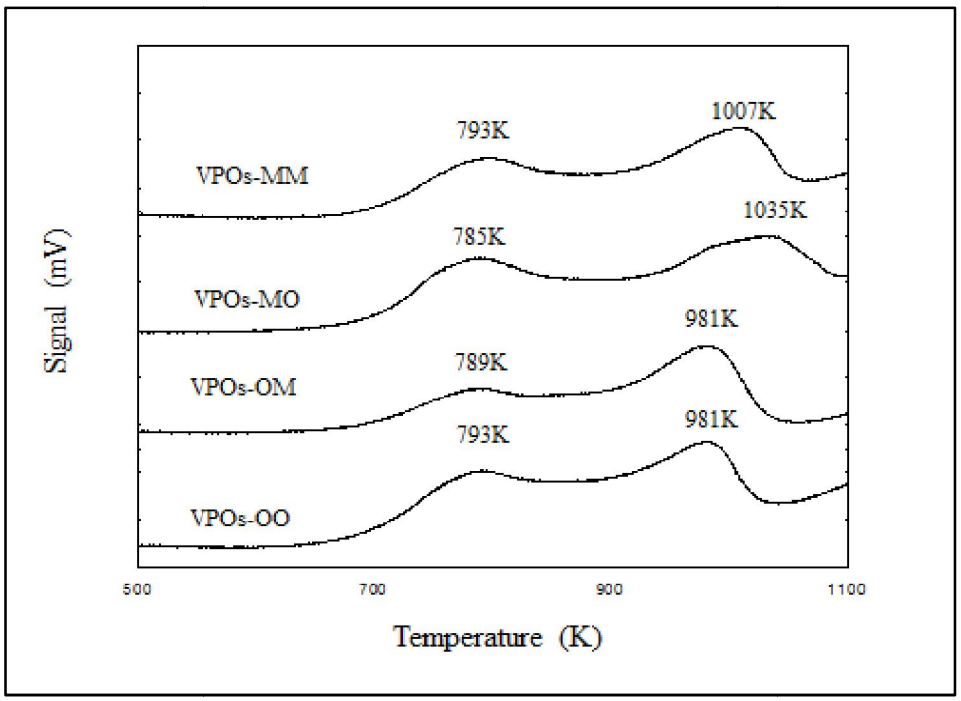

Figure 4.3: Series 1: TPR in H_2/N_2 profiles for bulk VPOs catalysts

For microwave-dried catalyst (VPOs-MM) both reduction temperatures appeared at higher temperatures than of conventionally dried catalyst (VPOs-OO). The increase in the reduction temperature indicated that the microwave-dried catalysts contain physically stronger pellets than those produced by conventional heating, which may caused by the moisture levelling achieved in microwave drying (Rownaghi et al., 2009c).

The amount of oxygen removed associated to V^{4+} phase (O^{-}-V^{4+}) and V^{5+} phase (O^{2-}-V^{5+}) were calculated and shown in Table 4.3. Catalyst VPOs-MM exhibited the highest amount of oxygen atoms removed (2.4871 x 10^{21} atom/g) as compared to VPOs-MO, VPOs-OM and VPOs-OO catalysts, which were 2.3141 x 10^{21} atom/g, 2.0624 x 10^{21} atom/g, and 1.8276 x 10^{21} atom/g, respectively. The total H_2 consumption was found to increase by 13 % to 36 % when the catalysts were dried with microwave irradiation as compared to conventionally dried catalyst (VPOs-OO). VPOs-MM exhibited the highest amount of oxygen atoms (O^{2-}) removed from V^{5+} phase (i.e. 9.0511 x 10^{20} atom/g). This is in agreement with the XRD analysis indicating that more prominent peaks assigned to V^{5+} phase were observed in the XRD profile. Comparatively, VPOs-MO, VPOs-OM and VPOs-OO exhibited lower amount of O^{2-}-V^{5+} could be removed from their lattice (i.e. 8.2375 x 10^{20} atom/g, 5.3319 x 10^{20} atom/g and 7.0289 x 10^{20} atom/g, respectively). The amount of oxygen associated to V^{4+} (O^{-}-V^{4+}) was found to increase by 33 % to 46 %, when the catalysts were dried by microwave irradiation in either stage 1 (VPOs-MO), stage 2 (VPOs-OM) or both stages (VPOs-MM). Higher total amount of H_2

consumption from microwave drying catalyst suggested that microwave irradiation is capable of producing highly active and selective VPOs catalysts.

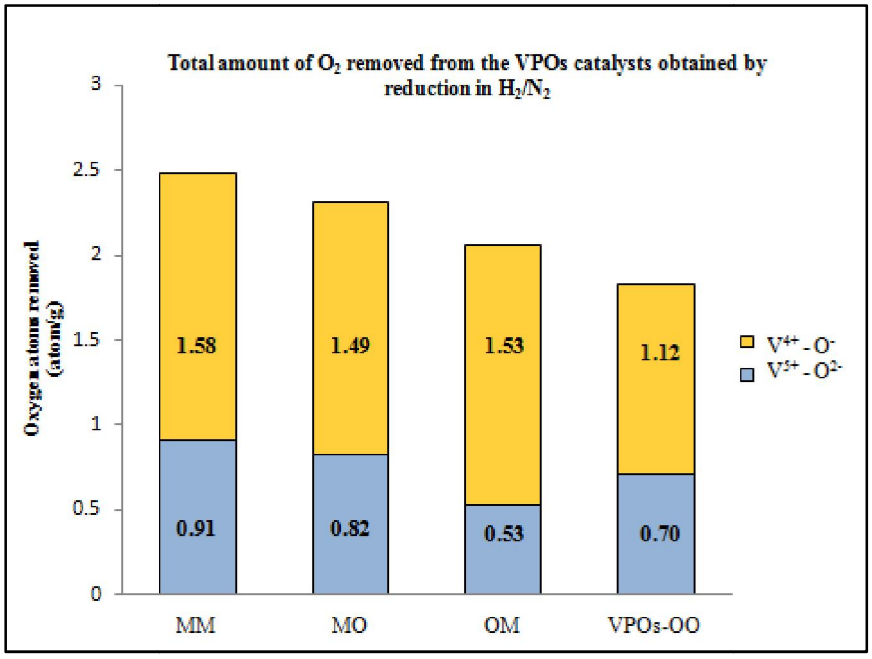

Figure 4.4: Series 1: Data chart of TPR in H_2/N_2 for bulk VPOs catalysts

Table 4.3: Series 1: Total amount of O_2 removed from the bulk VPOs catalysts obtained by reduction in H_2/N_2

Catalysts	T_{max} (K)	Reduction activation energy, E_r (kJ mol^{-1})	Oxygen atoms removed (mol/g)	Oxygen atoms removed (atom/g)
VPOs-MM	793	152.3667	1.5032×10^{-3}	9.0511×10^{20}
	1007	193.4845	2.6269×10^{-3}	1.5819×10^{21}
Total :			**4.1301×10^{-3}**	**2.4871×10^{21}**
VPOs-MO	785	150.8295	1.3679×10^{-3}	8.2375×10^{20}
	1035	198.8644	2.4749×10^{-3}	1.4904×10^{21}
Total :			**3.8427×10^{-3}**	**2.3141×10^{21}**
VPOs-OM	789	151.5981	8.8541×10^{-4}	5.3319×10^{20}
	981	188.4888	2.5393×10^{-3}	1.5292×10^{21}
Total :			**3.4247×10^{-3}**	**2.0624×10^{21}**
VPOs-OO	793	152.3667	1.1672×10^{-3}	7.0289×10^{20}
	981	188.4888	1.8677×10^{-3}	1.1247×10^{21}
Total :			**3.0349×10^{-3}**	**1.8276×10^{21}**

4.1.5 Series 1: Catalytic Oxidation of *n*-Butane to Maleic Anhydride

The catalytic performances of the bulk VPOs catalysts in Series 1 have been tested at an operating temperature (673 K) for VPO catalysts, with GHSV of 2400 h^{-1} (Leong et al., 2011). The selectivity and activity of catalysts were tested through catalytic test and the catalytic performances of the catalysts are shown in Figure 4.5 and Table 4.4.

The conversion of *n*-butane for VPOs-MM, VPOs-MO, VPOs-OM, and VPOs-OO are 25 %, 20 %, 28 %, and 18 %, respectively, whereas the selectivity to maleic anhydride of the same series catalysts are 91 %, 94 %, 87 %, and 87 %, respectively. Catalysts prepared via microwave irradiation (VPOs-OM, VPOs-MO, VPOs-MM) showed an increment in both activity and selectivity as compared to catalyst produced via conventional oven heating method in both stages (VPOs-OO). These results are in agreement with results obtained in Section 4.1.4 TPR analysis, which stated that microwave irradiation will increase both the selectivity and activity of the catalysts. Since V^{4+} phase contribute to activity while V^{5+} phase contribute to selectivity. VPOs-MO produced more V^{5+} instead of V^{4+} while VPOs-OM is the other way round. Thus, the conversion is higher in OM due to its high amount of V^{4+} which is shown Section 4.1.1 XRD profile, Section 4.1.2 redox titration analysis and Section 4.1.4 TPR analysis indicated that microwave drying in Stage 1 will enhance V^{5+} phase while microwave drying in Stage 2 will enhance V^{4+} phase..

Table 4.4 showed the Turnover Number (TON) of VPOs catalysts in Series 1. TON is the number of moles of substrate that a mole of catalyst can convert before it becomes inactivated. Activity is a function of area and TON is the activity per unit area (intrinsic activity). The catalyst Turnover Number (TON) is an important quantity used for comparing catalyst efficiency. Although the conversion of *n*-butane to maleic anyhydride of VPOs-MO is not the highest among the catalysts in Series 1, but when plotted against the specific surface area of the catalysts (Figure 4.6), it showed to gave the highest rate of conversion of *n*-butane, which might due to the mobility of oxygen associated with V^{4+} phase (showed in TPR, Section 4.1.4) at lower specific surface area.

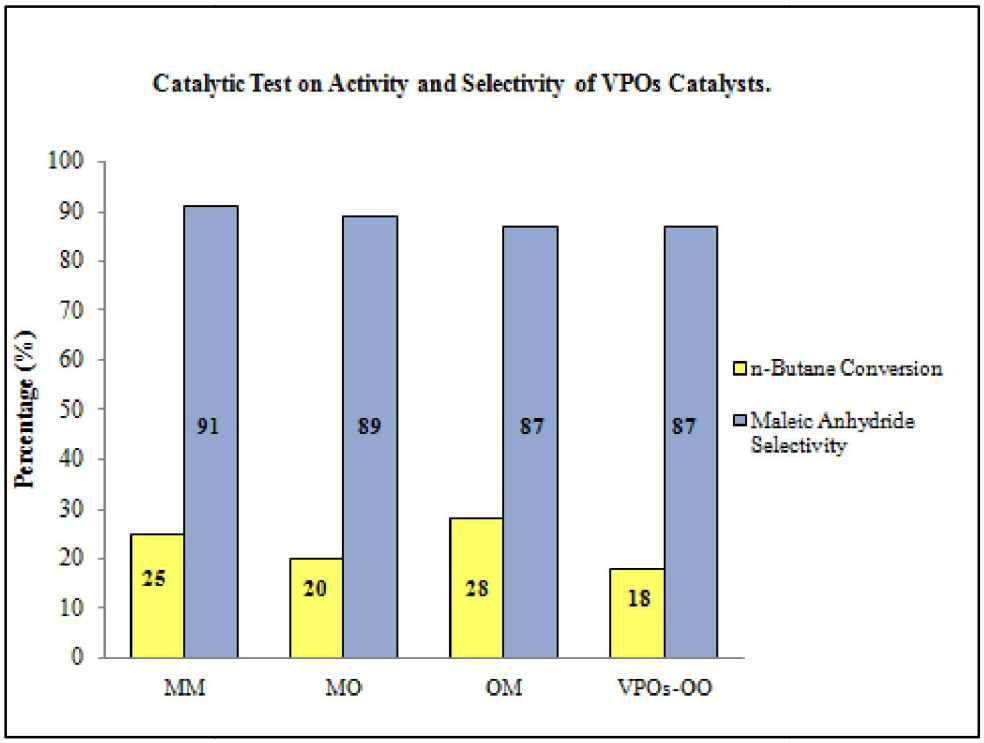

Figure 4.5: Series 1: Chart of catalytic performances for bulk VPOs catalysts

Table 4.4: Series 1: Catalytic performances of bulk VPOs catalysts

Catalyst	*n*-Butane conversion (%)	Turnover number (TON)	Product selectivity (%)		
			MA	CO	CO_2
VPOs-MM	25	1.39	91	3	6
VPOs-MO	20	1.67	89	8	3
VPOs-OM	28	1.33	87	5	8
VPOs-OO	18	1.20	87	6	7

4.1.6 Series 1: Conclusions

Catalysts dried via microwave irradiation drying method gave better catalytic performances with the increment in both activity and selectivity. The use of microwave drying method was observed to induce higher specific surface area and a significant change of morphology of the catalysts. The effect of the drying method of the catalyst precursors will be the key study of this series. Thus, VPOs-MM is used as control for further research in Series 2 and Series 3 due to its balance improvement in activity, selectivity and specific surface area.

4.2 Series 2: Effect of Gallium Dopant and Microwave Drying Method in the Synthesis of Vanadium Phosphorus Oxide Catalysts via sesquihydrate Route

A series of vanadyl pyrophosphate catalysts were prepared via sesquihydrate route and microwave drying added with gallium as dopant. 0.1 %, 0.3 % and 0.5 % of gallium were incorporated into the VPOs catalysts. All the VPOs catalysts in Series 2 were analysed and characterized to show the effect of Ga compared to the VPOs-MM catalyst. The activated catalysts were denoted as VPOs-MM, VPOs-Ga0.1%, VPOs-Ga0.3%, and VPOs-Ga0.5%, where s represents the preparation method, i.e. via sesquihydrate route; MM represents microwave irradiation drying method in both stages of precursor preparation without Ga dopant; and Ga0.1% - 0.5% represents catalysts prepared with microwave irradiation drying method in both stages of precursor preparation added with 0.1 % - 0.5 % Ga as dopant, respectively.

4.2.1 Series 2: X-ray Diffraction (XRD) Analyses

Figure 4.6 shows the XRD patterns for undoped and Ga-doped VPOs catalysts. All the catalysts showed similar diffraction patterns comprised of well-crystallised $(VO)_2P_2O_7$ phase on XRD profiles. Three main characteristic peaks appeared at 2θ = 22.9°, 28.4°, and 29.9°, which are corresponded to (0 2 0), (2 0 4), and (2 2 1) planes, respectively (JCPDS File No. 34-1381). At low level of Ga doping (VPOs-Ga0.1%), there was a slight increment on V^{5+} phase intensity. However, when the amount of dopant increased from 0.1% to 0.5%, the V^{5+} phase intensity decreased. The addition

of Ga gave a slight decreased in the intensity of the reflection peaks at all three characteristic peaks (2θ = 22.9°, 28.4° and 29.9°) corresponded to (0 2 0), (2 0 4), and (2 2 1) reflection planes. This is in agreement with the findings by Sartoni et al. (2004), which showed that the addition of higher concentrations of $Ga(acac)_3$ in catalyst prepared via hemihydrates and conventional heating, leads to a significant decrease in the intensity of the (0 0 1) reflection relative to the (2 2 0) reflection (Sartoni et al., 2004).

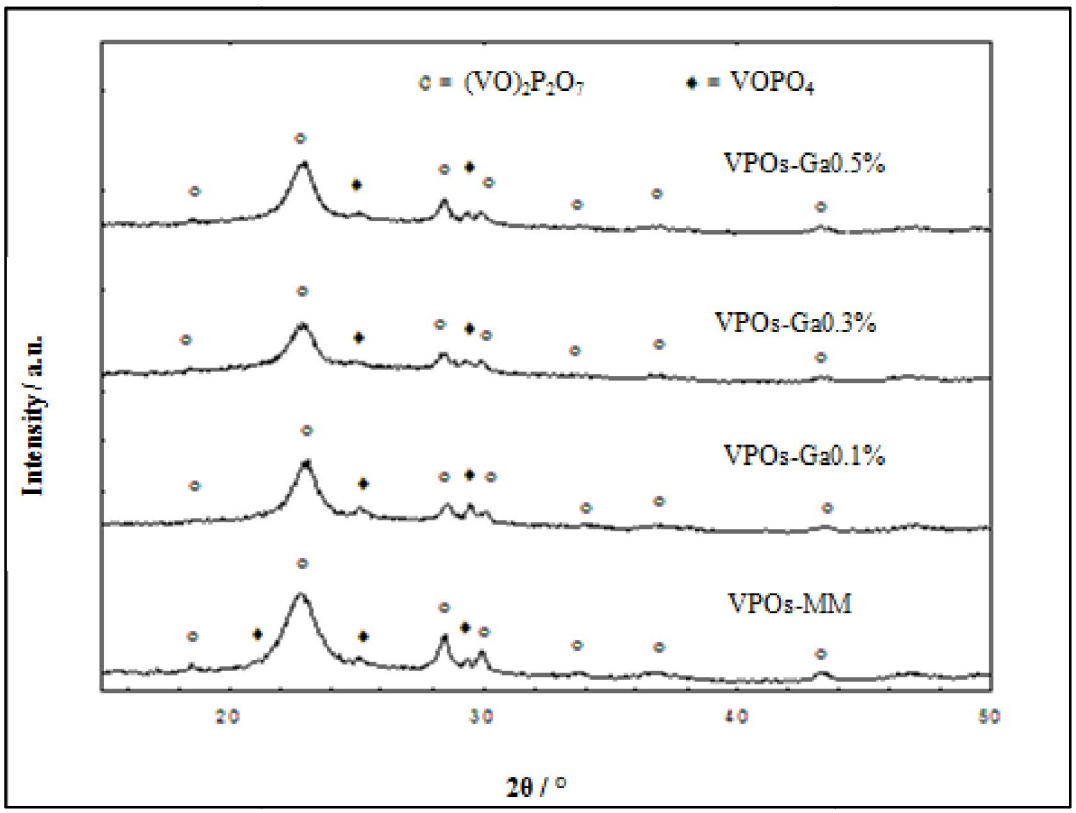

Figure 4.6: Series 2: Powder XRD pattern of VPOs catalysts

In Table 4.5, the crystallite size of (0 2 0) reflection plane for VPOs-MM, VPOs-Ga0.1%, VPOs-Ga0.3% and VPOs-0.5% were calculated as 54 Å, 69 Å, 69 Å and 65 Å, respectively. The crystallite size of (2 0 4) reflection plane for the same series of catalysts produced were 113 Å, 117 Å, 117 Å and 102 Å, respectively. Previous studies had proposed that the crystallite size and the activity of the VPOs catalysts are inversely proportional due to the reason that smaller crystallite size contributed to a better active phase for the oxidation of *n*-butane to MA. The incorporation of gallium into the VPOs catalysts produced catalysts with larger crystallite sizes in the (0 2 0) direction and (2 0 4), except for VPOs-Ga0.5% which showed a slightly smaller crystallite size in (2 0 4) reflection plane. This is in agreement with the XRD profile (Figure 4.6) which shows that V^{4+} is the predominant phases in VPOs-Ga0.5%.

Table 4.5: Series 2: XRD data of VPOs catalysts

Catalysts	Linewidth[a] (0 2 0) (°)	Linewidth[b] (2 0 4) (°)	Crystallite size[c] (0 2 0) (Å)	Crystallite size[c] (2 0 4) (Å)
VPOs-MM	1.4853	0.7180	54	113
VPOs-Ga0.1%	1.1551	0.6927	69	117
VPOs-Ga0.3%	1.1596	0.6957	69	117
VPOs-Ga0.5%	1.2252	0.7977	65	102

[a] Full-witdth half maximum (FWHM) of (020) reflection plane
[b] Full-witdth half maximum (FWHM) of (020) reflection plane
[c] Crystallite size by means of Scherrer's formula

4.2.2 Series 2: Brunauer-Emmett-Teller (BET) Surface Area Measurement and Chemical Analyses

As tabulated in Table 4.6, the specific surface area of VPOs catalysts are as follows; 18 m^2g^{-1} for VPOs-MM, 19 m^2g^{-1} for VPOs-Ga0.1%, 18 m^2g^{-1} for VPOs-Ga0.3%, and 13 m^2g^{-1} for VPOs-Ga0.5%. As compared to the VPOs-MM (18 m^2g^{-1}), Ga-doped catalysts did not show obvious increment on the specific surface area. As the Ga concentration increased from 0.1% to 0.5%, a reduce trend in specific surface area was observed. This suggests that gallium when added into VPOs catalysts prepared via sesquihydrate route with microwave drying method, does not gives rise to the standard promotion on surface area which was often happened on addition of metal cation to VPO catalysts synthesised via hemihydrates route (Sartoni et al., 2004). When the concentration of Ga increased in the VPOs catalysts, the specific surface area reduced due to the reason that the Ga dopant has caused the agglomerate of VPOs crystal platelets to form a bulkier structure which was confirmed with SEM in Section 4.2.3.

The average oxidation numbers of vanadium and the composition of V^{5+} and V^{4+} oxidation states are tabulated in Table 4.6. The P/V atomic ratio for VPOs-MM, VPOs-Ga0.1%, VPOs-0.3%, and VPOs-0.5% are 1.30, 1.22, 1.15, and 1.25 respectively. As for EDAX analyses, results observed for P/V ratio fall within the range of 1.05 to 1.33 (Centi, 1993). As shown in Table 4.6, Ga dopant does not significantly affect the average oxidation of the VPOs catalysts prepared via sesquihydrate route with the aid of microwave irradiation drying method.

Table 4.6: Series 2: Percentages of V^{4+} and V^{5+} oxidation states present, Specific BET surfaces areas, and chemical compositions of VPOs catalysts

Catalysts	Surface Area (m^2/g)	P/V Ratio (ICP-OES)	P/V Ratio (EDX)	Average oxidation numbers of vanadium		
				V^{4+} (%)	V^{5+} (%)	V_{AV}
VPOs-MM	18	1.30	1.33	53.57	46.43	**4.4643**
VPOs-Ga0.1%	19	1.22	1.02	52.94	47.06	**4.4706**
VPOs-Ga0.3%	18	1.15	1.01	45.78	54.22	**4.5422**
VPOs-Ga0.5%	13	1.25	1.04	56.31	43.69	**4.4369**

4.2.3 Series 2: Scanning Electron Microscopy (SEM) Analyses

Figure 4.7 showed the surface morphology of VPOs-MM, VPOs-Ga01%, VPOs-Ga0.3%, and VPOs-Ga0.5%. Previous studies had shown that VPO catalyst will formed secondary structures with different sizes of plate-like crystal, which were agglomerated into the characteristics of rosette-shape clusters (Leong et al., 2010). However, unlike catalyst prepared via conventional oven drying which shows the typical rosette-type structure, all the catalysts were dried using microwave irradiation and thus form a structure with crystal-like clusters that stacks up to form rosette shape. Due to the microwave irradiation as drying method in both stages of precursor

preparation, all the catalysts prepared in Series 2 failed to show the folded-edges structure which is the characteristic of catalysts prepared via sesquihydrate route.

Catalysts doped with gallium (Figure 4.7) show more compact structures with further agglomeration of the crystal-like clusters layering in rosette shape. At higher amount of gallium dopants (VPOs-Ga0.5%) a bulkier morphology is formed and thus decreased the specific surface area of the catalyst (as shown in Table 4.6). These results contradict with Sartoni et.al. (2004) study on hemihydrates VPO catalysts which indicated that the increasing amount of $Ga(acac)_3$ decreased the size of platelets. The high amount V^{5+} phase in the increasing concentration of Ga in VPOs catalysts is the main contribution to bulkier structure shown in SEM.

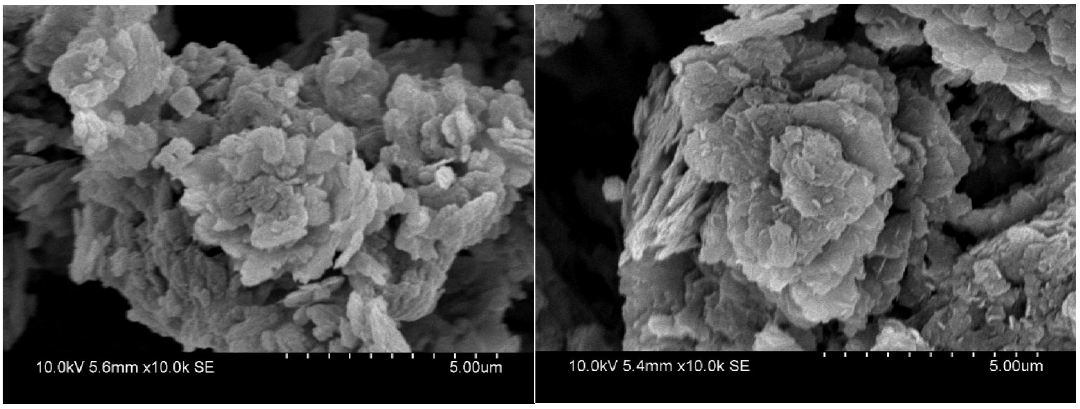

(a) **(b)**

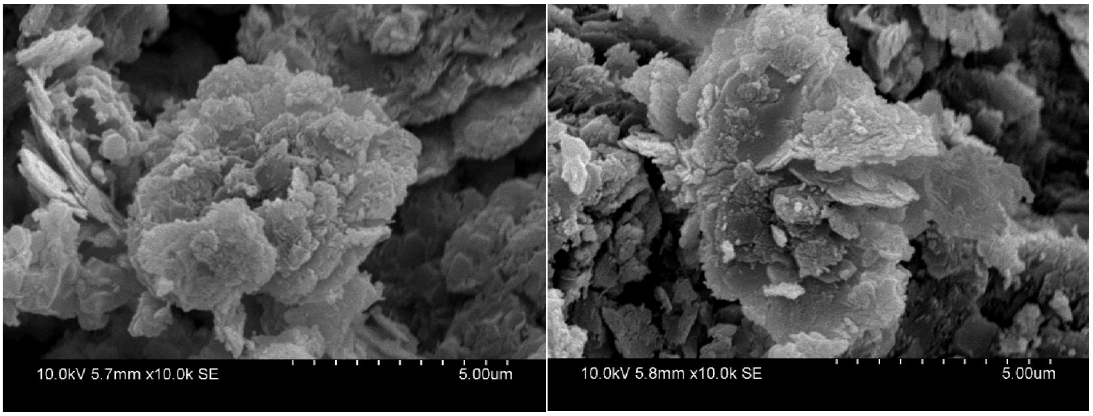

(c) **(d)**

Figure 4.7: SEM micrographs of (a) VPOs-MM (b) VPOs-Ga0.1% (c) VPOS-Ga0.3% and (d) VPOs-Ga0.5% catalysts

4.2.4 Series 2: Temperature Programmed Reduction (TPR of H_2/N_2)

From Figure 4.8, VPOs-MM catalyst showed 2 maxima peaks emerged at 793 K and 1007 K. VPOs-Ga0.1% catalyst, VPOs-Ga0.3%, and VPOs-Ga0.5% have maxima peaks at 786 K and 1030 K, 858 K and 963 K, 846 K and 1072 K, respectively. This observation showed two kinetically different reduction peaks appeared and thus implied the presence of two types of oxygen species being removed during the analysis. Previous chapter had stated that the first peak is the reduction of V^{5+} phases whereas the second peak is assigned to the removal of lattice oxygen from the active V^{4+} phase. Previously, electrical conductivity studies on VPO catalysts suggested that O^{2-} is related to V^{5+} phase, while O^{-} is associated with the V^{4+} phase (Taufiq-Yap, 2006).

Figure 4.8 showed that the reduction of V^{4+} species appeared to be more dominant for VPOs-Ga0.5% catalyst, which is well agreed with the redox titration and XRD profile; indicated that V^{4+} is the predominant species in this catalyst. The V^{5+} peak appeared to be more dominant on VPOs-Ga0.3%, which is in agreement with the redox titration indicating higher percentage of V^{5+} in this individual catalyst.

For higher Ga-doped catalysts (VPOs-Ga0.5%) second reduction peak temperature emerged at higher temperature as compared to undoped catalyst. The increment in the reduction temperature indicated that the gallium would strengthen the bonding between the oxygen species and the VPO matrix. This eventually increased the reduction activation energy of O^{-}-V^{4+} for Ga-doped VPOs catalysts.

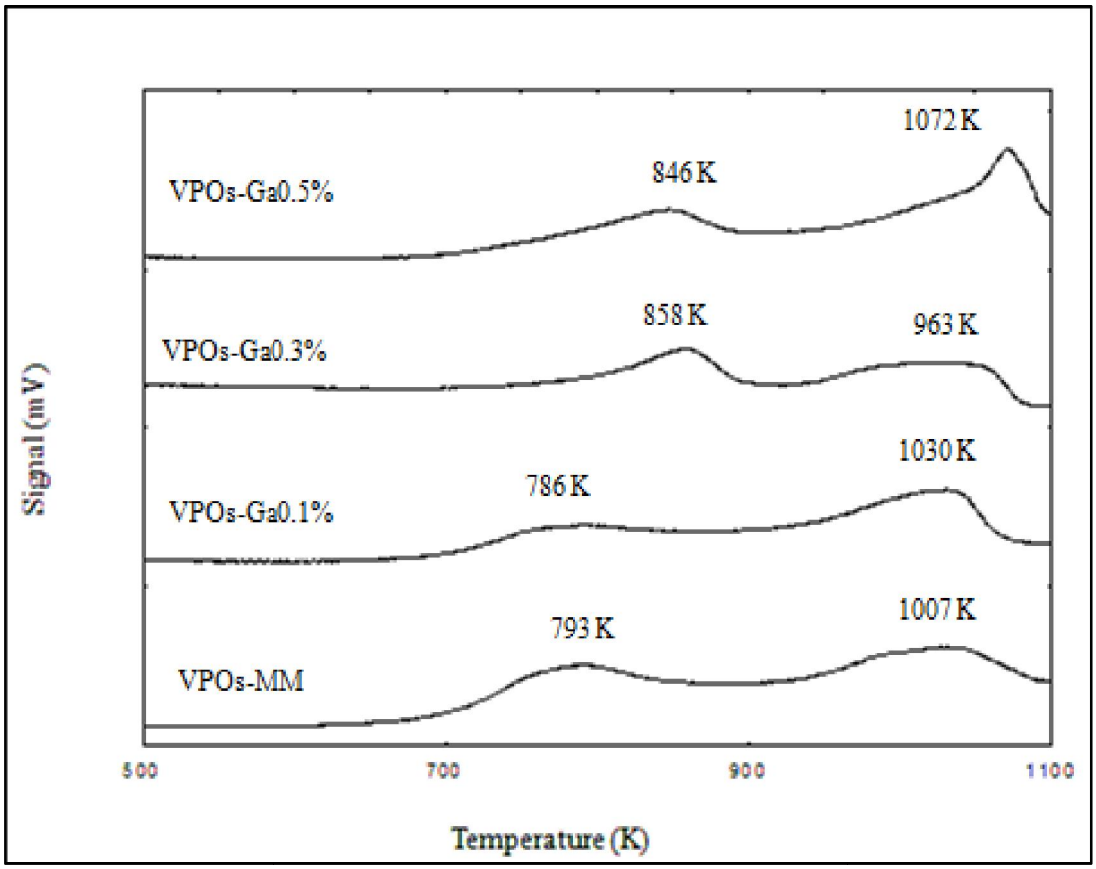

Figure 4.8: Series 2: TPR in H_2/N_2 profiles for VPOs catalysts

The amount of oxygen removed associated to V^{4+} phase (O^--V^{4+}) and V^{5+} phase (O^{2-}-V^{5+}) are calculated and shown in Table 4.7. VPOs-Ga0.5% exhibited the highest amount of oxygen atoms (O^-) removed from V^{4+} phase (i.e. 2.6624 x 10^{21} atom/g). This is in agreement with the XRD analysis indicating that more intense peaks assigned to V^{4+} phase were observed in the XRD profile. Comparatively, VPOs-MM, VPOs-Ga0.1% and VPOs-Ga0.3% exhibited lower amount of O^--V^{4+} could be removed from their lattice (i.e. 1.5819 x 10^{21} atom/g, 1.4194 x 10^{21} atom/g and 1.4339 x 10^{21} atom/g, respectively). The removal of oxygen species associated to V^{4+} (O^--V^{4+}) and V^{5+} (O^{2-}-V^{5+}) were found to increase by 68 % and 7 %

respectively, when the catalysts were doped at higher amount of gallium (VPOs-Ga0.5%) in comparison to VPOs-MM. The total amount of H_2 consumption increased by 46 % had suggested that catalyst doped with considerable amount of gallium is capable of producing VPOs catalysts with higher TON. This is in agreement with the XRD profile (Figure 4.6) where there was increment in the V^{4+} phase when the VPOs catalysts were doped with Ga dopant.

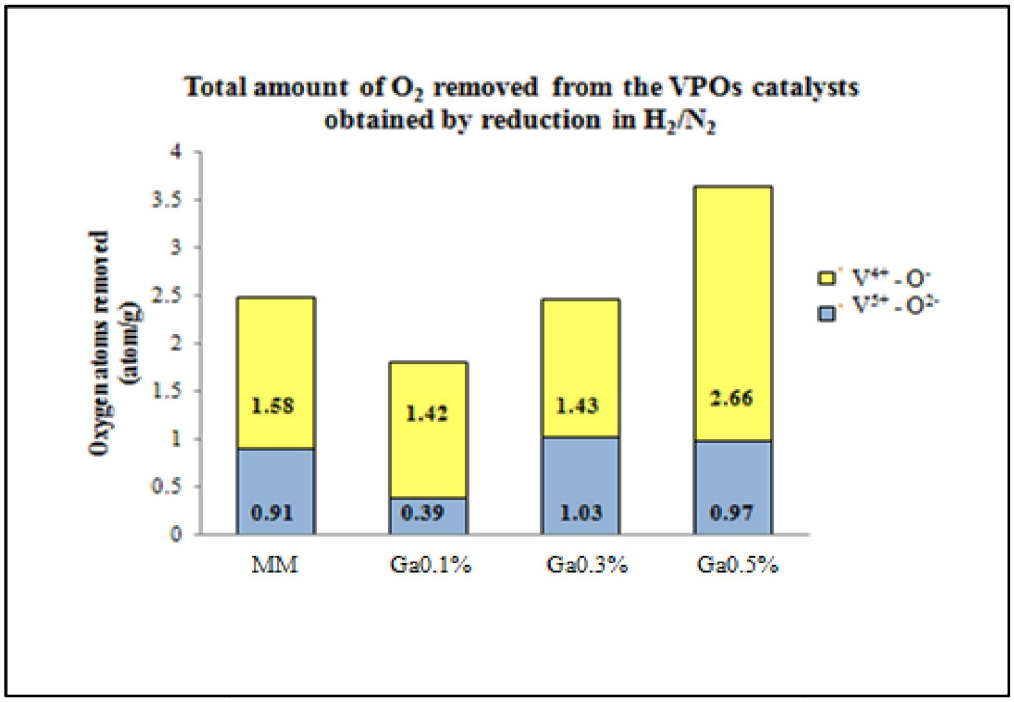

Figure 4.9: Series 2: Data chart of TPR in H_2/N_2 for VPOs catalysts

Table 4.7: Series 2: Total amount of O_2 removed from the VPOs catalysts obtained by reduction in H_2/N_2

Catalysts	T_{max} (K)	Reduction activation energy, E_r (kJ mol^{-1})	Oxygen atoms removed (mol/g)	Oxygen atoms removed (atom/g)
VPOs-MM	793	152.3667	1.5032×10^{-3}	9.0511×10^{20}
	1007	193.4845	2.6269×10^{-3}	1.5819×10^{21}
Total :			**4.1301×10^{-3}**	**2.4871×10^{21}**
VPOs-Ga0.1%	786	151.0217	6.4066×10^{-4}	3.8581×10^{20}
	1030	197.9037	2.3570×10^{-3}	1.4194×10^{21}
Total :			**2.9976×10^{-3}**	**1.8052×10^{21}**
VPOs-Ga0.3%	858	164.8557	1.7101×10^{-3}	1.0298×10^{21}
	963	185.0304	2.3811×10^{-3}	1.4339×10^{21}
Total :			**4.0912×10^{-3}**	**2.4637×10^{21}**
VPOs-Ga0.5%	846	162.5501	1.6140×10^{-3}	9.7195×10^{20}
	1072	205.9736	4.4212×10^{-3}	2.6624×10^{21}
Total :			**6.0352×10^{-3}**	**3.6344×10^{21}**

4.2.5 Series 2: Catalytic Oxidation of *n*-Butane to Maleic Anhydride

The selectivity and conversion of *n*-butane to maleic anhydride of catalysts were tested through catalytic test and the catalytic performances of the catalysts are shown in Table 4.8. The conversion of *n*-butane for VPOs-MM, VPOs-Ga0.1%, VPOs-Ga0.3%, and VPOs-0.5% are 25 %, 29 %, 28 %, and 23 %, respectively, whereas the selectivity to maleic anhydride of the same series catalysts are 91 %, 94 %, 95 %, and 95 %, respectively. Although the conversion of *n*-butane to maleic anyhydride decreased with increasing doping of gallium, but when plotted against the specific surface area of the catalysts (TON), it showed a trend of increasing which is in agreement will all the previous analysis indicating that VPOs-Ga0.5% gave the highest rate of conversion of *n*-butane. The high TON number of VPOs-0.5% has overcome its low specific surface area and low conversion rate due to the reason that

VPOs-Ga0.5% exhibited the highest amount of oxygen atoms (O^-) removed from V^{4+} phase as shown in Section 4.2.4.

Previous study of Sartoni et al. (2004) had proposed that lower Ga doping (0.1% mol) produced using $Ga(acac)_3$ shown to have the best activity. However, the activity and selectivity for VPO catalysts that produced through hemihydrates route with conventional heating method was not markedly affected by increasing amount of Ga dopant.

With respect to the results above, it could be concluded that Ga doped in catalyst prepared via sesquihydrate route and treated with microwave drying method could improve the mobility of oxygen atoms (O^-) associated with V^{4+} phase (Section 4.2.4) thus giving a high TON number. The incensement of TON gave an important improvement to the VPOs catalyst due to the reason that the conversion will be fairly high using only a small amount of catalyst.

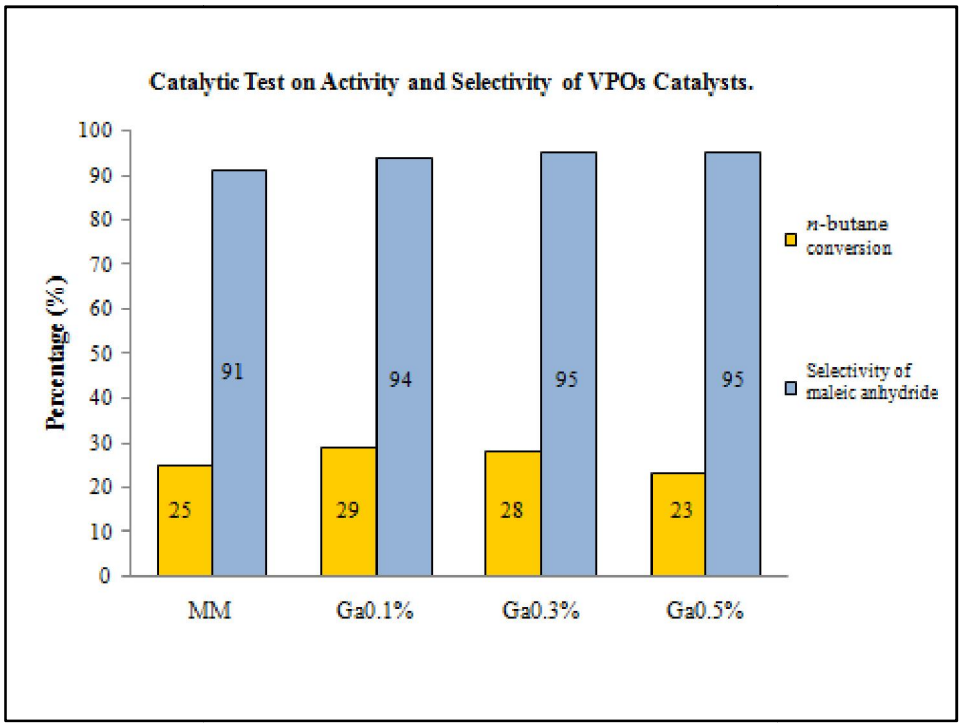

Figure 4.10: Series 2: Chart of catalytic performances for VPOs catalysts

Table 4.8: Series 2: Catalytic performances of VPOs catalysts

Catalyst	*n*-Butane conversion (%)	Turnover Number (TON)	Product selectivity (%)		
			MA	CO	CO_2
VPOs-MM	25	1.39	91	3	6
VPOs-Ga0.1%	29	1.53	94	5	1
VPOs-Ga0.3%	28	1.56	95	4	1
VPOs-Ga0.5%	23	1.77	95	4	1

4.2.6 Series 2: Conclusions

The use of higher gallium dopant concentration in catalysts prepared via microwave drying method was observed to induce higher V^{4+} phase and a significant change of morphology of the catalysts. It is believed that the preparation method via sesquihydrate, microwave irradiation, and additional of gallium has successfully increased the overall performance of the catalyst. The presence of Ga would induce higher removal of oxygen species and eventually increase the TON value of the synthesised VPOs catalysts. The combination of microwave energy level and Ga-dopant bonding in the VPOs catalysts has improved the mobility of oxygen atoms (O^-) associated with V^{4+} phase which cause VPOs-Ga0.5% to contribute highest conversion rate of *n*-butane to MA with minimal specific surface area used.

4.3 Series 3: Effect of microwave irradiation and reflux methods in the synthesis of vanadium phosphorus oxide catalysts via sesquihydrate route

A bulk catalyst, VPOs-R_sR_s (named as VPOs-MM in Series 1) produced by reflux synthesis process was used in Series 3 for the comparison of microwave irradiation effect in synthesis of VPOs catalysts. The activated catalysts were denoted as VPOs-M_sM_s, VPOs-R_sR_s, VPOs-R_sM_s and VPOs-M_sR_s where VPOs represents the catalyst prepared via sesquihydrate route; M_s represent microwave irradiation synthesis process; and R_s represents the reflux synthesis process. The position of M_s/R_s represents the Stage 1 and Stage 2 synthesis respectively.

4.3.1 Series 3: X-ray Diffraction (XRD) Analyses

Figure 4.11 shows the XRD patterns for VPOs-M_sM_s, VPOs-R_sR_s, VPOs-R_sM_s and VPOs-M_sR_s. All the catalysts showed similar diffraction patterns comprised of well-crystallised $(VO)_2P_2O_7$ phase. Three main characteristic peaks appeared at 2θ = 22.9 °, 28.4 °, and 29.9 °, which are corresponded to (0 2 0), (2 0 4), and (2 2 1) planes, respectively (JCPDS File No. 34-1381). The intensities of (0 2 0) and (2 0 4) for both VPOs-M_sM_s and VPOs-R_sR_s were found to be more intense as compared to VPOs-R_sM_s and VPOs-M_sR_s. As observed in Figure 4.11, there were additional weak peaks emerged at around 2θ = 21.3˚, 25.3˚, and 29.3˚ for VPOs-M_sM_s and VPOs-R_sR_s, which peaks are corresponded to various V^{5+} phases, such as β-$VOPO_4$ (JCPDS File No. 27-0948, 2θ= 21.3˚), and α_{II}-$VOPO_4$ (JCPDS File No. 34-1247, 2θ= 25.3˚ and 29.3˚) while VPOs-M_sR_s and VPOs-R_sM_s only showed an extra peak on 21.3˚. These indicated that catalysts synthesised using same method on both stages (VPOs-M_sM_s and VPOs-R_sR_s) would promote higher formation of V^{5+} phase at 2θ= 25.3˚ in the catalysts as clearly shown in Figure 4.11. As for VPOs-M_sM_s, the intensity of the V^{5+} phase at 2θ = 21.3˚ increases intensively.

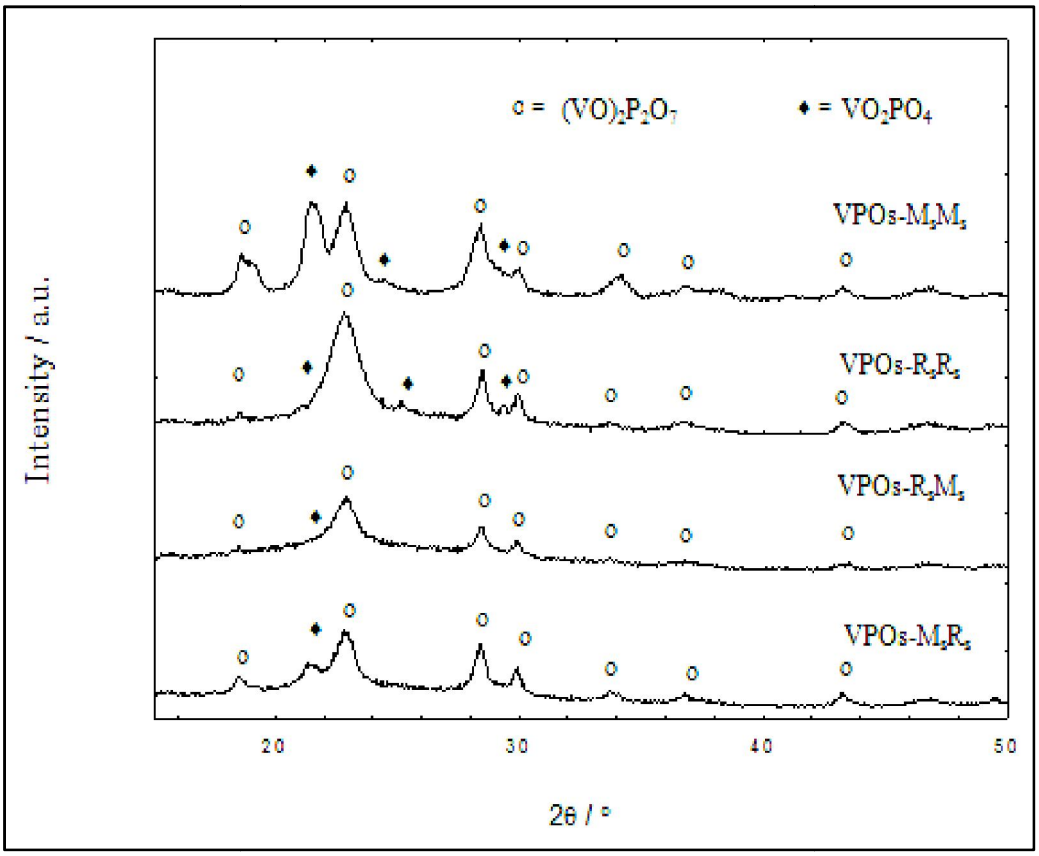

Figure 4.11: Series 3: Powder XRD pattern of bulk VPOs catalysts

Table 4.9: Series 3: XRD data of bulk VPOs catalysts

Catalysts	Linewidth[a] (0 2 0) (°)	Linewidth[b] (2 0 4) (°)	Crystallite size[c] (0 2 0) (Å)	Crystallite size[c] (2 0 4) (Å)
VPOs-M_sM_s	0.9346	0.8945	86	122
VPOs-R_sR_s	1.4853	0.7180	54	113
VPOs-R_sM_s	1.2191	0.6871	66	118
VPOs-M_sR_s	1.0404	0.6620	77	129

[a] Full-witdth half maximum (FWHM) of (020) reflection plane
[b] Full-witdth half maximum (FWHM) of (020) reflection plane
[c] Crystallite size by means of Scherrer's formula

The crystallite size of (0 2 0) reflection plane for VPOs-M_sM_s, VPOs-R_sR_s, VPOs-R_sM_s and VPOs-M_sR_s were calculated as 86 Å, 54 Å, 66 Å and 77 Å, respectively. The crystallite size of (2 0 4) reflection plane for the same series of catalysts produced were 122 Å, 113 Å, 118 Å and 129 Å, respectively. The microwave irradiation gave a different effect on the catalysts during synthesis in Stage 1 and Stage 2 separately. When microwave irradiation involved in Stage 1, both crystallite sizes of the catalysts (VPOs-M_sM_s and VPOs-M_sR_s) at (0 2 0) and (2 0 4) planes increased as compared to catalysts synthesised via reflux on stage 1 (VPOs-R_sM_s and VPOs-R_sR_s). These results showed that microwave irradiation, applied on Stage 1, has effect on increasing the crystallite size of bulk VPOs catalysts.

4.3.2 Series 3: Brunauer-Emmett-Teller (BET) Surface Area Measurement and Chemical Analyses

As tabulated in Table 4.10, the specific surface area of VPOs catalysts are as follows; 24 m^2g-^{1} for VPOs-M_sM_s, 18 m^2g^{-1} for VPOs-R_sR_s, 17 m^2g^{-1} for VPOs-R_sM_s, and 21 m^2g^{-1} for VPOs-M_sR_s. In previous study, Rownaghi and co-workers had reported that catalyst prepared via VPD method involving microwave irradiation exhibited larger specific surface area (Rownaghi et al., 2009b). This is somehow in agreement with catalysts prepared via VPS method as well, where catalyst synthesised by microwave on Stage 1 (VPOs-M_sR_s and VPOs-M_sM_s) has larger specific surface area as compared to catalysts synthesised via reflux on Stage 1 (VPOs-R_sM_s and VPOs-

R_sR_s). The comparison between these catalysts has indicated the improvement on specific surface area will only happened when the catalyst were prepared using microwave irradiation synthesis method on Stage 1.

It could be notified that VPOs catalysts prepared via microwave irradiation on both Stage 1 and Stage 2 exhibited the largest specific surface area as compared to other catalysts. Further analysis by secondary electron images from SEM micrographs proved that microwave irradiation altered the surface morphology of the synthesised catalysts.

From Table 4.10, the P/V atomic ratio for VPOs-M_sM_s, VPOs-R_sR_s, VPOs-R_sM_s, and VPOs-M_sR_s are 1.29, 1.30, 1.28, and 1.26 respectively. As for EDAX analyses, results observed for P/V ratio fall within the range of 1.05 to 1.35. As mentioned previously, the optimum P/V atomic ratio range in producing active and selective $(VO)_2P_2O_7$ phase fall within the range 1.0-1.2 (Centi, 1993). The high P/V atomic ratio observed for VPOs-R_sR_s indicated that both microwave drying method and reflux synthesised would induced the phosphorus surface enrichment.

The average oxidation numbers of vanadium and the composition of V^{5+} and V^{4+} oxidation states are tabulated in Table 4.10. VPOs-M_sM_s and VPOs-R_sR_s showed a higher average oxidation numbers of vanadium which is in agreement with the XRD (Section 4.3.1) profile and TPR (Section 4.3.4) indicated the V^{5+} phases in the VPOs catalysts could be induced when microwave (VPOs-M_sM_s) or reflux (VPOs-R_sR_s) method were employed in both stages during the synthesis.

Table 4.10: Series 3: Percentages of V^{4+} and V^{5+} oxidation states present, Specific BET surfaces areas, and chemical compositions of VPOs catalysts

Catalysts	Surface Area (m^2/g)	P/V Ratio (ICP-OES)	P/V Ratio (EDX)	Average oxidation numbers of vanadium		
				V^{4+} (%)	V^{5+} (%)	V_{AV}
VPOs-M_sM_s	24	1.29	1.14	47.72	52.28	**4.5228**
VPOs-R_sR_s	18	1.30	1.33	53.57	46.43	**4.4646**
VPOs-R_sM_s	17	1.28	1.24	57.14	42.86	**4.4286**
VPOs-M_sR_s	21	1.26	1.01	76.20	23.80	**4.2380**

4.3.3 Sereis 3: Scanning Electron Microscopy (SEM) Analyses

The surface morphology of VPOs-M_sM_s, VPOs-R_sR_s, VPOs-R_sM_s, and VPOs-M_sR_s catalysts are shown in Figure 4.12. In general, VPO catalyst will form secondary structures with different sizes of plate-like crystal, which were agglomerated into the clusters of $(VO)_2P_2O_7$ platelets that preferentially exposing the (1 0 0) crystal plane (Kiely et al., 1995). As observed in Figure 4.12, since all the catalysts were dried by microwave irradiation, thus, they formed agglomerated crystal-like clusters that stacked up in layer forming rosette shaped, except for VPOs-M_sM_s.

VPOs-M_sM_s showed a secondary structure of chrysanthemum needle-like morphology with sharp edges. These phenomena only occurred when the catalyst was synthesized via microwave irradiation on both stages. This interesting feature

had contributed to the higher specific surface area of the catalyst. The crystal growth is usually sensitive to the initial nucleation process. In conventional heating method, crystals tend to nucleate on container walls or impurity particles, leading to a slow growth rate due to rather few nuclei. Therefore, when microwave irradiation is employed for the synthesis of VPOs catalyst, the energy of microwave irradiation leads to rapid nucleation rate and induced the formation of massive nuclei throughout the bulk solution (Zhang and Zhu, 2008).

VPOs-M_sM_s and VPOs-M_sR_s showed to form thinner crystal platelets as compared to VPOs-R_sM_s and VPOs-R_sR_s which were in agreement with BET surface area analysis. VPOs-M_sM_s and VPOs-M_sR_s showed a larger specific surface area as compared to VPOs-R_sM_s and VPOs-R_sR_s.

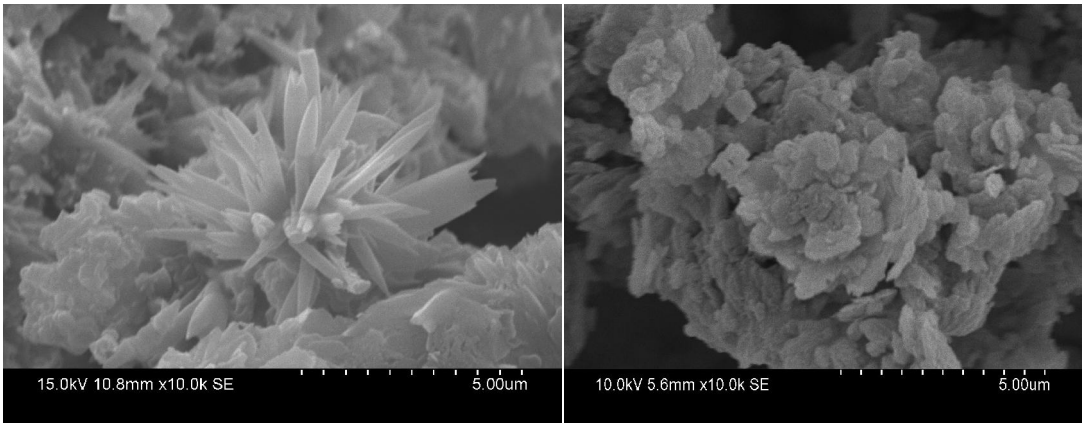

(a) **(b)**

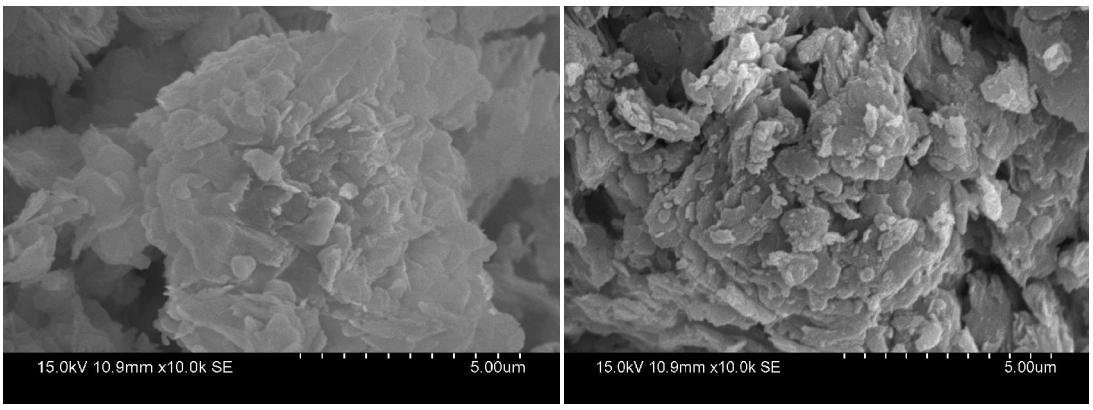

(c) **(d)**

Figure 4.12: SEM micrographs of (a)VPOs-M_sM_s (b)VPOs-R_sR_s (c)VPOs-R_sM_s and (d)VPOs-M_sR_s catalysts

4.3.4 Series 3: Temperature Programmed Reduction (TPR of H_2/N_2)

From Figure 4.13, VPOs- M_sM_s catalyst showed 2 peaks maxima at 866 K and 1056 K, while VPOs-R_sR_s catalyst and VPOs-M_sR_s both having peaks maximised at 793 K and 1007 K. As for VPOs-R_sM_s catalyst, the maxima peak appeared at 833 K and 1009 K.

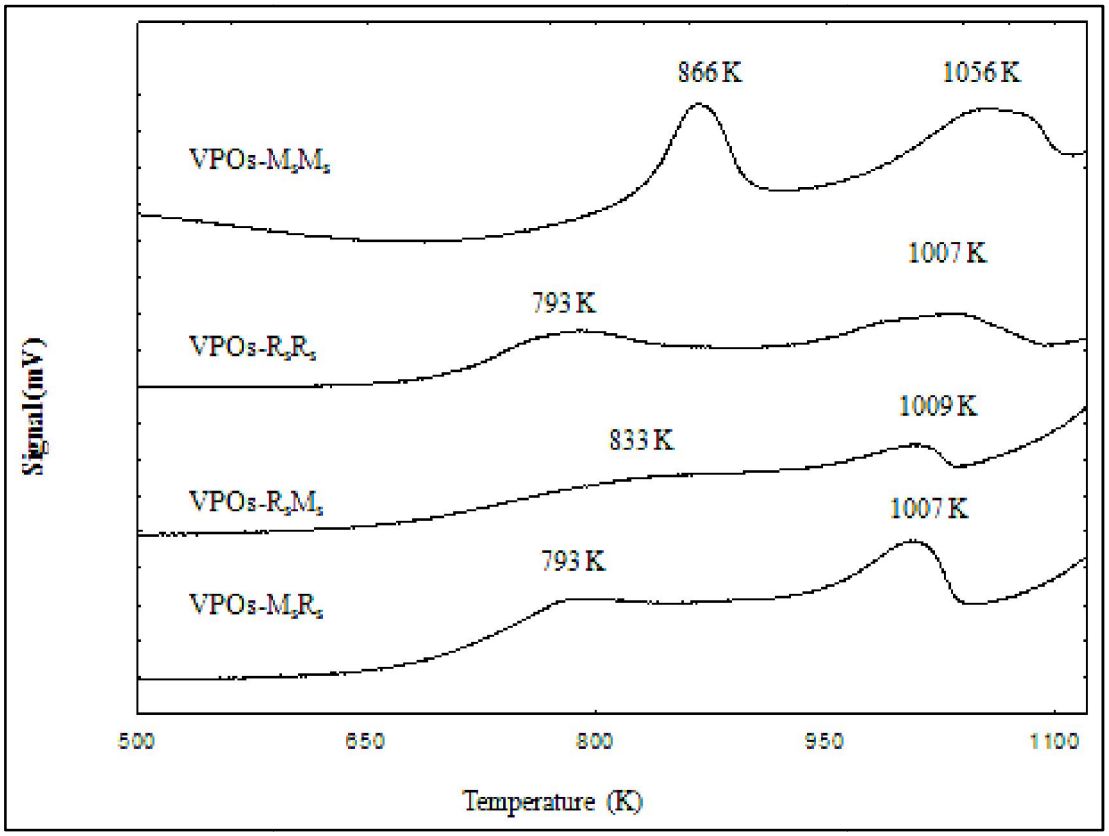

Figure 4.13: Series 3: TPR in H_2/N_2 profiles for VPOs catalysts

For VPOs-M_sM_s, both reduction temperatures appeared at higher values as compared to other catalysts. The increase in the reduction temperature indicated that the microwave-assisted catalysts contained physically stronger pellets than those produced by reflux method, which may due to the energy employed on the catalysts during synthesis.

The amount of oxygen removed associated to V^{4+} phase (O^--V^{4+}) and V^{5+} phase (O^{2-}-V^{5+}) were calculated and shown in Table 4.11. As mentioned in previous section, the first peak removal of O^{2-}-V^{5+} species, whereas the second peak was attributed to the removal of O^--V^{4+} species. Catalyst VPOs-R_sR_s exhibited the highest amount of oxygen atoms removed (2.4871 x 10^{21} atom/g) as compared VPOs-M_sM_s, VPOs-R_sM_s and VPOs-M_sR_s catalysts, which were 2.4278 x 10^{21} atom/g, 1.0004 x 10^{21} atom/g, and 1.8805 x 10^{21} atom/g, respectively. The total H_2 consumption was found to decrease by 2 % to 60 % when the catalysts were synthesised using microwave irradiation as compared to catalyst synthesized by reflux method only. As mentioned above, the microwave-assisted catalysts contain physically stronger pellets, thus the mobility of oxygen species was observed to be lower as compared to the catalyst synthesized via reflux methods. This is due to the higher bonding strength in between the oxygen species and VPO matrix.

VPOs-M_sM_s and VPOs-R_sR_s exhibited a high amount of oxygen atoms (O^-) removed from V^{4+} phase (i.e. 1.6692 x 10^{21} atom/g and 1.5818 x 10^{21} atom/g, respectively). This is in agreement with the XRD analysis indicating that more prominent peaks assigned to V^{4+} phase were observed in the XRD profile.

Comparatively, VPOs-R_sM_s and VPOs-M_sR_s exhibited lower amount of O^--V^{4+} could be removed from their lattice; i.e. 6.0425 x 10^{20} atom/g, 8.8036 x 10^{20} atom/g, respectively. The amount of oxygen associated to V^{5+} (O^{2-}-V^{5+}) was found to be higher on VPOs-R_sR_s catalysts among all the catalysts prepared. Higher total amount of H_2 consumption from microwave drying catalyst suggested that microwave irradiation is capable of producing active and selective VPOs catalysts.

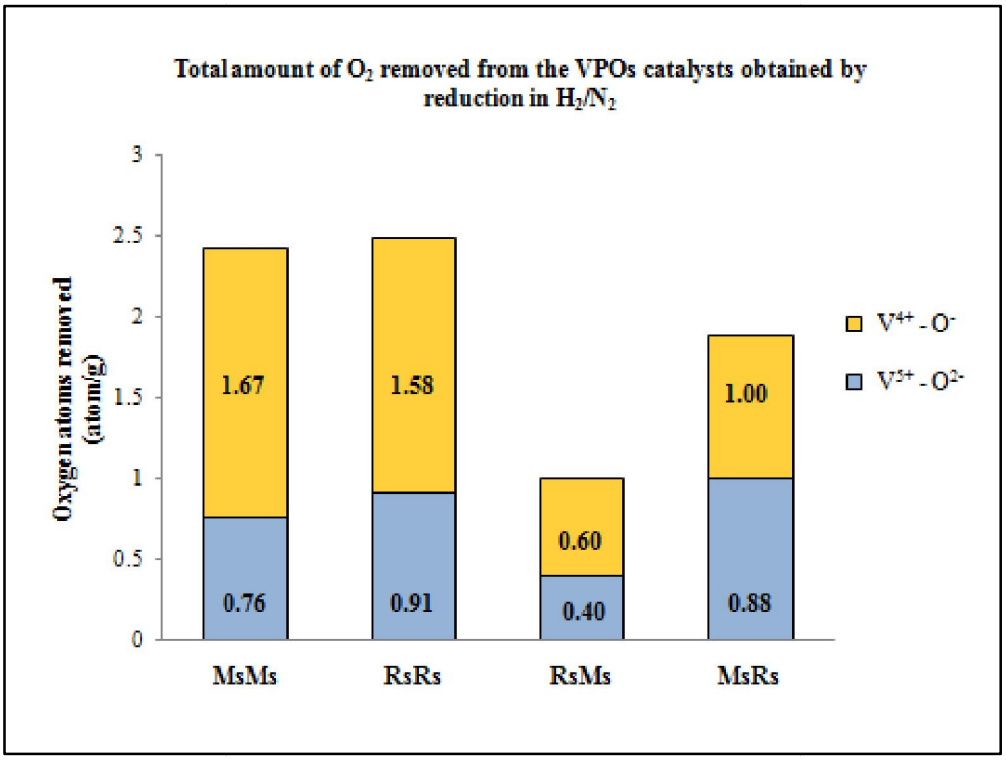

Figure 4.14: Series 3: Data chart of TPR in H_2/N_2 for VPOs catalysts

Table 4.11: Series 3: Total amount of O_2 removed from the VPOs catalysts obtained by reduction in H_2/N_2

Catalysts	T_{max} (K)	Reduction activation energy, E_r(kJ mol^{-1})	Oxygen atoms removed (mol/g)	Oxygen atoms removed (atom/g)
VPOs-M_sM_s	866	166.3929	1.2597×10^{-3}	7.5859×10^{20}
	1056	202.8993	2.7719×10^{-3}	1.6692×10^{21}
Total :			**4.0316×10^{-3}**	**2.4278×10^{21}**
VPOs-R_sR_s	793	152.3667	1.5032×10^{-3}	9.0523×10^{20}
	1007	193.4845	2.6267×10^{-3}	1.5818×10^{21}
Total :			**4.1301×10^{-3}**	**2.4871×10^{21}**
VPOs-R_sM_s	833	160.0522	6.5780×10^{-4}	3.9613×10^{20}
	1009	193.8688	1.0034×10^{-3}	6.0425×10^{20}
Total :			**1.6612×10^{-3}**	**1.0004×10^{21}**
VPOs-M_sR_s	793	152.3667	1.6608×10^{-3}	1.0001×10^{21}
	1007	193.4845	1.4619×10^{-3}	8.8036×10^{20}
Total :			**3.1227×10^{-3}**	**1.8805×10^{21}**

4.3.5 Series 3: Catalytic Oxidation of *n*-Butane to Maleic Anhydride

The activity and selectivity of catalysts were analysed through catalytic test results are shown in Table 4.12. The conversion of *n*-butane for VPOs- M_sM_s, VPOs-R_sR_s, VPOs-R_sM_s, and VPOs-M_sR_s are 34%, 25%, 19%, and 23%, respectively, whereas the selectivity to maleic anhydride of the catalysts mentioned above are 95%, 91%, 88%, and 93%, respectively. Catalyst prepared via microwave irradiation on both Stage 1 and Stage 2 (VPOs-M_sM_s) showed the highest amount in both activity and selectivity among the same series catalysts. These results are in agreement with results obtained in XRD, which stated that microwave irradiation would increase both the selectivity and activity of the catalysts.

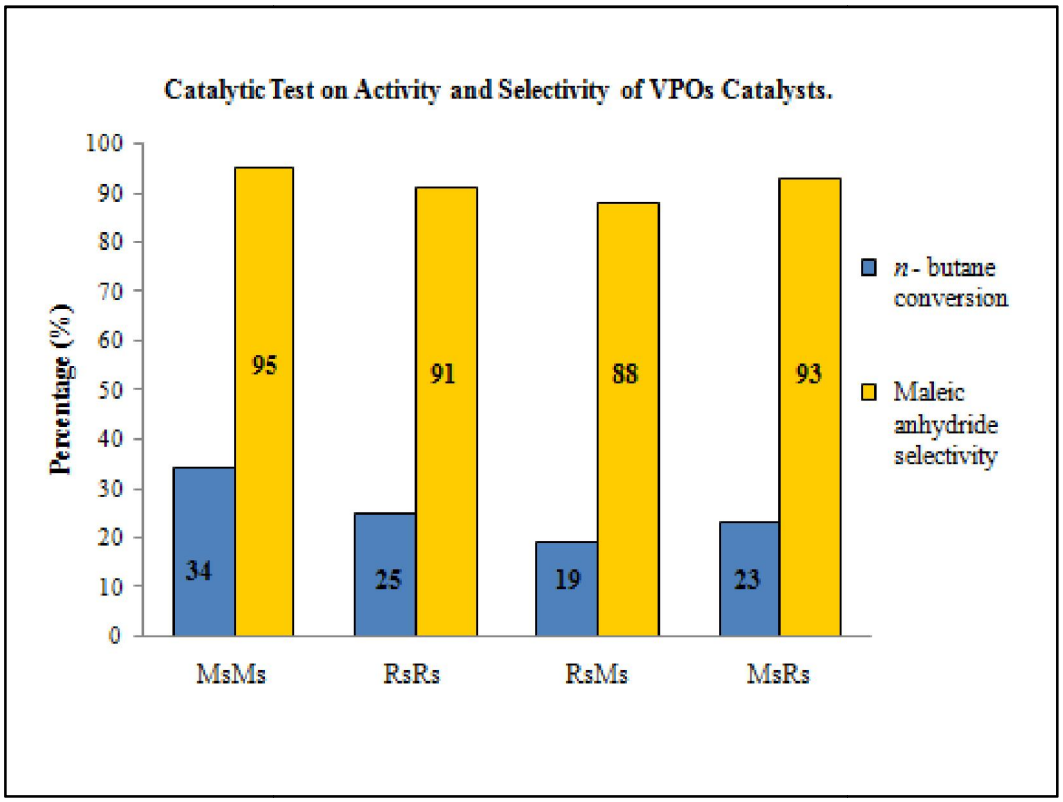

Figure 4.15: Series 3: Chart of catalytic performances for VPOs catalysts

The Turnover Number (TON) of VPOs catalysts in Series 3 showed that VPOs-M_sM_s has the highest *n*-butane conversion rate as per surface area among all the catalysts prepared. This showed that catalyst synthesized via microwave irradiation method on both stages gave better catalytic performances with the increment in both activity and selectivity which is in agreement with most of the analysis results obtained.

Table 4.12: Series 3: Catalytic performances of VPOs catalysts

Catalyst	*n*-Butane conversion (%)	Turnover Number (TON)	Product selectivity (%)		
			MA	CO	CO_2
VPOs-M_sM_s	34	1.42	95	2	3
VPOs-R_sR_s	25	1.39	91	3	6
VPOs-R_sM_s	19	1.12	88	4	8
VPOs-M_sR_s	23	1.10	93	3	4

4.3.6 Series 3: Conclusions

VPOs-M_sM_s showed to be the best catalyst among Series 3 due to its ability to produce more maleic anhydride with minimum by-products. Extra secondary structure of chrysanthemum needle-like morphology appeared on VPOs-M_sM_s with high surface area indicated that microwave irradiation could structurally affect the morphology of the catalysts during synthesis stages. By using microwave irradiation as synthesis method, the time consumed for preparation of VPO catalyst can be shortened tremendously.

CHAPTER 5

CONCLUSION

5.1 The effects of microwave irradiation drying method, Gallium dopant, and microwave irradiation synthesis method in VPOs catalysts

Microwave irradiation drying method was capable of increasing not only specific surface area as well as on activity and selectivity. When microwave irradiation used in both drying and synthesis, the overall catalytic performances were enhanced. The presence of gallium dopant and microwave irradiation drying process could further enhance the specific surface area and catalytic performances of VPOs catalysts. The realisation of chemical reactions in a very short time period by direct interaction of microwave irradiation energy can certainly be considered as "green technology" due to the reason that microwave irradiation reduced the energy consumption and synthesis duration. VPOs-M_sM_s showed to be the best catalyst among all the 3 series due to its ability to produce more maleic anhydride with minimum by-products. In short, microwave irradiation had increased the efficiency of catalytic reaction with lower cost and time consumed.

LIST OF ABBREVIATIONS

°C	Degree Celcius
K	Absolute temperature in Kelvin
Ea	Activation energy
t	Crystallite size for (h k l) phase
λ	X-ray wavelength of radiation for CuKα
$\beta_{h\,k\,l}$	Full-width at half maximum (FWHM) at (h k l) phase
$\theta_{h\,k\,l}$	Diffraction angle for (h k l) phase
A_r	Pre-exponential factor
ΔH_1	Heat of adsorption of the first layer
ΔH_2	Heat of liquefaction
ppm	Part-per-million
T_{max}	Temperature of the peak maximum
T	Temperature
D	Duration
P/V	Phosphorus-to-vanadium ratio
α-, β-, γ-$VOPO_4$,	Vanadyl phosphate in α (alpha), β (beta), and γ (gamma) phases
β-, γ- $(VO)_2P_2O_7$	Vanadyl pyrophosphate in α (alpha), β (beta), and γ (gamma) phases
o-H_3PO_4	*ortho*-Phosphoric acid
Ag	Argentum

BET	Brunauer-Emmett-Teller surface Area Measurements
CFB	Circulating fluidised bed
$CH_3(CH_2)_3OH$	1-Butanol
Co	Cobalt
CO	Carbon monoxide
CO_2	Carbon dioxide
Cr	Chromium
Cs	Cesium
EDX	Energy-dispersive X-ray spectroscopy
Fe	Iron
Ga	Gallium
$Ga(acac)_3/Ga(C_5H_7O_2)_3$	Gallium(III) Acetylacetonate
Ga_2O_3	Gallium(III) oxide
$GaPO_4$	Gallium phosphate
GHSV	Gas hourly space velocity (Reactant Gas Flow Rate)
H_3PO_4	Phosphoric acid
HNO_4	Nitric acid
ICP-OES	Inductively Coupled Plasma-Optical Emission Spectrometry
MA	Maleic anhydride
Mo	Molybdenum
N_2	Gas nitrogen
O_2	Gas oxygen
PO_4	Phosphate

SEM	Scanning electron Microscopy
TCD	Thermal conductivity detector
TON	Turnover Number
TPDRO	Temperature Programmed Desorption Reduction Oxidation
TPR	Temperature Programmed Reduction
V_2O_5	Vanadium (V) pentoxide
VHP	Vanadium phosphorus oxide catalyst prepared via hemihydrates route
$VOHPO_4 \cdot 0.5H_2O$	Vanadyl (IV) hydrogen phosphate hemihydrates
$(VO)_2P_2O_7$	Vanadyl pyrophosphate
$VOPO_4 \bullet 2H_2O$	Vanadyl phosphate dehydrate
VPA	Vanadium phosphorus oxide catalyst prepared via aqueous method
VPD	Vanadium phosphorus oxide prepared via dihydrates route
VPO	Vanadium phosphorus oxide prepared via organic method
VPOs	Vanadium phosphorus oxide catalyst prepared via sesquihydrate route
VPOs-Ga0.1%	Vanadium phosphorus oxide catalyst prepared via sesquihydrate route doped with 0.1% of Gallium
VPOs-Ga0.3%	Vanadium phosphorus oxide catalyst prepared via sesquihydrate route doped with 0.3% of Gallium
VPOs-Ga0.5%	Vanadium phosphorus oxide catalyst prepared via sesquihydrate route doped with 0.5% of Gallium
VPOs-MM	VPOs catalyst dried by microwave irradiation on both stages
VPOs-MO	VPOs catalyst dried via microwave irradiation in Stage 1 and conventional oven-dried in Stage 2

VPOs-OM	VPOs catalyst prepared via conventional oven drying in Stage 1 and microwave drying in Stage 2
VPOs-OO	VPOs catalyst dried using conventional oven on both stages
VPOs-M_sM_s	VPOs catalyst synthesised using microwave irradiation method on both stages
VPOs-M_sR_s	VPOs catalyst synthesised using microwave irradiation method in Stage 1 and reflux method in Stage 2
VPOs-R_sM_s	VPOs catalyst synthesised using reflux method in Stage 1 and microwave irradiation method in Stage 2
VPOs-R_sR_s	VPOs catalyst synthesised using reflux method on both stages
XRD	X-Ray Diffractometer
Zn	Zinc
Zr	Zirconium

REFERENCES

Abdelouahab, F.B. et al., 1995. The role of Fe and Co dopants during the activation of the $VO(HPO_4)\cdot 0.5H_2O$ precursor of the vanadium phosphorus catalyst as studied by in Situ Laser Raman Spectroscopy. *Journal of Catalysis*, 157(2), pp. 687–697.

Asghar, A., Taufiq-yap, Y.H., and Rezaei, F., 2010. Innovative process for the synthesis of vanadyl pyrophosphate as a highly selective catalyst for *n*-butane oxidation. *Chemical Engineering Journal*, 165(1), pp. 328–335.

Bartholomew, C.H. and Farrauto, R.J., 2006. *Catalysts or industrial application. In: Fundamentals of industrial catalytic processes*. New Jersey: John Wiley & Sons Inc., pp. 1–49.

Bond, G.C., 1987. Basic principles of catalysts. In: Heterogeneous Catalysis. *Principles and Application*, 2nd ed., Oxford Clarendon Press, pp. 1-11.

Bordes, E., 1987. Crystallochemistry of V-P-O phases and application to catalysis. *Catalysis Today*, 1(5), pp. 499-526.

Boudart, M., Thomas, J.M. and Zamaraev, K.I., 1992. *In: Perspectives in Catalysis*. Blackwell: Oxford, pp. 183.

Brunauer, S., Emmett, P.H. and Teller, E., 1938. Adsorption of gases in multimolecular layers. *Journal of the American Chemical Society*, 60(2), pp. 309-319.

Cavani, F. and Trifirò, F., 1994a. Catalyzing butane oxidation to make maleic anhydride. *Chemtech*, 24, pp. 18-25.

Cavani, F. and Trifirò, F., 1994b. *Selective oxidation of C4 paraffins*, *catalysis*. The Royal Society of Chemistry, Cambridge, 11.

Cavani, F. and Trifirò, F., 2004. Basic principles in applied catalysis: *Oxidation of n-butane to maleic anhydride*. New York: Springer, pp. 19-84.

Centi, G. et al., 1988. Mechanistic aspects of maleic anhydride synthesis from C4 hydrocarbons over phosphorus vanadium oxide. *Chemical Reviews*, 88(1), pp. 55-80.

Centi, G., 1993. Vanadyl pyrophosphate catalysts. *Catal. Today*, 16(5).

Centi, G., Cavini, F., and Trifirò, F., 2001. New reactor technology options. In: *Selective oxidation by heterogeneous* catalysis. New York: Kluwer Academic/Plenum Publishers, pp. 37-53.

Cheng, W. and Wang, W., 1997. Effect of calcinations environment on the selective oxidation of *n*-butane to maleic anhydride over promoted and unpromoted VPO catalyst. *Applied Catalysis A: General*, 156(1), pp. 57-69.

Chorkendoff, I. and Niemantsverdrient, J.W., 2003. Introduction to Catalysis. In: *Concepts of Modern Catalysis and Kinetics*. WILEY-VCH, pp. 1-20.

Chorkendorff, I. and Niemantsverdriet, J.W., 2007. Introduction to catalysis: In: *Concepts of modern catalysis and kinetics*. 2nd Edition, WILEY-VCH Verlag GmbH & Co. KGaApp., pp. 2-167.

Conde, L.D. et al., 2001. Frequency effects in the catalytic oligomerization of methane via microwave heating. *J. Catal*, pp. 204-324.

Clugston, M.J. et al., 1998. *The New Penguin Dictionary of Science*. London: New York, pp. 24-36.

Ellison, I.J. et al., 1994. Control of the composition and morphology of vanadium phosphate catalyst precursors from alcohol treatment of $VOPO_4 \cdot 2H_2O$. *Journal of the Chemical Society, Chemical Communications*, 8(9), pp. 1093-1094.

Fadoni, M. and Lucarelli, L., 1999. Temperature programmed desorption, reduction, oxidation and flow chemisorptions for the characterisation of heterogeneous catalysts-Theoretical aspects, instrumentation and applications. *Studies in Surface Science and Catalysis*, 120(a), pp. 177-255.

Felthouse, T.R. et al., 2000. *Maleic anhydride, maleic acid, and fumaric acid.* In: Kirk-Othmer (Ed.). *Kirk-Othemer Encylopedia of Chemical Technology*. New York: John Wiley & Sons, Inc., pp. 893-928.

Felthouse, T. et al., 2001. *Maleic anhydride, maleic acid and fumaric acid.* In: Kirk-Othmer (Ed.), *Kirk-Othmer Encyclopedia of Chemical Technology*. New York: John Wiley.

Funada, C. and Greiner, E., 2011, *Maleic Anhydride* [Online]. Available at: http://www.sriconsulting.com/CEH/Public/Reports/672.5000/ [Accessed: 19 December 2011].

Frey, J. et al., 2010. Quantitative solid-state NMP investigation of V^{5+} species in VPO catalysts upon sequential selective oxidation of *n*-butane. *Journal of Catalysis*, 272(1), pp. 131-139.

González-Cortés, S.L. and Imbert, F.E., 2013. Fundamentals, properties and applications of solid catalysts prepared by solution combustion synthesis (SCS). *Applied Catalysis A: General*, 452, pp. 117-131.

Gopal, R. and Calvo, C., 1972. Crystal structure of βVPO_5. *Journal of Solid State Chemistry,* 5(3), pp. 432-435.

Hartley, F.R., 1985. *Introduction, Supported Metal Complexes*. 3rd edition, United States: Oxford, pp. 1-3.

Hodnett, B.K., Permanne, P.h. and Delmon, B., 1983. Influence of P/V ratio on the phase composition and catalytic activity of vanadium phosphate based catalysts. *Applied Catalysis*, 6(2), pp. 231-244.

Hodnett, B.K., 2000. *Heterogeneous catalytic oxidation – fundamental and technology aspects of the selective and total oxidation of organic compounds*. Brisbane: John Wiley & Sons Ltd.

Hutchenson, K.W. et al., 2010. Applied Catalysis A: General parametric study of *n*-butane oxidation in a circulating fluidized bed reactor. *Applied Catalysis A, General*, 376(1-2), pp. 91-10.

Hutching, G.J., 1991. Effect of promoters and reactant concentration on the selective oxidation of *n*-butane to maleic anhydride using vanadium phosphorus oxide catalysts. *Applied Catalysis*, 72, pp. 1-32.

Hutching, G.J. and Higgins, R., 1996. Effect of promoters on the selective oxidation of *n*-butane with vanadium-phosphorus oxide catalysts. *Journal of Catalysis,* 162, pp. 153-168.

Hutching, G.J., and Higgins, R., 1997. Selective oxidation of *n*-butane to maleic anhydride with vanadium phosphorus catalysts prepared by comminution in the presence of dispersants. *Applied Catalysis A: General*, 154(1-2), pp. 103-115.

Hutchings, G.J. et al., 1997. Improved method of preparation of vanadium phosphate catalysts. *Catalysis Today*, 33(1-3), pp. 16-171.

Hutching, G.J., 2001. Promotion in heterogeneous catalysis: a topic requiring a new approach. *Catalysis Letters*, 75(1-12).

Hutchings, G.J., 2004. Vanadium phosphate: A new look at the active component of catalysts for the oxidation of butane to maleic anhydride. *Journal of Materials Chemistry*, 14(23), pp. 3385-3395.

Horowitz, H. et al., 1988. V-P-O catalysts for oxidation of butane to maleic anhydride: Influence of $(VO)_2H_4P_2O_9$ precursor morphology on catalytic properties. *Applied Catalysis*, 38, pp. 193-210.

Ishimura, T., Sugiyama, S. and Hayashi, H., 2000. Vanadyl hydrogenphosphate sesquihydrate as a precursor for preparation of $(VO)_2P_2O_7$ and cobalt-incorporated catalysts. *Journal of Molecular Catalysis A: Chemical*, 158, pp. 559-565.

Johnson, J.W. et al., 1984. Preparation and characterization of vanadyl hydrogen phosphate hemihydrates and its topotactic transformation to vanadyl pyrophosphate. *Journal of the American Chemical Society*, 106(26), pp. 8123-8128.

Kiely, C.J. et al., 1995. Electron microscopy studies of vanadium phosphorus oxide catalysts derived from $VOPO_4 \cdot 2H_2$. *Catal. Lett*, 33, pp. 357.

Klug, P.H. and Alexander, L.E., 1974. *X-ray diffraction procedures for polycrystalline and amorphous materials.* In: X-ray diffraction procedures. 2nd Edition, New York: John Wiley & Sons, pp. 177-424.

Kourtakis, K., 2010. Direct grafting of alkoxide promoters on vanadium hydrogen phosphate precursor: Improved catalysts for the selective oxidation of *n*-butane. *Applied Catalysis A: General,* 376(1-2), pp. 40-46.

Ledoux, M.J. et al., 2001. High-yield butane to maleic anhydride direct oxidation on vanadyl pyrophosphate supported on heat-conductive materials: β-SiC, Si3N4, and BN. *Journal of Catalysis*, 203(2), pp. 495-508.

Leong, L.K., Chin, K.S. and Taufiq-Yap, Y.H., 2011. The effect of Bi promoter on vanadium phosphate catalysts synthesized via sesquihydrate route. *Catalysis Today,* 164(1), pp. 341-346.

Leong, L.K., Chin, K.S. and Taufiq-Yap, Y.H., 2012. Effect of varying reflux durations on the physico-chemical and catalytic performance of vanadium phosphate catalysts synthesized via vanadyl hydrogen phosphate sesquihydrate *Applied Catalyst,* 415-416, pp. 53-58.

Ma, L. et al., 2012. Influence of calnination temperature on Fe/HBEA catalyst for the selective catalytic reduction of NOx with NH_3. *Catalysis Today*, 184(1), pp. 145-152.

Maleic Anhydride Market For Unsaturated Polyester Resins (UPR), 1, 4-Butanediol (BDO), Additives (Lubricants & Oil), Copolymers and Other Applications - Global Industry Analysis, Size, Share, Growth, Trends and Forecast, 2012 – 2018, 2013. [Online] Available at: http://www.transparencymarketresearch.com/maleic-anhydride-market.html#sthash.9t9RNSMf.dpuf [Accessed: 30 September 2013]

Matsuura, I., Ishimura, T. and Kimura, N., 1995. Preparation and characterization of vanadyl hydrogen phosphate hydrates; $VO(HPO_4)\cdot 1.5H_2O$ and $VO(HPO_4)\cdot 0.5H_2O$. *Chemistry Letters*, 9, pp. 769-770.

Misono, M., 2002. Selective oxidation of butanes toward green/sustainable chemistry. *Topics in Catalysis*, 21(1-3), pp. 89-96.

Mota, S. Et al., 2000. Selective oxidation of *n*-butane on a VPO catalyst: Study under fuel-rich conditions. *Journal of Catalysis*, 193 (2), pp. 308-318.

Nakamura, M., Kawai, K. and Fujiwara, Y., 1974. The structure and the activity of vanadyl phosphate catalysts. *Journal of Catalysis*, 34(3), pp. 345-355.

Nie, W. et al., 2001. A study on VPO specimen supported on aluminium-containing MCM-41 for partial oxidation of *n*-butane to MA. *Catalysis Letters*, 76(3-4), pp. 201-206.

Nie, W. et al., 2003. Comparative studies on the VPO specimen supported on mesoporous Al-containing MCM-41 and large pore silica. *Applied Catalysis A: General*, 244(2), pp. 265-272.

Niwa, M. and Murakami, Y., 1982. Reaction mechanism of ammoxidation of toluene IV. Oxidation state of vanadium oxide and its reactivity for toluene oxidation. *Journal of Catalysis*, 76(1), pp, 9-16.

O'Mahony, L. et al., 2004. Surface species during the crystallization of VOHPO4 · 0.5H2O. *Journal of Catalysis*, 227(2), pp. 270–281.

O'Mahony, L. et al., 2005. Phase development and morphology during the thermal treatment of $VOHPO_4 \cdot 0.5H_2O$. *Applied Catalysis*, 285, pp. 36-42.

Ramaswamy, A.V., 2002. *Catalysis and theoretical concepts.* In: Catalysis-Principles and Applications. 3rd Edition, Narosa Publishing House, pp. 206-219.

Ravichandran, S. and Karthikeyan, E., 2011. Microwave Synthesis - A Potential Tool for Green Chemistry. *ChemTech*, 3(1), pp. 466–470.

Robert, W.W. and Glenn, L.S., 1986. Vanadium-phosphorus-oxygen industrial catalysts for *n*-butane oxidation: characterization and kinetic measurement. *Ind*, 25, pp. 612-620.

Rownaghi, A.A., Taufiq-Yap, Y.H. and Rezaei, F., 2009a. High surface area vanadium phosphate catalysts for *n*-butane oxidation. *Ind. Eng. Chem. Res*., 48, pp. 7517-7528.

Rownaghi, A.A., Taufiq-Yap, Y.H., and Jiunn, T.W., 2009b. Influence of the ethylene glycol, water treatment and microwave irradiation on the characteristics and performance of VPO catalysts for *n*-butane oxidation to maleic anhydride. *Catalysis Letters*, 130(3-4), pp. 593-603.

Rownaghi, A.A., Taufiq-Yap, Y.H. and Rezaei, F., 2009c. Influence of rare-earth and bimetallic promoters on various VPO catalysts for partial oxidation of *n*-butane. *Catalysis Letters*, 130(3-4), pp. 504-516.

Rownaghi, A.A., Taufiq-Yap, Y.H. and Rezaei, F., 2010. Innovative process for the synthesis of vanadyl pyrophosphate as a highly selective catalyst for *n*-butane oxidation. *Chemical engineering Journal*, 165, pp. 328-335.

Ruiz, P. Et al., 1993. New aspects of the cooperation between phases in vanadium phosphate catalysts. *Catalysis Today*, 16, pp. 99-111.

Sartoni, L. et al., 2004. Promotion of vanadium phosphate catalysts using gallium compounds: effect of low Ga/V molar ratios. *Journal of Molecular Catalysis A: Chemical*, 220(1), pp. 85–92.

Sharp D. W.A., 2003, *The Penguin Dictionary of Chemistry,* pp. 56-98.

Sheldon, R., 2000. Atom utilization, E factors and the catalytic solution. *Comptes Rendus de I'Académie ddes Science-Series IIIC-Chemistry*, 3(7), pp. 541-551.

Sheldon, R., Arends, I. and Hanefeld, U., 2007. *Catalytic oxidation.* In: Green chemistry and catalysis. WILEY-VCH Verlag GmbH & Co. KGaA, pp. 133-221.

Taufiq-Yap, Y.H., et al., 2001. The effect of the duration of *n*-butane/air pretreatment on the morphology and reactivity of $(VO)_2P_2O_7$ catalysts. *Catalysis Letters*, 74(1), pp. 99–104.

Taufiq-Yap Y.H. et al., 2004. Synthesis and characterization of vanadyl pyrophosphate catalysts via vanadyl hydrogen phosphate sesquihydrate precursor. *Catalysis* Today, 93-95, pp. 715-722.

Taufiq-Yap Y.H., 2006. Effect of Cr and Co promoters addition on vanadium phosphate catalysts for mild oxidation of *n*-butane. *Journal of Natural Gas Chemistry*, 15(2), pp. 144-148.

Taufiq-Yap, Y.H. et al., 2007. Preparation of vanadium phosphate catalysts from $VOPO_4 \cdot 2H_2O$: Effect of microwave irradiation on morphology and catalytic property. *Catalysis Letters*, 119(1–2), pp. 64–71.

Taufiq-Yap, Y.H. et al., 2009. Synthesis of self assembled nanorod vanadium oxide bundles by sonochemical treatment. *Journal of Natural Gas Chemistry*, 18(3), pp. 312–318.

Thomas, J.M. and Thomas, W.J., 1997. *Principles and pratice of heterogeneous catalysis.* Wiley: VCH, Berlin.

Trivedi, B.C. and Culbertson, B.M., 1982. *Maleic anhydride*. New York: Plenum Press.

Upadhyaya D.J. and Samant D.S., 2013. New insights into the bifunctionality of vanadium phosphorous oxides: A chemical switch between oxidative scission and pinacol rearrangement of vicinal diols. *Catalysis Today*, 208, pp. 60-65.

Védrine, J.C., Hutchings, G.J., and Kiely, C.J., 2013. Molybdenum oxide model catalysts and vanadium phosphates as actual catalysts for understanding heterogeneous catalytic partial oxidation reactions: A contribution by Jean-Claude Volta. *Catalysis Today*, pp. 1–8.

Wu, N.L. et al., 2004. Effect of calcination atmosphere on TiO_2 photocatalysis in hydrogen production from methanol/water solution. *Journal of Photochemistry and Photobiology A: Chemistry*, 163(1-2), pp. 277–280.

Zhang, L. and Zhu, Y.J., 2008. Microwave-assisted solvothermal synthesis of AlOOH hierarchically nanostructured microscospheres and their transformation to γ-Al2O3 with similar morphologies. *J. Phys. Chem. C*, 112, pp. 16764-16768.

APPENDICES

APPENDIX A

Calculation for the Gallium Dopant Used

Molecular weight of $VOPO_4 \cdot 2H_2O$ = 197.9426 g mol^{-1}

$$10\text{g of } VOPO_4 \cdot 2H_2O = \frac{10\text{ g}}{197.9426\text{ g mol}^{-1}}$$

$$= 0.0505\text{ mol}$$

Moelcular weight of gallium (III) acetylacetonate, $Ga(acac)_3$ / $Ga(C_5H_8O_2)_3$

= 69.723 g mol^{-1} +3 x $[(5 \times 12.0107\text{ gmol}^{-1}) + (8 \times 1.0079\text{ gmol}^{-1}) + (2 \times 15.9994\text{ gmol}^{-1})]$

= 370.0695 g mol^{-1}

Example of calculation:

For VPOs-Ga0.1%

To obtain Ga/V = 0.001;

V = 0.0505 mol and Ga = 0.0000505 mol,

Total mass of Ga needed to obtain Ga = 0.0000505 mol,

$$\frac{\text{Mass of Ga, x}}{\text{Molecular weight of Ga(acac)}_3} = \text{mol of Ga}$$

$$\frac{\text{Mass of Ga, x}}{370.0695\ \text{g mol}^{-1}} = 0.0000505\ \text{mol}$$

$$x = 0.018689\ \text{g}$$

Thus, 0.018689 g of $Ga(acac)_3$ needed to produce VPOs-Ga0.1%.

APPENDIX B

Preparation of Solutions Used in Redox Titration

Preparation of 2M sulphuric acid, H_2SO_4 solution

Concentrated H_2SO_4 (95-98 %)

1 L = 1.84 kg = 1840 g/ 1000 cm^3

= 1.84 g/ cm^3

M_r of H_2SO_4 = 98.07 g/mol

Concentration of 95-98 % H_2SO_4 = $\frac{1.84\,g/\,cm^3}{98.07\,g/\,mol} \times \frac{95}{100} \times 1000 = 17.82\,M$

$M_1V_1=M_2V_2$ where M_1 = concentration of 95-98 % H_2SO_4

M_2 = concentration of diluted H_2SO_4 (2 M)

V_1 = volume of 95-98 % H_2SO_4

V_2 = volume of diluted H_2SO_4 (2 M)

(17.82 M)(V_1) = (2 M)(1000 cm^3)

V_1 =112.23 cm^3

Preparation of 0.1 M sulphuric acid, H_2SO_4 solution

$M_1V_1 = M_2V_2$ where M_1 = concentration of 95-98 % H_2SO_4

M_2 = concentration of diluted H_2SO_4 (0.1 M)

V_1 = volume of 95-98 % H_2SO_4

V_2 = volume of diluted H_2SO_4 (0.1 M)

$(17.82\ M)(V_1) = (0.1\ M)(1000\ cm^3)$

$V_1 = 5.61\ cm^3$

Preparation of 0.01 N potassium permanganate, $KMnO_4$

Normality, N (eq/L) = M (mol/L) x *n* (eq/mol)

$MnO^{4-} + 8\ H^+ + 5e^- \leftrightarrow Mn^{2+} + 4\ H_2O$

$$\text{Molarity, M (mol/L)} = \frac{\text{N (eq/L)}}{n\ \text{(eq/mol)}}$$

$$= \frac{0.01}{5}$$

$= 0.002$ M

M_r of $KMnO_4$ = 158.04 g/mol

Weight for $KMnO_4$ in 1000 cm^3 diluted (0.1 M) H_2SO_4 = 0.002 x 158.04

= 0.3161 g

Preparation of 0.01 N ammonium iron (II) sulphate, $(NH_4)_2Fe(SO_4)_2 \cdot 6H_2O$

Normality, N (eq/L) = M (mol/L) x *n* (eq/mol)

$Fe^{2+} + e^- \leftrightarrow Fe^{3+}$

$$\text{Molarity, M (mol/L)} = \frac{\text{N (eq/L)}}{n\,\text{(eq/mol)}}$$

$$= \frac{0.01}{1}$$

$$= 0.01\,\text{M}$$

Mr of $(NH_4)_2Fe(SO_4)_2{\cdot}6H_2O$ = 391.99 g/mol

Weight for $(NH_4)_2Fe(SO_4)_2{\cdot}6H_2O$ in 1000 cm^3 diluted (0.1 M) H_2SO_4

= 0.01 x 391.99

= 3.9199 g

Preparation of Diphenylamine, Ph_2NH, indicator

1 g of diphenylamine was weighed and dissolved in a few ml of concentrated sulphuric acid, H_2SO_4. Then the solution was transferred to a 100 ml volumetric flask and further top up with concentrated H_2SO_4.

APPENDIX C

Calculation for Average Oxidation State of Vanadium (V_{AV})

According to Niwa and Murakami,

$V^{4+} + 2V^{3+} = 20\ [MnO_4^-]\ V_1$

$V^{5+} + V^{4+} + V^{3+} = 20\ [Fe^{2+}]\ V_2$

$V^{5+} = 20\ [Fe^{2+}]\ V_3$

$[MnO_4^-] = 0.01$

$[Fe^{2+}] = 0.01$

$V^{4+} + 2V^{3+} = 0.2\ V_1 \quad (1)$

$V^{5+} + V^{4+} + V^{3+} = 0.2\ V_2 \quad (2)$

$V^{5+} = 0.2\ V_3 \quad (3)$

(2)-(3),

$V^{4+} + V^{3+} = 0.2\ V_2 - 0.2\ V_3 \quad (4)$

$V^{4+} = 0.2\ V_2 - 0.2\ V_3 - V^{3+} \quad (5)$

Substitute (5) to (1),

$0.2\ V_2 - 0.2\ V_3 - V^{3+} + 2V^{3+} = 0.2\ V_1$

$V^{3+} = 0.2\ V_1 - 0.2\ V_2 + 0.2\ V_3$ (6)

Substitute (6) to (5),

$V^{4+} = 0.4\ V_2 - 0.4\ V_3 - 0.2\ V_1$

Therefore;

$V^{5+} = 0.2V_3$

$V^{4+} = 0.4\ V_2 - 0.4\ V_3 - 0.2\ V_1$

$V^{3+} = 0.2\ V_1 - 0.2\ V_2 + 0.2\ V_3$

Average Oxidation State:

$$V_{AV} = \frac{3\,V^{3+} + 4\,V^{4+} + 5\,V^{5+}}{V^{3+} + V^{4+} + V^{5+}}$$

Example calculation:

For VPOs-MM

$V_1 = 6.05 \qquad V_2 = 11.30 \qquad V_3 = 6.40$

$V^{3+} = 0.2(6.07) - 0.2(11.33) + 0.2(6.40) = 0.23$

$V^{4+} = 0.4(11.33) - 0.4(6.40) - 0.2(6.07) = 0.75$

$V^{5+} = 0.2(6.40) = 1.28$

$$V_{AV} = \frac{3(0.23) + 4(0.75) + 5(1.28)}{0.23 + 0.75 + 1.28}$$

= **4.4646**

VPOs-MO	$KMnO_4$ (V_1)		$(NH_4)_2Fe(SO_4)_2$ (V_2)		$(NH_4)_2Fe(SO_4)_2$ (V_3)	
	1	2	1	2	1	2
Initial (cm^3)	0.00	5.40	0.00	12.00	25.00	0.00
Final (cm^3)	5.40	10.8	11.20	23.30	32.25	7.35
Volume used (cm^3)	5.40	5.40	11.20	11.30	7.25	7.35
Average (cm^3)	**5.40**		**11.25**		**7.30**	
V_{AV} = 4.5200	**V^{4+} = 48.00 %**			**V^{5+} = 52.00 %**		

VPOs-OM	$KMnO_4$ (V_1)		$(NH_4)_2Fe(SO_4)_2$ (V_2)		$(NH_4)_2Fe(SO_4)_2$ (V_3)	
	1	2	1	2	1	2
Initial (cm^3)	12.00	20.00	25.00	0.00	13.00	20.00
Final (cm^3)	18.35	26.25	36.10	11.00	19.25	26.35
Volume used (cm^3)	6.35	6.25	11.10	11.00	6.25	6.25
Average (cm^3)	**6.30**		**11.05**		**6.25**	
V_{AV} = 4.4299	**V^{4+} = 57.01 %**			**V^{5+} = 42.99 %**		

VPOs-OO	$KMnO_4$ (V_1)		$(NH_4)_2Fe(SO_4)_2$ (V_2)		$(NH_4)_2Fe(SO_4)_2$ (V_3)	
	1	2	1	2	1	2
Initial (cm^3)	15.00	25.00	0.00	13.00	0.00	10.00
Final (cm^3)	21.25	31.15	11.10	24.10	6.30	16.40
Volume used (cm^3)	6.25	6.15	11.10	11.10	6.30	6.40
Average (cm^3)	**6.20**		**11.10**		**6.35**	
V_{AV} = 4.4419	**V^{4+} = 55.81 %**			**V^{5+} = 44.19 %**		

VPOs-Ga0.1%	$KMnO_4$ (V_1)		$(NH_4)_2Fe(SO_4)_2$ (V_2)		$(NH_4)_2Fe(SO_4)_2$ (V_3)	
	1	2	1	2	1	2
Initial (cm^3)	0.00	8.00	9.00	22.00	0.00	10.00
Final (cm^3)	6.20	14.30	21.25	34.25	8.40	18.40
Volume used (cm^3)	6.20	6.30	12.25	12.25	8.40	8.40
Average (cm^3)	**6.25**		**12.25**		**8.40**	
V_{AV} = 4.4706	**V^{4+} = 52.94 %**			**V^{5+} = 47.06 %**		

VPOs-Ga0.3%	$KMnO_4$ (V_1)		$(NH_4)_2Fe(SO_4)_2$ (V_2)		$(NH_4)_2Fe(SO_4)_2$ (V_3)	
	1	2	1	2	1	2
Initial (cm^3)	18.00	25.00	0.00	13.00	18.00	0.00
Final (cm^3)	23.10	30.20	11.25	24.25	25.30	7.40
Volume used (cm^3)	5.10	5.20	11.25	11.25	7.30	7.40
Average (cm^3)	**5.15**		**11.25**		**7.35**	
V_{AV} = 4.5422	**V^{4+} = 45.78 %**			**V^{5+} = 54.22 %**		

VPOs-Ga0.5%	$KMnO_4$ (V_1)		$(NH_4)_2Fe(SO_4)_2$ (V_2)		$(NH_4)_2Fe(SO_4)_2$ (V_3)	
	1	2	1	2	1	2
Initial (cm^3)	0.00	10.00	0.00	13.00	25.00	10.00
Final (cm^3)	6.30	16.20	11.15	24.05	31.35	16.35
Volume used (cm^3)	6.30	6.20	11.15	11.05	6.35	6.35
Average (cm^3)	**6.25**		**11.10**		**6.35**	
V_{AV} = 4.4369	**V^{4+} = 56.31 %**			**V^{5+} = 43.69 %**		

VPOs-M_sM_s	$KMnO_4$ (V_1)		$(NH_4)_2Fe(SO_4)_2$ (V_2)		$(NH_4)_2Fe(SO_4)_2$ (V_3)	
	1	2	1	2	1	2
Initial (cm^3)	23.00	34.00	20.00	0.00	22.00	0.00
Final (cm^3)	32.15	43.15	39.30	19.40	35.60	13.60
Volume used (cm^3)	9.15	9.15	19.30	19.40	13.60	13.60
Average (cm^3)	**9.15**		**19.35**		**13.60**	
V_{AV} = 4.5228	**V^{4+} = 47.72 %**		**V^{5+} = 52.28 %**			

VPOs-R_sM_s	$KMnO_4$ (V_1)		$(NH_4)_2Fe(SO_4)_2$ (V_2)		$(NH_4)_2Fe(SO_4)_2$ (V_3)	
	1	2	1	2	1	2
Initial (cm^3)	23.00	32.00	20.00	0.00	13.00	25.00
Final (cm^3)	29.40	38.40	31.25	11.15	19.20	31.10
Volume used (cm^3)	6.40	6.40	11.25	11.15	6.20	6.10
Average (cm^3)	**6.40**		**11.20**		**6.15**	
V_{AV} = 4.4286	**V^{4+} = 57.14 %**		**V^{5+} = 42.86 %**			

VPOs-M_sR_s	$KMnO_4$ (V_1)		$(NH_4)_2Fe(SO_4)_2$ (V_2)		$(NH_4)_2Fe(SO_4)_2$ (V_3)	
	1	2	1	2	1	2
Initial (cm^3)	0.00	12.00	25.00	0.00	20.00	0.00
Final (cm^3)	8.40	20.50	41.85	16.75	38.45	18.45
Volume used (cm^3)	8.40	8.50	16.85	16.75	18.45	18.45
Average (cm^3)	**8.45**		**16.80**		**18.45**	
V_{AV} = 4.2380	**V^{4+} = 76.20 %**		**V^{5+} = 23.80 %**			

APPENDIX D

Crystallite Size Measurements by Using Powder XRD Technique

According to Scherrer's formula,

$$\text{Crystallite size, T (Å)} = \frac{0.89\lambda}{\beta_{hkl}\cos\theta_{hkl}}$$

Given that λ for CuKα = 1.54 Å

$$\beta_{h\,k\,l} = \text{FWHM (rad)} = \text{FWHM (°)} \times \left(\frac{\pi}{180°}\right)$$

Example of calculation:

For VPOs-MM,

3 strongest peaks from XRD:

Peak no.	2θ	θ	FWHM (°)	FWHM (rad)
5	22.8173	11.4087	1.48530	0.0259
8	28.4366	14.2183	0.71800	0.0125
9	29.6302	14.8151	1.25160	0.0218

Peak appears at 2θ = 22.8173 corresponds to (020) plane

$$\text{T (Å)} = \frac{0.89 \times 1.54}{0.0259 \times \cos 11.4087}$$

$$= 53.9856 \text{ Å}$$

Peak appears at 2θ = 28.4366 corresponds to (204) plane

$$T\ (Å) = \frac{0.89 \times 1.54}{0.0125 \times \cos 14.2183}$$

$$= 113.1130\ Å$$

For VPOs-MO

Peak no.	2θ	θ	FWHM (°)	FWHM (rad)
5	22.8062	11.4031	1.26480	0.0221
7	28.3975	14.1988	0.66310	0.0117
8	29.8554	14.9277	0.68290	0.0119

For VPOs-OM

Peak no.	2θ	θ	FWHM (°)	FWHM (rad)
5	22.7080	11.3540	1.74840	0.0305
7	28.4447	14.2224	0.66940	0.0117
8	29.8942	14.9471	0.68410	0.0119

For VPOs-OO

Peak no.	2θ	θ	FWHM (°)	FWHM (rad)
5	22.7086	11.3543	1.47730	0.0258
7	28.4057	14.2029	0.70670	0.0123
8	29.8416	14.9208	0.73180	0.0128

VPOs-Ga0.1%

Peak no.	2θ	θ	FWHM (°)	FWHM (rad)
4	22.9837	11.4919	1.15510	0.0202
6	28.5631	14.2816	0.69270	0.0121
7	29.6806	14.8403	1.11330	0.0194

VPOs-Ga0.3%

Peak no.	2θ	θ	FWHM (°)	FWHM (rad)
5	22.8543	11.4272	1.15960	0.0202
8	28.4395	14.2198	0.6957	0.0121
9	29.8800	14.9400	0.73340	0.0128

VPOs-Ga0.5%

Peak no.	2θ	θ	FWHM (°)	FWHM (rad)
5	22.8474	11.4237	1.22520	0.0214
8	28.4468	14.2234	0.7977	0.0139
9	29.8400	14.9200	0.75740	0.0132

VPOs-M_sM_s

Peak no.	2θ	θ	FWHM (°)	FWHM (rad)
6	22.8191	11.4096	1.04040	0.0182
9	28.3790	14.1900	0.66200	0.0116
10	29.8502	14.9251	0.63230	0.0110

VPOs-R_sM_s

Peak no.	2θ	θ	FWHM (°)	FWHM (rad)
9	22.8209	11.4105	1.21910	0.0213
12	28.4064	14.2032	0.68710	0.0120
13	29.8733	14.9367	0.62670	0.0109

VPOs-M_sR_s

Peak no.	2θ	θ	FWHM (°)	FWHM (rad)
5	22.9200	11.4600	0.93460	0.0163
8	28.3780	14.1890	0.89450	0.0156
9	29.8800	14.9400	0.66660	0.0116

APPENDIX E

Preparation of Solutions Used in ICP-OES

i. Preparation of 8 M HNO_3

$$\text{Molarity for 65 \% of } HNO_3 = \frac{\text{Density of } HNO_3}{\text{Molecular Weight of } HNO_3} \times \frac{65}{100} \times 1000$$

$$= \frac{1.4090 \text{ g cm}^{-1}}{63.0130 \text{ g mol}^{-1}} \times \frac{65}{100} \times 1000$$

$$= 14.5343 \text{ mol L}^{-1}$$

$$= 14.5343 \text{ M}$$

$M_1V_1 = M_2V_2$

where,

M_1 = concentration of 65 % of HNO_3 (14.5343 M)

V_1 = volume of 65 % of HNO_3

M_2 = concentration of 8 M HNO_3

V_2 = volume of 8 M HNO_3

$M_1V_1 = M_2V_2$

(14.5343 M) V_1 = (8 M)(250 mL)

$$V_1 = \frac{(8 \text{ M})(250 \text{ mL})}{14.5343 \text{ M}}$$

= 137.65 mL

Thus, 137.65 mL of 65 % of HNO_3 was diluted to 250 mL with deionised water.

ii. Preparation of Stock Solution of Phosphorus, P

Molecular weight of $NH_4H_2PO_4$

= (14.0067 + 10079 x 4 + 30.9738 + 15.9994 × 4) g mol-1

= 115.0255 g mol^{-1}

Atomic weight of P = 30.9738 g mol^{-1}

50 ppm of stock solution for P = 50 mg L^{-1}

= 0.05 g L^{-1}

$$\text{Number of mole of P} = \frac{0.05 \text{ g L}^{-1}}{30.9738 \text{ g mol}^{-1}}$$

= 1.6145×10^{-3} mol L^{-1}

Mass of $NH_4H_2PO_4$ = 1.6145×10^{-3} mol L^{-1} × 115.0255 g mol^{-1}

= 0.1857 g L^{-1}

Thus, 0.1857 g of $NH_4H_2PO_4$ was transferred into 1000 mL volumetric flask and top up with deionised water.

Preparation of standard solution of phosphorus, P

$M_1V_1 = M_2V_2$

where,

M_1 = concentration of stock solution (50 ppm)

V_1 = volume of stock solution

M_2 = concentration of standard solution

V_2 = volume of standard solution (250 mL)

Example of calculation for standard solution of 20 ppm

$M_1V_1 = M_2V_2$

(50 ppm) V_1 = (20 ppm)(250 mL)

$$V_1 = \frac{(20 \text{ ppm})(250 \text{ mL})}{50 \text{ ppm}}$$

= 100 mL

Thus, 100 mL of stock solution for phosphorus was dissolved in 8 M HNO_3 then diluted to 250 mL with deionised water to produce 20 ppm standard solution of phosphorus.

iii. Preparation of Stock Solution of Vanadium, V

Preparations of Reagents for ICP-OES

Molecular weight of NH_4VO_3

$= (14.0067 + 10079 \times 4 + 50.9415 + 15.9994 \times 3)\ g\ mol^{-1}$

$= 116.9780\ g\ mol^{-1}$

Atomic weight of V = $50.9415\ g\ mol^{-1}$

50 ppm of stock solution for V = $50\ mg\ L^{-1}$

$= 0.05\ g\ L^{-1}$

Mass of $NH_4VO_3 = 9.8155 \times 10^{-4}\ mol \times 116.9780\ g\ mol^{-1}$

$= 0.1148\ g\ L^{-1}$

Thus, 0.1148 g of NH_4VO_3 was transferred into 1000 mL volumetric flask and top up with deionised water.

Preparation of standard solution of vanadium, V

$M_1V_1 = M_2V_2$

where,

M_1 = concentration of stock solution (50 ppm)

V_1 = volume of stock solution

M_2 = concentration of standard solution

V_2 = volume of standard solution (250 mL)

Example of calculation for standard solution of 10 ppm

$M_1V_1 = M_2V_2$

(50 ppm) V_1 = (10 ppm)(250 mL)

$$V_1 = \frac{(10 \text{ ppm})(250 \text{ mL})}{50 \text{ ppm}}$$

= 50 m L

Thus, 50 mL of stock solution for phosphorus was dissolved in 8 M HNO_3 then diluted to 250 mL with deionised water to produce 10 ppm standard solution of phosphorus.

iv. Preparation of Stock Solution of Gallium, Ga

Moelcular weight of $Ga(acac)_3$ / $Ga(C_5H_8O_2)_3$

$= 69.723 \text{ g mol}^{-1} + 3 \times [(5 \times 12.0107 \text{ gmol}^{-1}) + (8 \times 1.0079 \text{ gmol}^{-1}) + (2 \times 15.9994 \text{ gmol}^{-1})]$

$= 370.0695 \text{ g mol}^{-1}$

Atomic weight of Ga = $69.723 \text{ g mol}^{-1}$

50 ppm of stock solution for V = 50 mg / L

= 0.05 g / L

$$\text{Number of mole of Ga} = \frac{0.05 \text{ g L}^{-1}}{69.723 \text{ g mol}^{-1}}$$

$$= 7.1712 \times 10^{-4} \text{ mol L}^{-1}$$

Mass of $Ga(acac)_3 = 7.1712 \times 10^{-4} \text{ mol L}^{-1} \times 370.0695 \text{ g mol}^{-1}$

$= 0.2654 \text{ g L}^{-1}$

Thus, 0.2654 g of $Ga(acac)_3$ was transferred into 1000 mL volumetric flask and top up with deionised water.

Preparation of standard solution of gallium, Ga

$M_1V_1 = M_2V_2$

where,

M_1 = concentration of stock solution (50 ppm)

V_1 = volume of stock solution

M_2 = concentration of standard solution

V_2 = volume of standard solution (250 mL)

Example of calculation for standard solution of 5 ppm

$M_1V_1 = M_2V_2$

(50 ppm) V_1 = (5 ppm)(250 mL)

$$V_1 = \frac{(5 \text{ ppm})(250 \text{ mL})}{50 \text{ ppm}}$$

$= 50 \text{ m L}$

Thus, 25 mL of stock solution for phosphorus was dissolved in 8 M HNO_3 then diluted to 250 mL with deionised water to produce 10 ppm standard solution of phosphorus.

v. Preparation of 100 ppm sample solution

$$0.025 \text{ g sample in } 250 \text{ mL} = \frac{0.025 \text{ g}}{250 \text{ mL of } HNO_3}$$

$$= \frac{0.1 \text{ g}}{1000 \text{ mL of } HNO_3}$$

$$= 0.1 \times 10^3 \text{ mg } L^{-1}$$

$$= 100 \text{ ppm}$$

Thus, 0.0250 g of sample was transferred into 250 mL volumetric flask and dissolved by 10 mL of 8 M HNO_3. Then, top up to 250 mL with deionised water to produce 100 ppm sample solution.

APPENDIX F

Calculation of P/V and Ga/V mole ratio by using ICP-OES analysis

$$\frac{P}{V} = \frac{\text{Concentration of P/Atomic Weight of P}}{\text{Concentration of V/ Atomic Weight of V}}$$

$$\frac{Ga}{V} = \frac{\text{Concentration of Ga/Atomic Weight of Ga}}{\text{Concentration of V/ Atomic Weight of V}}$$

Example of calculation

For VPOs-Ga0.1%

$$\frac{P}{V} = \frac{22.81\ mgL^{-1}/30.9738\ mgL^{-1}}{30.68\ mgL^{-1}/\ 50.9415\ mgL^{-1}}$$

= 1.2228

$$\frac{Ga}{V} = \frac{0.0415\ mgL^{-1}/69.723\ mgL^{-1}}{30.68\ mgL^{-1}/\ 50.9415\ mgL^{-1}}$$

= 0.001

APPENDIX G

Calculation of TPR in H_2 Analysis

Total oxygen removed (atom g^{-1})

= Amount of oxygen removed (μ mol g^{-1}) × 6.022 × 10^{23} atom mol^{-1}

= Amount of oxygen removed (atom g^{-1})

Example of calculation

For VPOs-MM

Total oxygen atom removed = (1503.1891 + 2626.9095) μmol/g

= 4.1301 x 10^{-3} mol/g

= 4.1301 x 10^{-3} mol/g x 6.022 x 10^{23} atom/mol

= 2.4871 x 10^{21} atom/g

APPENDIX H

Calculation of Reduction Activation Enerygy (Er) for TPR in H_2 Analysis

Calculation step to obtain reduction activation energy, E_r

H_2 (c) + O (s) → H_2O (g) + □

where (s) = surface or lattice oxygen species; (c) = chemisorbed species

(g) = gaseous species; □ = oxygen vacancy

Rate = $k[H_2]_m[O_s]$

$$-\frac{d[H_2]}{dt} = A\ exp\ \left(\frac{-E_r}{RT_m}\right)[H_2]_m[O_s] \quad (1)$$

Setting the derivative of equation (1) to zero at T_m gives the modified version of Redhead (1962) equation:

$$\frac{E_r}{RT_m{}^2} = \left(\frac{A_r}{\beta}\right)[H_2]_m \exp\left(\frac{-E_r}{RT_m}\right) \quad (2)$$

From the Arrhenius (1889) equation,

$$k_1 = A \exp\frac{-E_r}{RT_m} \quad (3)$$

Therefore from equation (2),

$$k_2 = A[H_2]_m \exp\frac{-E_r}{RT_m} \quad (4)$$

Since k_1 and k_2 are the same at T_m and let k = χ at T_m

$$\frac{\chi}{A[H_2]_m} = \exp\left(\frac{-E_r}{RT_m}\right) \qquad or \qquad \frac{A[H_2]_m}{\chi} = \exp\left(\frac{E_r}{RT_m}\right)$$

$$\frac{E_r}{RT_m} = \ln\left(\frac{A[H_2]_m}{\chi}\right)$$

$$E_r = RT_m \ln\left(\frac{A[H_2]_m}{\chi}\right)$$

where, R = 0.001987 kcal K^{-1} mol^{-1}; 82.056 cm^3 atm K^{-1} mol^{-1}

A = 10^{13} s^{-1}

T_m = maxima temperature of the peak

E_r = reduction activation energy

APPENDIX I

BET Analysis: Nitrogen Adsorption Curves.

For VPOs-MM/VPOs-R_sR_s:

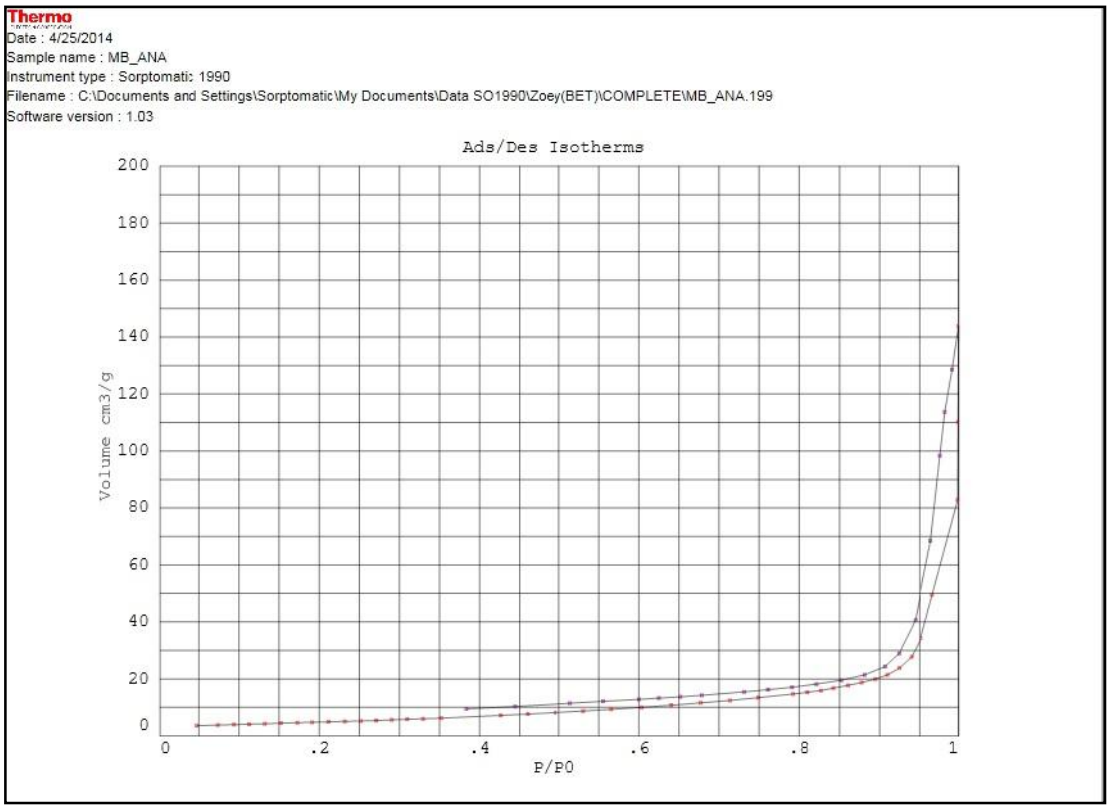

For VPOs-MO:

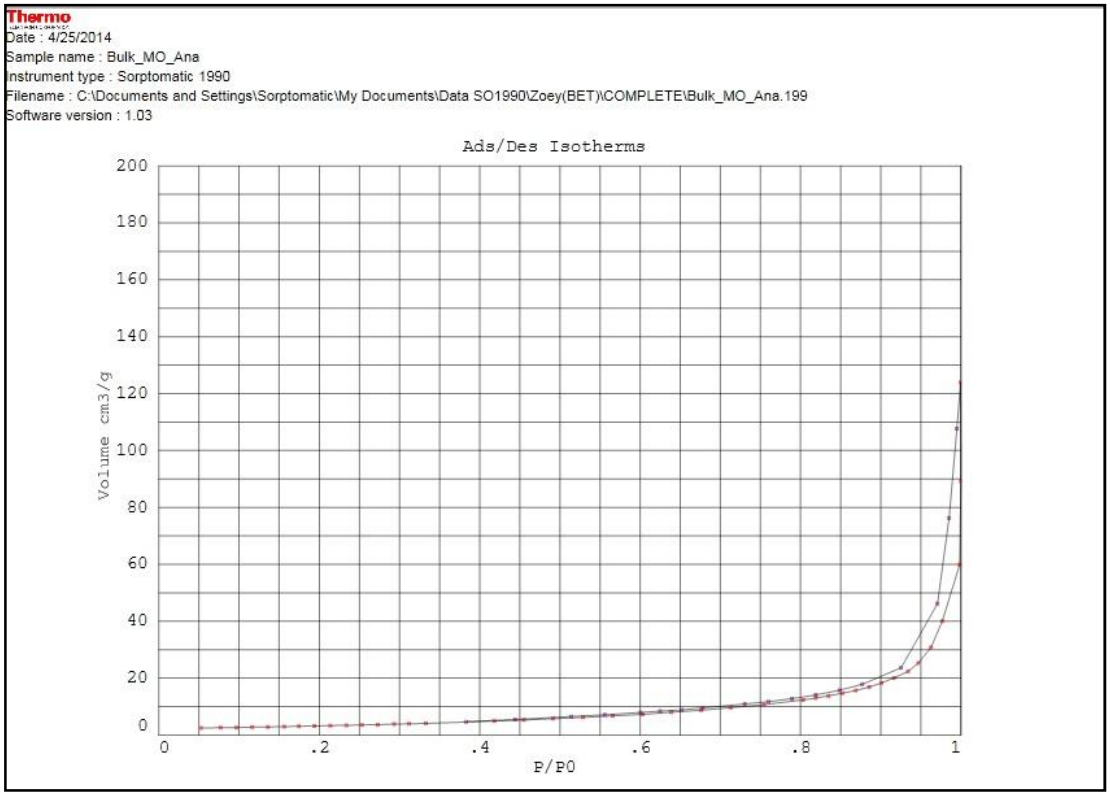

VPOs-OM:

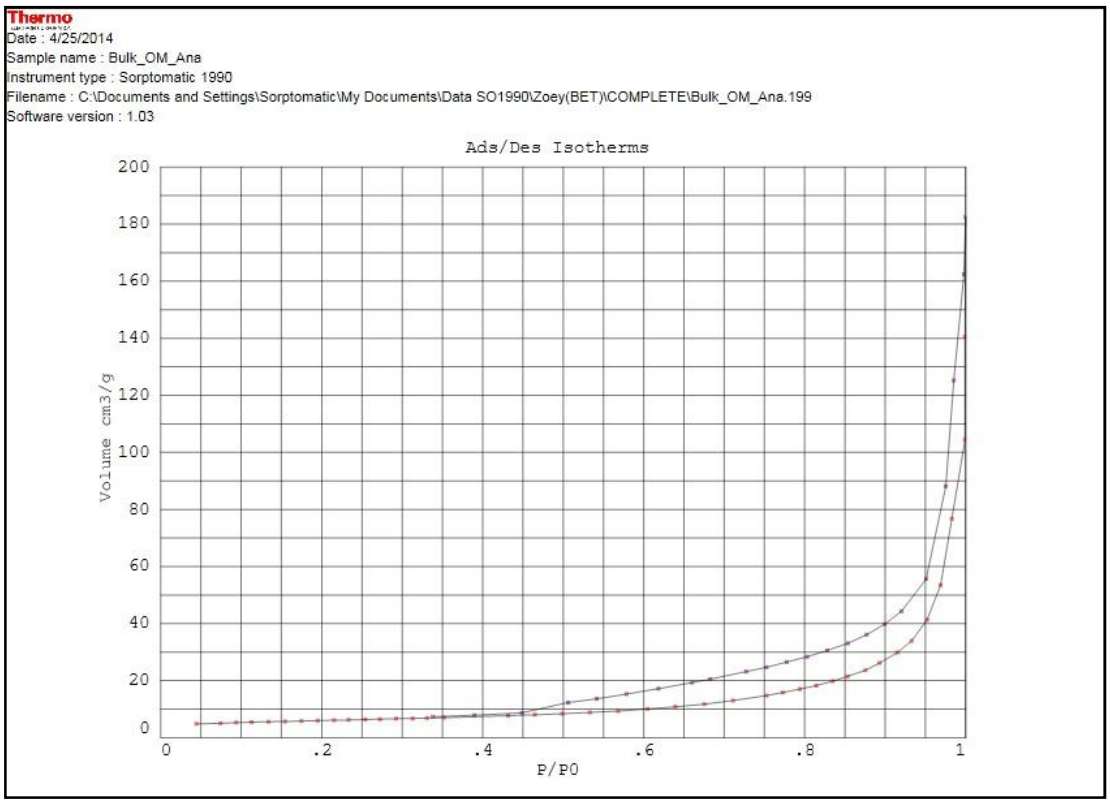

VPOs-OO:

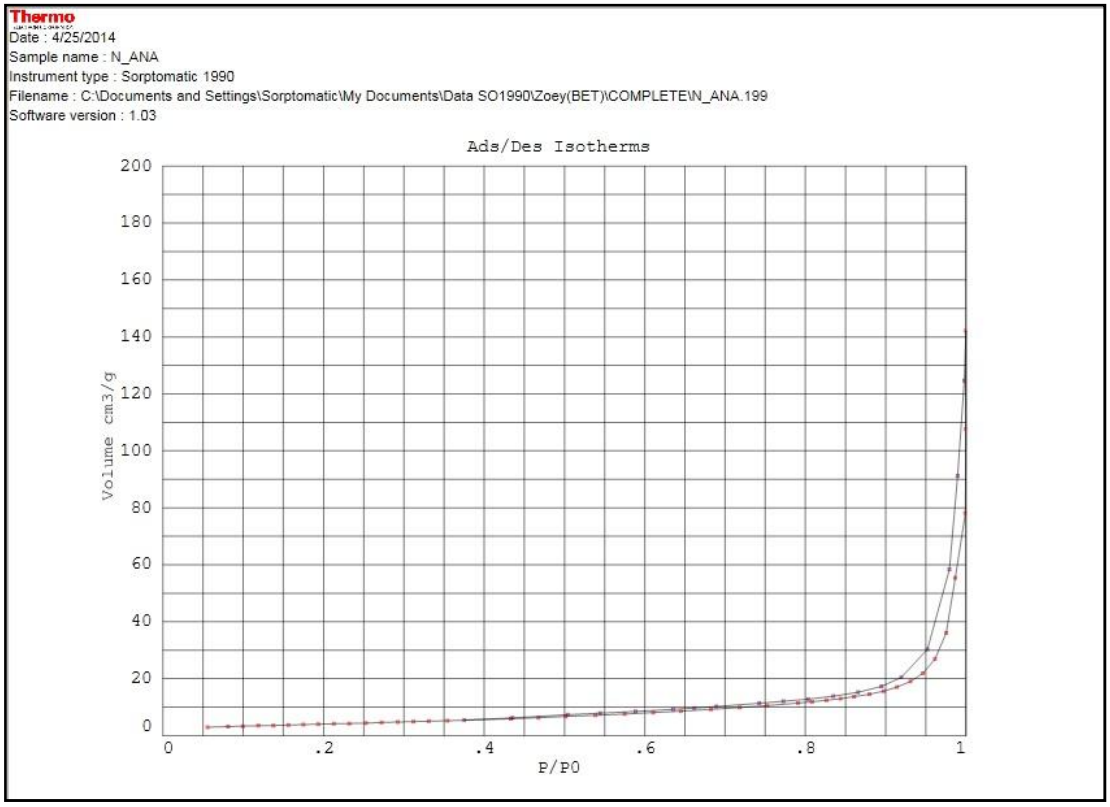

VPOs-Ga0.1%:

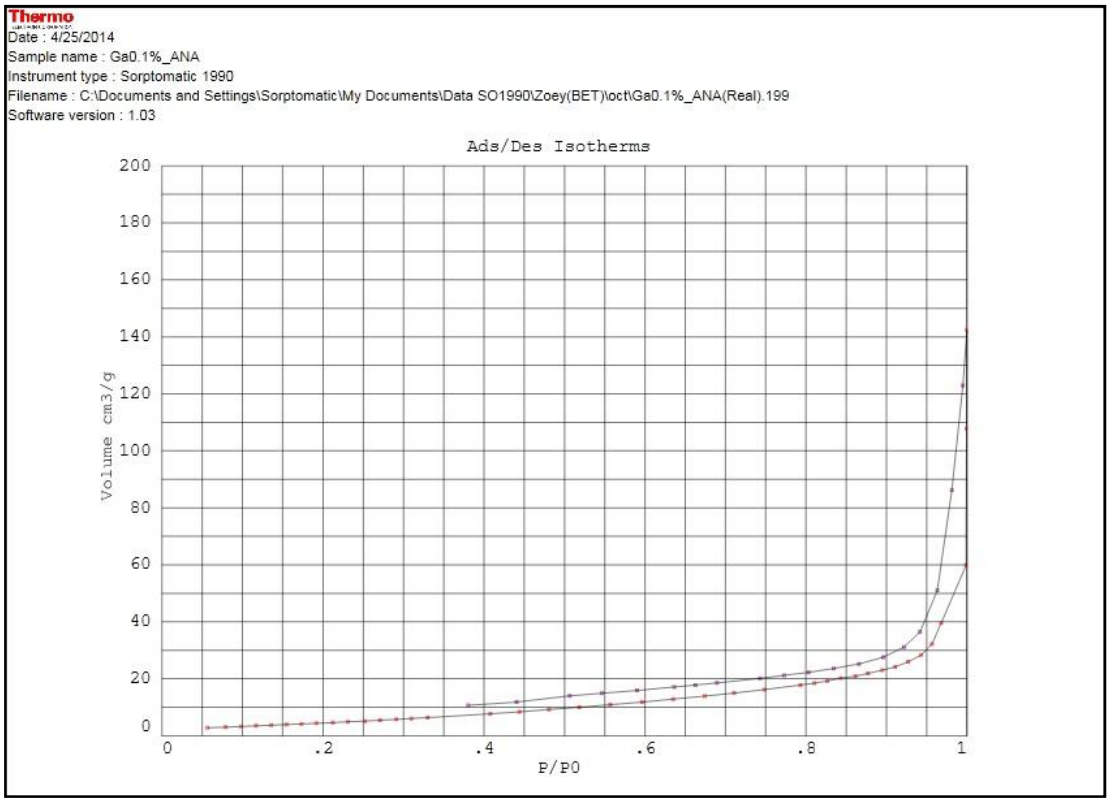

VPOs-Ga0.3%:

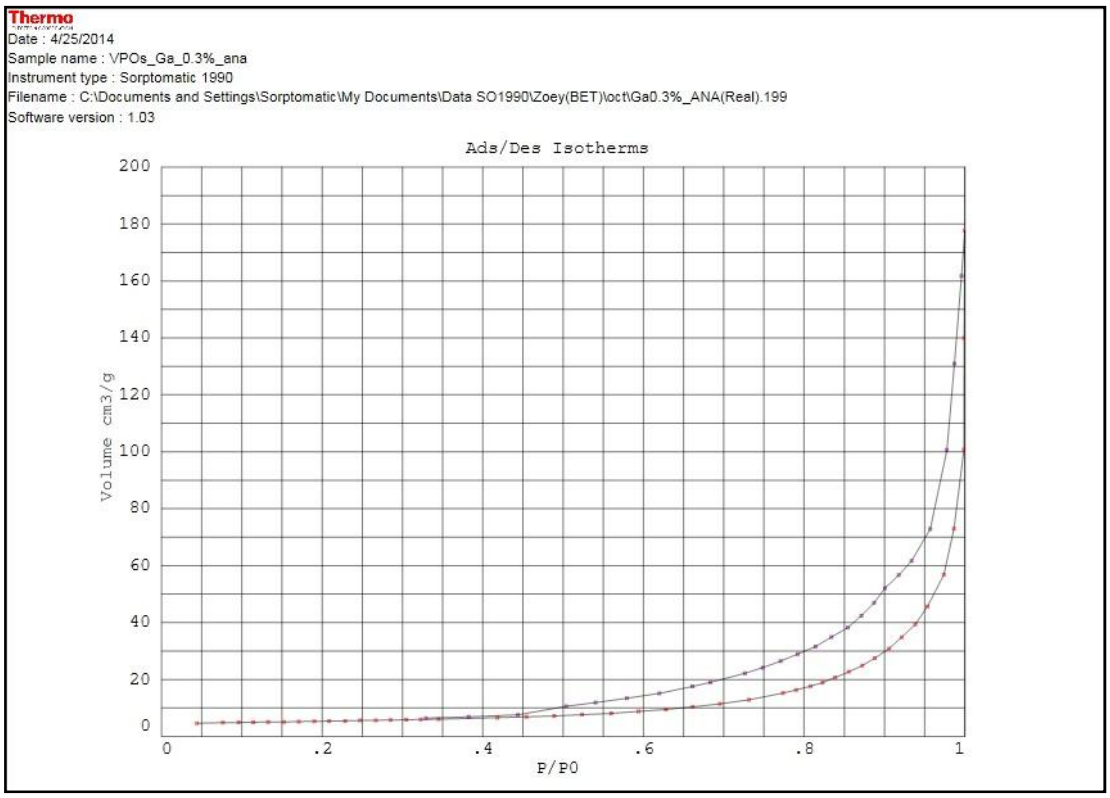

VPOs-Ga0.5%:

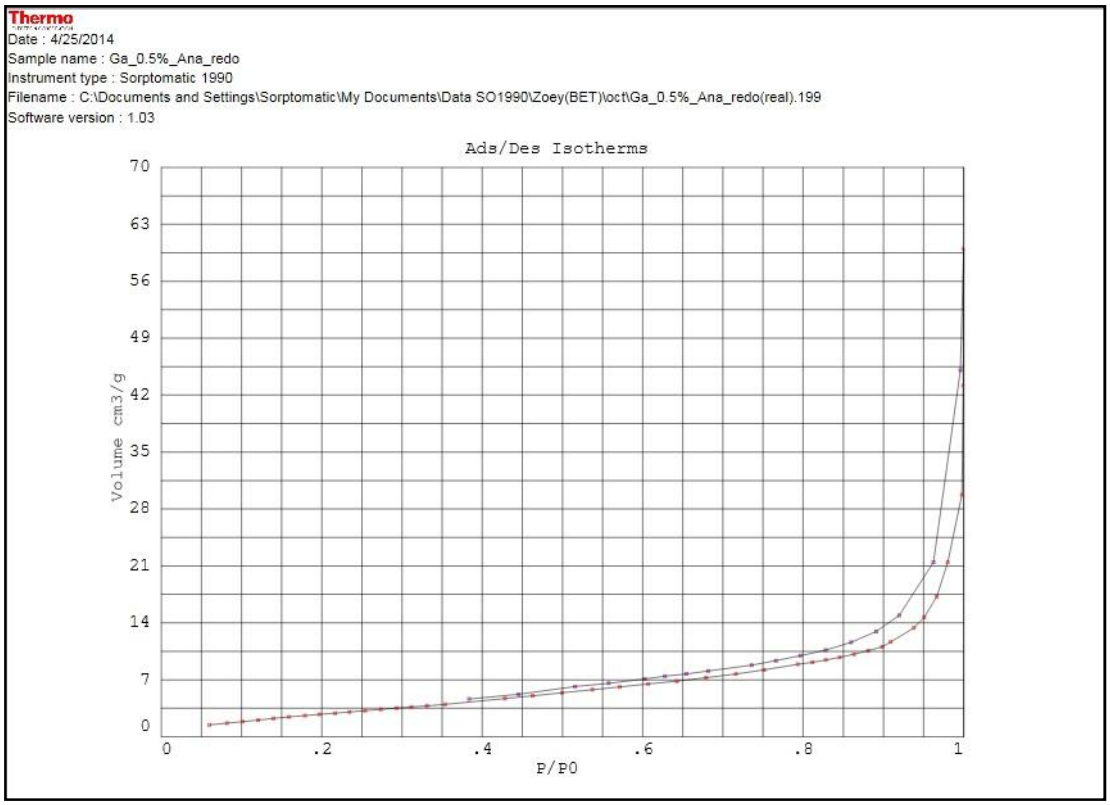

VPOs-M_sM_s:

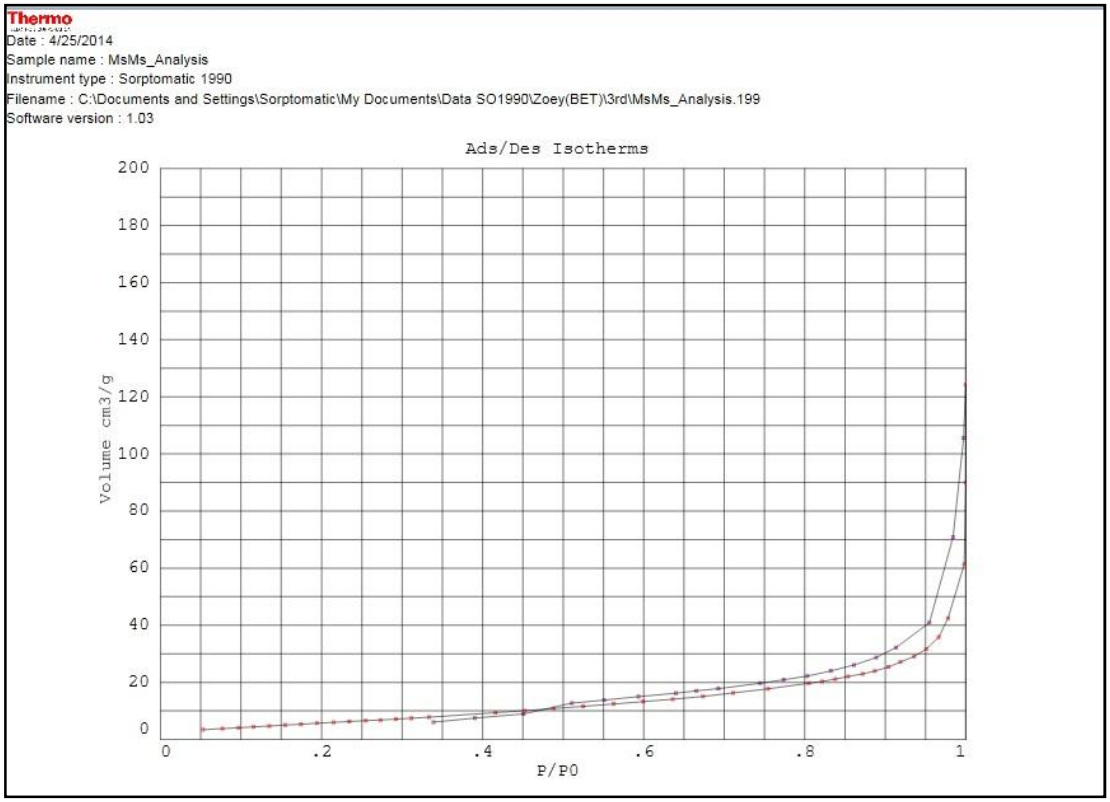

VPOs-R_sM_s:

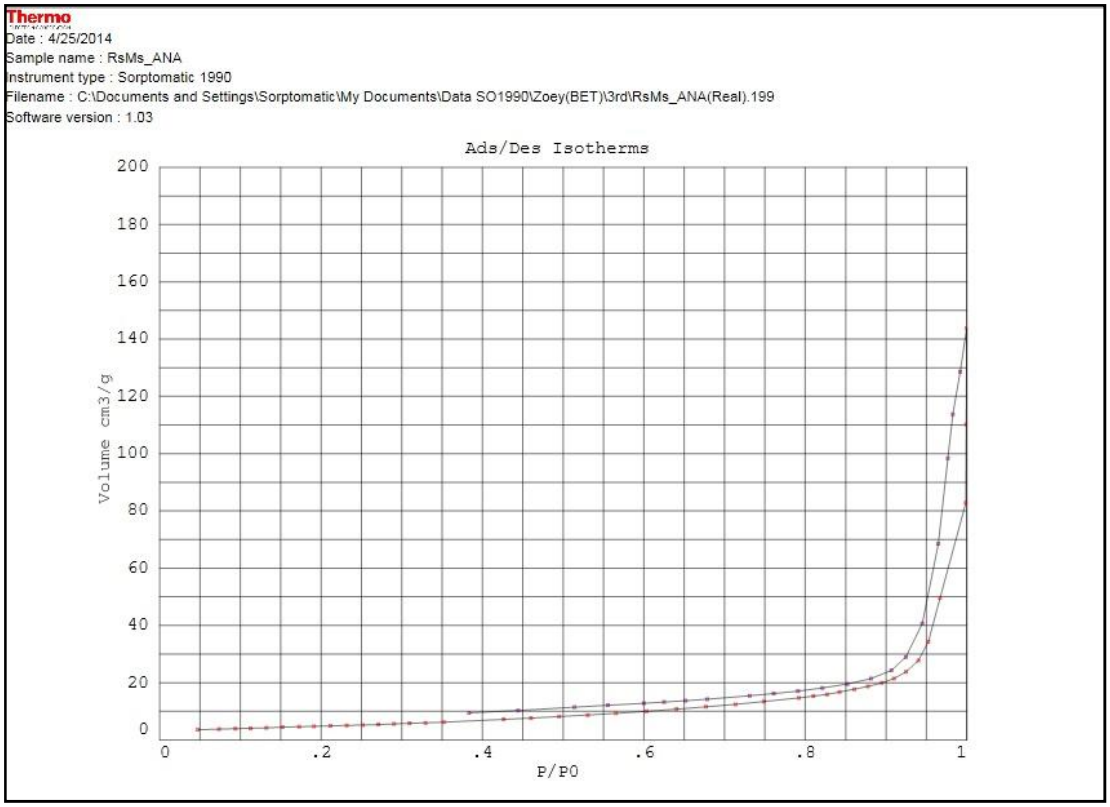

VPOs-M_sR_s:

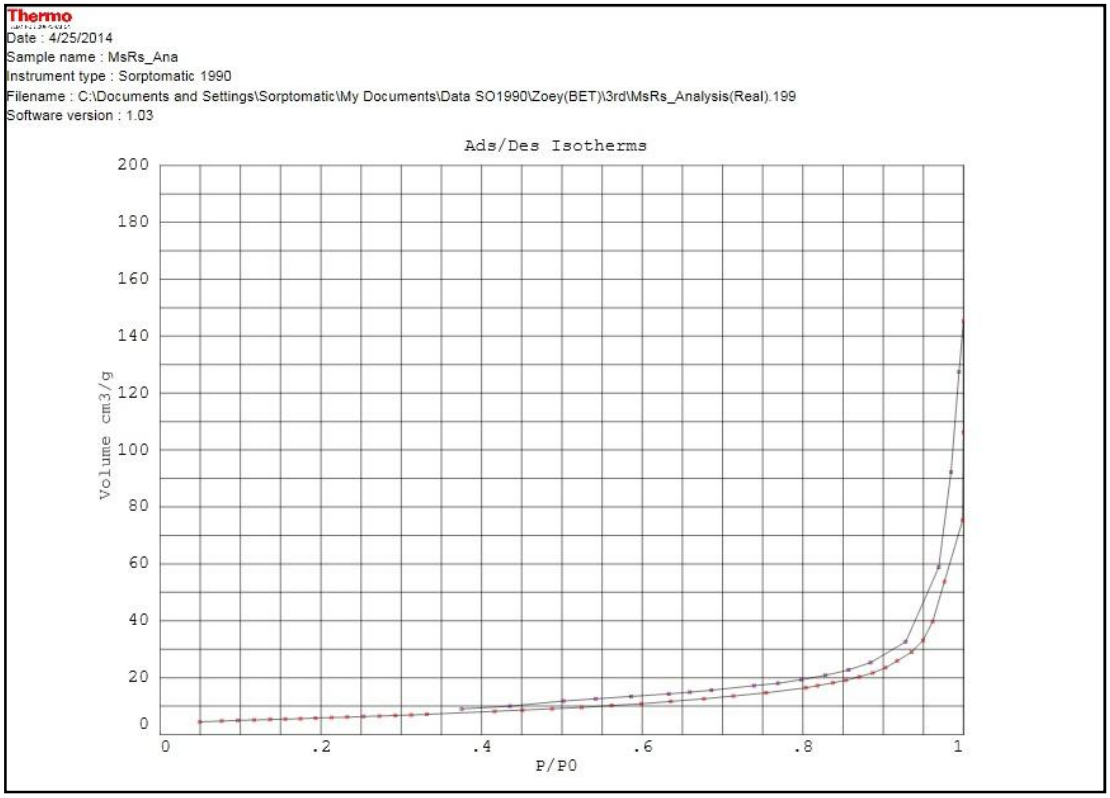
Thermo
Date : 4/25/2014
Sample name : MsRs_Ana
Instrument type : Sorptomatic 1990
Filename : C:\Documents and Settings\Sorptomatic\My Documents\Data SO1990\Zoey(BET)\3rd\MsRs_Analysis(Real).199
Software version : 1.03
Ads/Des Isotherms
Volume cm3/g
200
180
160
140
120
100
80
60
40
20
0
0
.2
.4
.6
.8
1
P/P0